
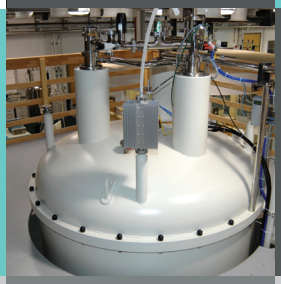
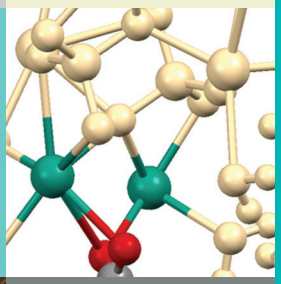


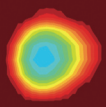

The UK 850 MHz Solid-State NMR Facility

Annual Report 2012

The UK 850 MHz Solid-State NMR Facility

In the first **3** years of operation:

947 days have been allocated to

35 PIs from **19** different UK institutions

with **1357** days being requested

Attendees at the 2012 Annual Symposium that took place at the University of Warwick on Thursday 29th March.

Contents

Introduction

We are pleased to present our third annual report showcasing the breadth of high-quality scientific research that has been performed at the UK 850 MHz Solid-State NMR Facility in the last year. The Facility was funded by a £3.7 M grant from EPSRC (with a 10% contribution from BBSRC) to a consortium of UK solid-state NMR spectroscopists who form the National Management Committee of the Facility, with additional financial contributions from the University of Warwick (in part through the Birmingham Science City Advanced Materials Projects 1 and 2, supported by Advantage West Midlands) and the European Regional Development Fund. Having welcomed the first visitors in February 2010, the Facility has demonstrated itself to be an extremely valuable shared resource for the UK scientific community, with researchers from 18 different institutions carrying out experiments in a range of disciplines including chemistry, materials science, Earth sciences, biology and physics.

The use of high magnetic fields in NMR spectroscopy brings increases in both resolution and sensitivity, and so the 850 MHz Facility enables experiments to be performed that are simply impossible at lower fields. High magnetic fields are particularly important for quadrupolar nuclei (such as ^{17}O, ^{25}Mg, ^{43}Ca and ^{71}Ga), with an additional gain in resolution owing to the reduction in quadrupolar line broadening. This report presents descriptions of the research carried out at the Facility in its third year of operation. Examples of this work have been published in leading international journals, including Angew. Chem., Chem. Sci. and J. Am. Chem. Soc., while ^{17}O NMR investigations of ionothermally-prepared zeolites carried out at the Facility were featured in Chemistry World in May 2012. Particular highlights in this report include a number of multinuclear NMR investigations of battery and fuel cell materials, ^{13}C NMR studies of amyloid fibrils, ^{17}O NMR studies of bone and biomimetic materials, ^{14}N NMR investigation of hydrogen bonding in pharmaceutical molecules and experiments that aim to understand polymorph formation by following the process of crystallization within the NMR rotor.

For NMR spectroscopy of solids, many experiments are performed using the technique of magic-angle spinning (MAS), where the sample is rapidly rotated to remove the significant line broadening observed for many systems. This year, the facility has benefitted from the installation of Europe's first 1 mm double-resonance MAS probe, supplied by Jeol, enabling rotation rates up to 80 kHz to be achieved, thereby widening the range of nuclei and systems that can be studied. This has proven to be particularly useful for the ^{71}Ga NMR investigation of microporous gallium phosphate materials and ^{1}H NMR studies of hydrogen bonding in small organic molecules. Visitors to the Facility have also taken advantage of the access to a double-rotation (DOR) probe that provides an alternative experimental approach for acquiring high-resolution spectra for quadrupolar nuclei. The report details impressive ^{11}B NMR results using this approach.

The second Annual Symposium of the facility was held in March 2012, and attracted over 60 attendees, with talks by graduate students, postdoctoral researchers and PIs from 9 different institutions. This meeting presents an excellent opportunity for researchers around the country to discuss new scientific advances, and provides graduate students in particular with the opportunity to meet each other and to present their work. The Facility is looking forward to welcoming both experienced and new users during the upcoming year, with the Facility Manager available to advise those less familiar with the technique, before, during and after a visit.

In conclusion, we hope you enjoy reading about the exciting science carried out at the UK 850 MHz Solid-State NMR Facility, and we look forward to another successful and productive year.

Further details of the Facility can be found on our website: **http://go.warwick.ac.uk/850mhz/**

The National Management Committee

Sharon E Ashbrook
(St Andrews)

Steven P Brown
(Chair, Warwick)

Melinda J Duer
(Cambridge)

Ray Dupree
(Warwick)

Robin K Harris
(Durham)

Mark E Smith
(Lancaster)

Jeremy J Titman
(Nottingham)

Stephen Wimperis
(Glasgow)

Organization and Management of the Facility

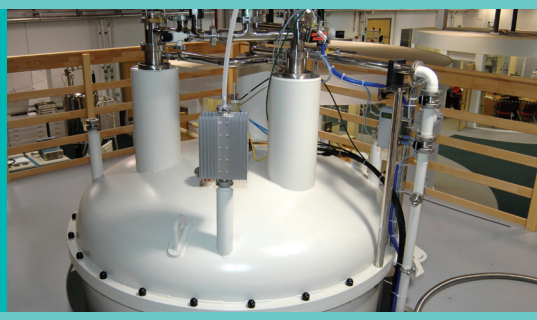

The UK 850 MHz solid-state NMR Facility was established with the aid of several linked research grants from EPSRC. The eight investigators on the grant comprise the National Management Committee (NMC) which determines the strategic objectives for the Facility and the procedures by that these are to be achieved. The NMC meets twice a year, communicating informally more frequently as the need arises. The operation of the Facility is the responsibility of the Local Management Team (LMT) comprising the Facility Manager (FM) who is an ex-officio member of the NMC and the Warwick-based NMC chair. The duties of the Facility Manager include maintaining the instrumentation and assisting visitors to the Facility with their experiments. The management of the Facility is overseen by the International Advisory Board (IAB) which is made up of three eminent solid-state NMR spectroscopists from overseas: Marc Baldus (Utrecht, until April 2012), Chris Jaroniec (Ohio, from May 2012), Arno Kentgens (Nijmegen), Roderick Wasylishen (Alberta). The terms of reference of the NMC and IAB, the remit of the LMT and the duties of the FM are available on the Facility website.

Time Allocation Process

All UK academics who are eligible to apply for Research Council funding, as well as UK researchers of similar standing in industry, may apply for an allocation of spectrometer time at the Facility. Users are expected to run their own experiments with the assistance of the Facility Manager, so personnel with previous solid-state NMR experience should be identified to visit the Facility and carry out the research (inexperienced users should contact the facility manager in advance, to agree a collaborative arrangement with the Facility Manager relating to the Facility Manager's role in carrying out the experiments). A minimum of 80% of the available time is allocated by an independent Time Allocation Panel (TAP) that comprises three UK scientists, including one member of the NMC, as well as the Facility Manager in an *ex-officio* capacity. The balance is allocated by the NMC and is reserved for fast-track applications, measurements referred from the EPSRC solid-state NMR service, the Facility Manager's designated research time, to compensate users who were unable to take up their allocated time because of instrument down-time, and a small number of maintenance days. Members of the TAP normally serve for a two-year term.

There are two allocation rounds each year for time, each covering a six-month period, starting in either February or August, corresponding to deadlines of November 30th and May 31st. Previous users of the Facility are notified of upcoming deadlines by email. Previous time allocations and instructions for applicants are given on the Facility website. The main criterion for allocating time is overall scientific merit, as well as the quality of the case made for high-field solid-state NMR. Where appropriate, the TAP will consider additional factors, such as the quality of publications arising from previous allocations of time and whether the research is supported by peer-reviewed grants or involves students funded by EPSRC or BBSRC. The TAP is charged with ensuring that the balance of the allocated time broadly reflects the research objectives of the original grant and with providing feedback for unsuccessful applicants. During the TAP meeting, the Facility Manager gives advice on the feasibility of the proposed experiments and the spectrometer time required.

The maximum time that can be requested by an individual applicant during any allocation round is 28 days, but this can be split between several applications. It is a condition that the Facility is mentioned in any publication arising wholly or partly from an allocation of time. Furthermore, a user report must be produced by the original applicant no later than the 7th of the month following the end of the specific six-month time-allocation period, i.e., 7th February or 7th August. Applications are not accepted from users who have outstanding reports from previous allocations of time. The code for all NMR pulse sequences implemented by users on the Facility's spectrometer must be deposited in a shared database. If the experiment is a new one, the code will only be made available to other users after the pulse sequence has been published. Reasonable travel costs associated with the use of the facility will be paid to academic users. The Facility rents accommodation on the University of Warwick campus for use by Facility visitors.

TAP membership (2012): Chair: Jeremy Titman, Nottingham; non-NMC members: Kenneth Harris, Cardiff, David Middleton, Liverpool (for the February 2012 round) & Philip Williamson, Southampton (for the August 2012 round onwards).

What is the Facility?

UK 850 MHz solid-state NMR facility probes

No	Probe
1	1.3 mm probe HXY (+19F) conventional insert design H13863
2	2.5 mm HXY DBB (double-broadband) H13856
3	2.5 mm HX (+19F) H13889
4	2.5 mm HFX H13894
5	3.2 mm HXY DBB (double-broadband) H13857
6	3.2 mm HXY low E field for biosolids LLC H13900
7	3.2 mm HXY conventional insert design H13888
8	4 mm HXY conventional insert design (+19F) H13694
9	4 mm HX (low gamma) H13892
10	7 mm X (low gamma) H13895
11	Static
12	1 mm HX (produced by Jeol)
13	DOR probe (produced by Samoson group, Tallinn, Estonia)

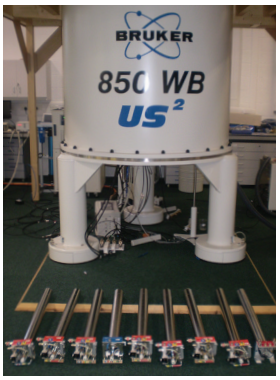

850 MHz spectrometer and probes

Probes 1 to 11 were supplied by Bruker. Maximum MAS frequencies: 4 mm probes 15 kHz; 3.2 mm probes 24 kHz, 2.5 mm probes 35 kHz; 1.3 mm probe 65 kHz. All 3.2 mm and 4 mm MAS probes are equipped with DVT stators and can operate between –140 °C and + 150 °C.

Probe usage 2010 and 2012

Year 1 to Year 3 (Round 1 to Round 6)

Nuclei tested in Double Resonance Mode

Probe in double Resonance mode	Mode	X-Nucleus																										
		^{31}P	^{119}Sn	^{87}Rb	^{11}B	^{71}Ga	^{65}Cu	^{23}Na	^{27}Al	^{13}C	^{79}Br	^{93}Nb	^{45}Sc	^{69}Ga	^{29}Si	^{2}H	^{6}Li	^{17}O	^{135}Ba	^{15}N	^{35}Cl	^{14}N	^{91}Zr	^{43}Ca	^{25}Mg	^{89}Y	^{39}K	^{87}Sr
1.3 mm HXY (+^{19}F) conventional insert design	DR ^{1}H-X DR ^{19}F-X ●	■	★	★	★	■	★	★	★	■ ■	■	■	■	■	★	★	★	■	★	■	★	■						
2.5 mm HX (+^{19}F) 2.5 mm HFX 2.5mm HXY DBB	DR ^{1}H-X DR ^{19}F-X ●	■	★	■	★	■	★	★	■ ■	■ ■	■	★	■	■	★	■	★	■	★	■	★	■	★	★	■				
3.2 mm HXY low E field for biosolids LLC	DR ^{1}H-X			★	★	★	★	★	★	■	■	★	★	★	★	★	★	★	★	■	★	★							
3.2 mm HXY conventional insert design 3.2mm HXY DBB	DR ^{1}H-X			■	■	■	★	■	■	■	■	★	★	★	★	★	★	■	★	■	■	■							
4 mm HXY conventional insert design (+^{19}F)	DR ^{1}H-X DR ^{19}F-X ●	■	■	★	★	★	★	■	■	■ ■	■	★	★	★	■	★	★	★	★	■ ■	★	★							
4 mm HX (low gamma)	DR ^{1}H-X									■	■	■	★	★	★	■	■	■	★	■	★	■	■	■	■	■	■		
7 mm X (low gamma)	X																	★	■	★	■	■	★	■	★	■	■	■	
Static	X	■	★	★	★	■	■	★	★	■	★	■	★	★	★	■	★	★	★	★	■	■	★	★	★	★	■	★	
DOR	X			■	■	■	★	■	■	★	★	★	★	★	★	★	★	■	★	★	★	★	★	■	★				
Jeol 1 mm HX	DR ^{1}H-X				★	■	★	★	★	■	★	★	★	★	★	★	★	★	★	★	★	★							

■ *Experiments performed at the facility to date*

★ *Bench tests indicate should be possible*

● *Other ^{19}F-X DR combinations have not yet been investigated*

For triple-resonance capabilities, refer to the facility website

Time Allocation

366 days requested by 26 PIs from 13 different institutions (Aston, Cambridge, Cardiff, Durham, Glasgow, ISIS, Lancaster, Liverpool, Loughborough, Nottingham, St. Andrews, University College London and Warwick.). 312 days allocated by the Time Allocation Panel.

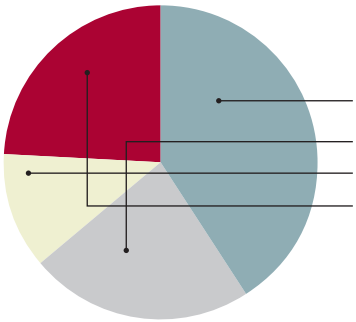

Requested time

Outside Warwick and non-NMC **41%**
NMC outside Warwick **23%**
Warwick NMC **12%**
Warwick non-NMC **24%**

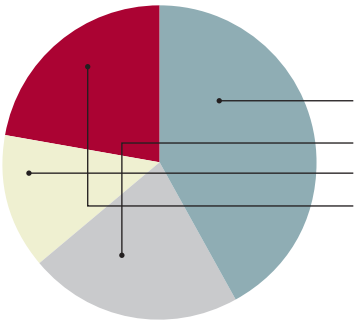

Allocated time

Outside Warwick and non-NMC **42%**
NMC outside Warwick **22%**
Warwick NMC **14%**
Warwick non-NMC **22%**

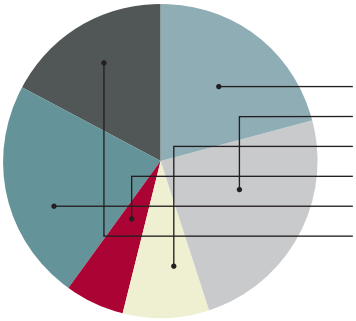

Requested time

Advanced materials **21%**
Bio materials **24%**
Energy materials **9%**
Methods development **6%**
Proteins **23%**
Pharmaceuticals and self assembly **17%**

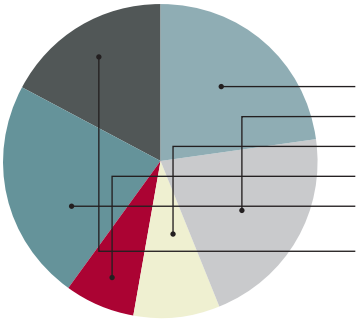

Allocated time

Advanced materials **23%**
Bio materials **21%**
Energy materials **9%**
Methods development **7%**
Proteins **23%**
Pharmaceuticals and self assembly **17%**

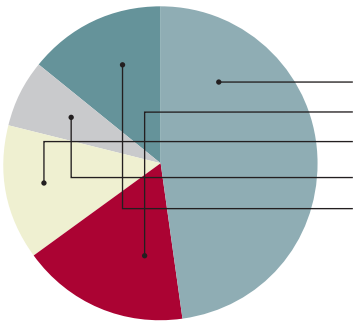

Requested time

EPSRC **48%**
BBSRC **17%**
Other agencies **14%**
Industrial **7%**
No external funding **14%**

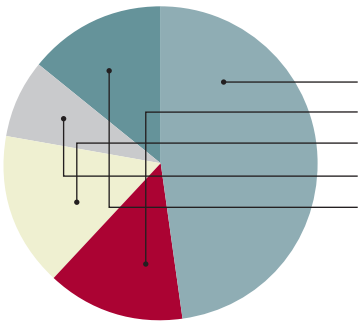

Allocated time

EPSRC **48%**
BBSRC **14%**
Other agencies **16%**
Industrial **8%**
No external funding **14%**

Projects with more than one funding source were counted only once. Other agencies that are funding facility users are: STFC, Leverhulme Trust, British Heart Foundation, Royal Society, EU, Swedish, US and Chile funding agencies.

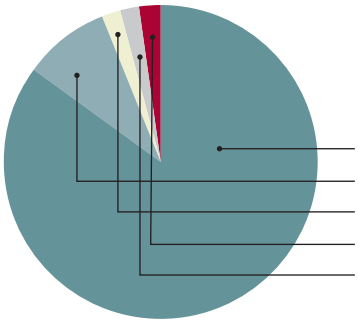

Spectrometer time

Feb 1 2012 – Jan 31 2013 (the facility operates 24 hours a day, 7 days a week)

TAP allocated days **85%**
Facility manager research **9%**
Maintenance **2%**
Fast track **2%**
Compensation **2%**

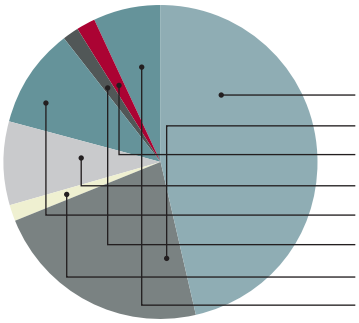

Facility users

Feb 1 2012 – Jan 31 2013

PIs + 1 UK academic **27**
EPSRC PhD students* **13**
BBSRC PhD student **1**
Other PhD or MSc students** **5**
PDRAs*** **6**
Research staff **1**
Industry **1**
Overseas collaborators **4**

* *Some students are partially funded by STFC and industry*
** *1 Marie Curie, 1 Cambridge Commonwealth Trust, 1 Becas Chile and 2 self funded*
*** *1 BBSRC, 1 Leverhulme Trust, 1 Welcome Trust, 1 EU and 1 US funding agency, 1 Newton fellow Royal Society*

Results from User Questionnaire Feb 2012 – Jan 2013

Feedback questionnaires are sent to each PI allocated time at the Facility and contain a series of questions and the opportunity for visitors to make comments and suggestions. The responses are graded from 1 (least satisfied) to 5 (most satisfied). Figure 1 shows the average scores based on the results from 18 responses from visits over the period February 2012 to January 2013.

Section 1 to be completed by the PI

Application for time

1 Ease of application process
2 Transparency of application process
3 Feedback on any unsuccessful time request

Scheduling of time awarded

4 Scheduling of your time by the facility

Overall impact

5 Quality of results obtained

Section 2 to be completed by the visitor

Accommodation

6 Ease of arranging accommodation
7 Quality of accommodation
8 Location of accommodation

At the 850 facility

9 Support from the Facility Manager upon arrival
10 Support from the Facility Manager throughout your visit
11 Quality of the NMR facilities
12 Quality of the sample preparation area and storage facilities
13 Ease of access to the facility out of hours
14 Your overall time at the facility

Post visit experience

15 Arrangements for accessing data
16 Arrangements for returning any samples
17 Reimbursement of expenses

Average scores from feedback questionnaire over period Feb 2012 – Jan 2013

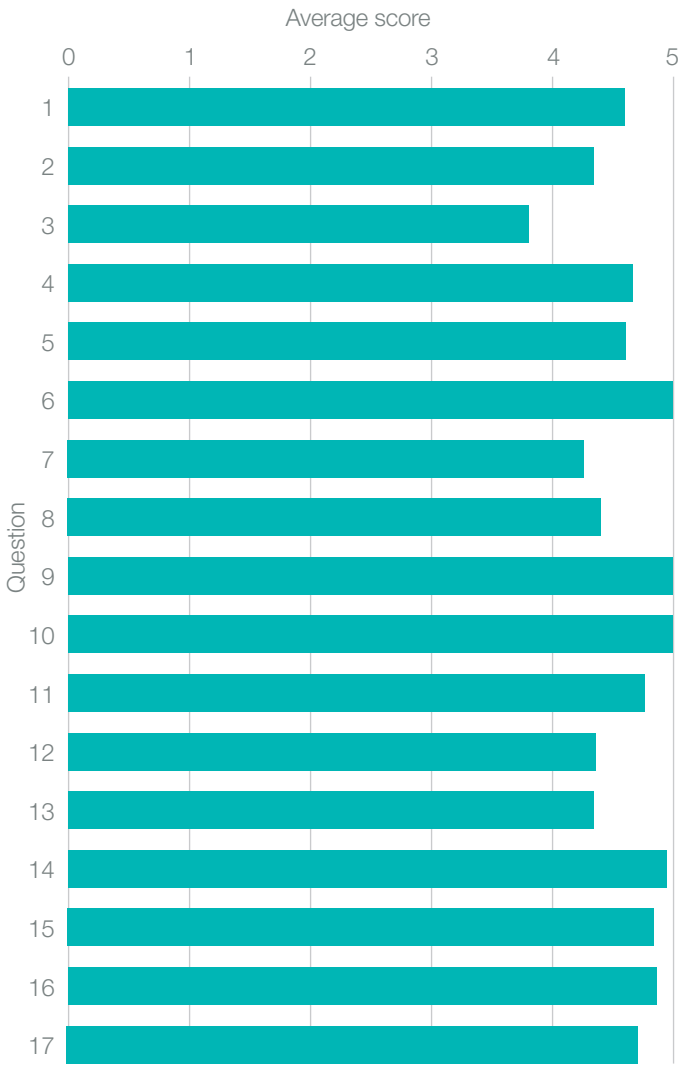

UK 850 MHz Solid-State NMR Facility
2nd Annual Symposium

Thursday 29 March 2012
Millburn House, University of Warwick
Symposium Organiser: **Ray Dupree**

List of talks

1 ***'Solid-State NMR of Pharmaceuticals using the UK 850 MHz SSNMR Facility at Warwick'***
Tran Pham *(GSK)*

2 ***'Solid-State NMR Investigation into Local Structure and Order in the Aluminophosphate STA-2'***
Valerie Seymour *(St Andrews)*

3 ***'In-Situ NMR Studies of Crystallization Processes in Polymorphic Systems'***
Andrew Williams *(Cardiff)*

4 ***'^{11}B Double Rotation NMR as a Probe of Local and Intermediate Structure in Crystalline Borates'***
Oliver Alderman *(Warwick)*

5 ***'Ion Mobility and Trapped Defects in Doped Perovskites by NMR Spectroscopy'***
Frédéric Blanc *(Cambridge)*

6 ***'Multi-nuclear NMR Studies of the Hydrogen Storage System $LiBH_4 + MgH_2$'***
Greg Martin *(Nottingham)*

7 ***'Solid-State NMR Study of Strontium and Magnesium Substitution in Fluorapatite'***
Nasima Kanwal *(Queen Mary)*

8 ***'Antibiotic/Target Recognition in Lipid Membranes'***
Boyan Bonev *(Nottingham)*

9 ***'High-Field Solid-State NMR Analysis of the Structural Modification of Aβ Fibrils and Oligomers by Glycosaminoglycans'***
Jillian Madine *(Liverpool)*

10 ***'A Solid State ^{31}P, ^{29}Si and ^{43}Ca MAS and DOR and GIPAW DFT Study of α-Tricalcium Phosphate and Silicon-Substituted α-Tricalcium Phosphate Bioactive Materials'***
James McDonald *(Warwick)*

11 ***'Improved Background Suppression in MAS NMR'***
Steve Wimperis *(Glasgow)*

Publications

'Identifying the Intermolecular Hydrogen-Bonding Supramolecular Synthons in an Indomethacin-Nicotinamide Cocrystal by Solid-State NMR'
K. Maruyoshi, D. Iuga, O.N Antzutkin, A. Alhalaweh, S. Velaga, S.P. Brown,
Chem. Commun., 48, 10844-10846 (2012)

'Hydrogen Bonding in Alzheimer's Amyloid-β, Fibrils Probed by $^{15}N\{^{17}O\}$ REAPDOR Solid-State NMR Spectroscopy'
O.N. Antzutkin, D. Iuga, A.V. Filippov, R.T. Kelly, J. Becker-Baldus, S.P. Brown, R. Dupree
Angew. Chem. Int. Ed., 51, 10289-10292 (2012)

'A Multinuclear Solid-State NMR Study of Templated and Calcined Chabazite-Type GaPO-34'
M. Amri, S.E. Ashbrook, D.M. Dawson, J.M. Griffin, R.I. Walton, S. Wimperis
J. Phys. Chem. C, 116, 15048-15057 (2012)

'Double Rotation ^{11}B NMR Applied to Polycrystalline Barium Borates'
L.G. Alderman, D. Iuga, A.P. Howes, D. Holland, R. Dupree
Phys. Chem. Glasses: Eur. J. Glass Sci. Technol. B., 53, 132-140 (2012)

'^{87}Sr Solid-State NMR as a Structurally Sensitive Tool for the Investigation of Materials: Antiosteoporotic Pharmaceuticals and Bioactive Glasses'
C. Bonhomme, C. Gervais, N. Folliet, F. Pourpoint, C.C. Diogo, J. Lao, E. Jallot, J. Lacroix, J.M. Nedelec, D. Iuga, J.V. Hanna, M.E. Smith, Y. Xiang, J. Du, D. Laurencin
J. Am. Chem. Soc., 134, 12611-12628 (2012)

'Ionothermal ^{17}O Enrichment of Oxides using Microlitre Quantities of Labelled Water'
J.M. Griffin, L. Clark, V.R. Seymour, D.W. Aldous, D.M. Dawson, D. Iuga, R.E. Morris, S.E. Ashbrook
Chem. Sci., 3, 2293-2300 (2012)
(Featured in *Chemistry World*, 2nd May 2012)

'Probing Intermolecular Interactions and Nitrogen Protonation in Pharmaceuticals by Novel ^{15}N-Edited and 2D ^{14}N-^{1}H Solid-State NMR'
A.S. Tatton, T.N. Pham, F.G. Vogt, D. Iuga, A.J. Edwards, S.P. Brown
CrystEngComm, 14, 2654-2659 (2012)

'Exploiting the Chemical Shielding Anisotropy to Probe Structure and Disorder in Ceramics: ^{89}Y MAS NMR and First-Principles Calculations'
M.R. Mitchell, D. Carnevale, R. Orr, K.R. Whittle, S.E. Ashbrook
J. Phys. Chem. C., 116, 4273- 4286 (2012)

'Thermal Phase Transformation in $LaGaO_3$ and $LaAlO_3$ Perovskites: an Experimental and Computational Solid-State NMR Study'
F. Blanc, D.S. Middlemiss, J.L. Palumbo, L. Buannic, I. Farnan, C.P. Grey
Solid State Nucl. Magn. Reson., 42, 87-97 (2012)

'A Novel Structural Form of MIL-53 Observed for the Scandium Analogue and its Response to Temperature Variation and CO_2 Adsorption'
J.P.S. Mowat, V.R. Seymour, J.M. Griffin, S.P. Thompson, A.M.Z. Slawin, D. Fairen-Jimenez, T. Düren, S.E. Ashbrook, P.A. Wright
Dalton Trans., 41, 3937-3941 (2012)

'Applications of High-Resolution ^{1}H Solid-State NMR'
S.P. Brown
Solid State Nucl. Magn. Reson., 41, 1-27 (2012)

'Probing Cation and Vacancy Ordering in the Dry and Hydrated Yttrium Substituted $BaSnO_3$ Perovskite by NMR Spectroscopy and First Principles Calculations: Implications for Proton Mobility.'
L. Buannic, F. Blanc, D.S. Middlemiss, C.P. Grey
J. Am. Chem. Soc., 134, 14483-14498 (2012)

'^{14}N-^{1}H Heteronuclear Multiple-Quantum Correlation Magic-Angle Spinning NMR Spectroscopy of Organic Solids'
A.S. Tatton, J.P. Bradley, D. Iuga, S.P. Brown
Z. Phys. Chem., 226, 1187-1204 (2012)

'Exploiting In-Situ Solid-State NMR for the Discovery of New Polymorphs during Crystallization Processes'
C.E. Hughes, P.A. Williams, T.R. Peskett, K.D.M. Harris
J. Phys. Chem. Lett., 3, 3176-3181 (2012)

'Direct Detection of Discharge Products in Lithium–Oxygen Batteries by Solid-State NMR Spectroscopy'
M. Leskes, N.E. Drewett, L.J. Hardwick, P.G. Bruce, G.R. Goward, C.P. Grey
Angew. Chem. Int. Ed., 51, 8560-8563 (2012)

'An Examination of the Calcium and Strontium Site Distribution in Bioactive Glasses through Isomorphic Neutron Diffraction, X-ray Diffraction, EXAFS and Multinuclear Solid State NMR'
R.A. Martin, H.L. Twyman, G.J. Rees, E.R. Barney, R.M. Moss, J.M. Smith, R.G. Hill, G. Cibin, T. Charpentier, M.E. Smith, J.V. Hanna and R.J. Newport
J. Mater. Chem., 22, 22212-22223 (2012)

'Site-Specific Identification of an Aβ Fibril–Heparin Interaction Site by Using Solid-State NMR Spectroscopy'
J. Madine, M.J. Pandya, M.R. Hicks, A. Rodger, E.A. Yates, S.E. Radford, D.A. Middleton
Angew. Chem. Int. Ed., 51, 13140-13145 (2012)

'New Strategies for Exploring Crystallization Processes of Organic Materials'
K.D.M. Harris, C.E. Hughes, B.A. Palmer and F. Guillaume
Trans. Am. Cryst. Assoc. 43, 97-112 (2012)

In addition, there were 57 talks and 25 posters at conferences and seminars in 2012, where results obtained at the UK 850 MHz Solid-State NMR Facility were presented.

PhD Theses

Student	Department	University	Supervisor	Title	Date
Andrew S. Tatton	Physics	Warwick	Steven P. Brown	*'Development of solid-state NMR techniques for the characterisation of pharmaceutical compounds'*	Sep 2012
Erika Davies	Chemistry	Cambridge	Melinda J. Duer	*'Finding a place for citrate: an NMR crystallographic approach to the study of bone material'*	Oct 2012

User Comments

"The facility enabled us to obtain structural details on an amyloid fibril, which could not be obtained with the resolution and sensitivity provided by our in-house 400 MHz spectrometer."

David Middleton, Liverpool

"This high-field solid-state NMR instrumentation has enabled very effective methods for probing the ^{71}Ga nucleus in glassy environments. The quadrupolar characteristics of the ^{71}Ga nucleus have precluded these measurements being undertaken at lower fields with any real effectiveness and accuracy. The reduced quadrupolar dominated linewidths afforded at 20 T, and the advent of MAS frequencies ≥ 60 kHz, have facilitated the study of more quadrupolar nuclei in the NMR Periodic Table."

John Hanna, Warwick

"The improved resolution and sensitivity afforded by the higher field, combined with the fast MAS and VT capabilities allowed high-quality data to be acquired in a reasonable timescale. The facility proved particularly valuable in this work owing to the combination of fast MAS and VT (heating and cooling), which is not available at our lower-field facility."

Sharon Ashbrook, St Andrews

"To study crystallization via in-situ solid-state NMR we require high signal to noise to gain sufficient time resolution to observe the crystallization process as it occurs. In systems with natural abundance levels of ^{13}C this is often not possible at lower fields. In addition, high spectral resolution is important to allow different polymorphic forms to be distinguished."

Kenneth Harris, Cardiff

"Access to the 850MHz facility allowed us to identify most of the species formed in the lithium-air battery, a crucial step in the development of a viable energy storage system. The high field and fast magic angle spinning (60 kHz) significantly narrows the signals arising from the various oxygen species. As a result, despite the small samples recovered from working batteries, the signal intensity is sufficient to reliably assign the spectra obtained at the 850 MHz facility."

Clare Grey, Cambridge

The UK 850 MHz Solid-State NMR Facility PhD Travel Fund

Supported by Bruker

The UK 850 MHz Solid-State NMR Facility PhD travel fund supported by Bruker provides funding for: (a) attendance at an internationally recognised, high-profile conference where a PhD student presents results he/she obtained at the 850 MHz Facility, or (b) a "start-up" visit to another lab to learn new methods to be implemented at the 850 MHz Facility. For further details see: **http://go.warwick.ac.uk/850mhz/travel_fund/**

2012 Awards

- **Daniel M. Dawson** (University of St Andrews) awarded £1000 to attend the Solid-State NMR Symposium at the 54th Rocky Mountain Conference on Analytical Chemistry in Colorado, USA (July 2012) and give a talk entitled *Using Solid-State ^{13}C MAS NMR Spectroscopy to Study Paramagnetic Metal-Organic Frameworks Loaded with Multiple Guests*.
- **Smita Odedra** (University of Glasgow) awarded £1000 to attend the Solid-State NMR Symposium at the 54th Rocky Mountain Conference on Analytical Chemistry in Colorado, USA (July 2012) and give a poster entitled *Improved Background Suppression in MAS NMR using Composite Pulses*.
- **Luke Sperrin** (University of Cambridge) awarded £773 to attend the Solid State Protonic Conductors (SSPC16) conference in Grenoble, France (Sept 2012) and present a poster entitled *Solid State NMR Studies of Yttrium doped $BaZrO_3$: Defect Arrangement and Protonic Conduction Pathways*.

User Reports

Proline and Hydroxyproline Dynamics in Collagen and Peptides

Abil E. Aliev and Denis Courtier-Murias

Department of Chemistry, University College London

Overview

There is a long-standing interest in the dynamics of individual amino acid residues in solid proteins, including the influence of water on protein dynamics.[1] Amongst various amino acid residues, proline (Pro) and 4-hydroxy-proline (Hyp) are unique in terms of their structure and dynamics,[2,3] as the ring puckering of the Pro and Hyp residues and the ratio of the *trans*- and *cis*-rotamers about the peptide bonds are expected to influence the stability of ordered protein structures, including collagen triple helices. Another attribute of Pro is its hinge-like function, which enhances the probability of β-turns.

The well-known example of Pro and Hyp containing protein is collagen. The structure of collagen is described as a triple-helix of three individual protein strands. Each strand consists of repeated -Gly-Xaa-Yaa- units, the most common fragment being -Gly-Pro-Hyp-. Previous studies have shown that by adding water to collagen it is possible to induce large angle motions of the collagen atoms.[2,4] Specifically, the increase of water content may result in the increase of the amplitude Φ of the oscillation about internal bond directions, as illustrated in Figure 1 for a C-C$^{\alpha}$ bond in -Hyp-Gly-Pro-. We show here that solid-state ^{13}C CP MAS measurements can be successfully applied for monitoring the changes in dynamics of amino acid residues in peptides and collagen as a function of water content. The ^{1}H-^{13}C dipolar-dephasing experiment proved very useful for quantifying the changes in motional amplitudes.

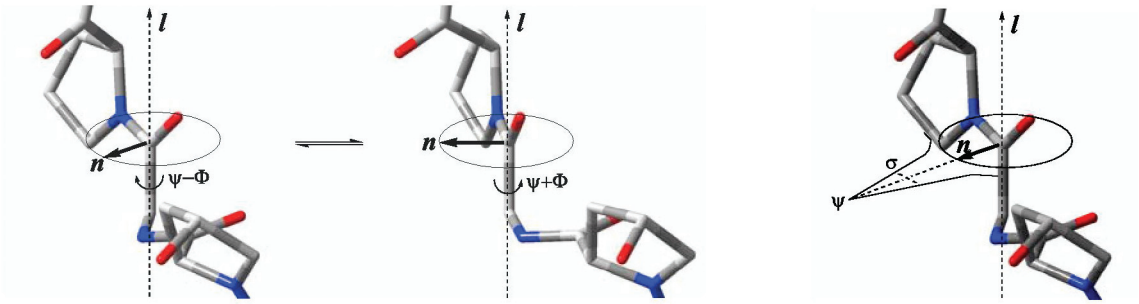

Figure 1. Internal bond libration about the C-C$^{\alpha}$ bond axis. The normal (n) of the Gly peptide plane is shown to librate about the bond axis (l) between two sites with dihedral angles $\psi-\Phi$ and $\psi+\Phi$ (left) or about its averaged position with a Gaussian uncertainty σ (right).[2]

^{13}C CSA and ^{1}H-^{13}C Dipolar Dephasing for Dynamics Studies in Solids

One of the reasons for relatively modest applications of solid-state NMR compared to its solution counterpart is due to the fact that diffraction techniques can be applied for direct structure determinations of solids where a single crystal is available. In the field of solids dynamics characterizations, however, the leading position of NMR is well recognized. Within the limits of such a widely exploited nucleus as ^{13}C, motional averaging of the chemical shift anisotropy (CSA) and ^{1}H-^{13}C dipolar interactions provides a straightforward mean for dynamics studies. With the introduction of high-field solid-state NMR equipment, CSA measurements of aliphatic carbons become feasible. We have exploited this in our comparative analysis of ^{13}C sites in amino acids. For example, our measurements at 850 MHz show that CSAs of the three methylene carbons of L-proline reduce in a sequence of C$^{\delta}$ > C$^{\beta}$ > C$^{\gamma}$. The lower value for C$^{\gamma}$ (30 ppm) compared to C$^{\beta}$ (35 ppm) can be attributed to relatively higher mobility of the C$^{\gamma}$ site. The results of our ^{13}CO CSA measurements on collagen samples containing different amounts of added heavy water showed that ^{13}CO CSAs decrease on increasing the water content. The changes in the values of ^{13}CO CSAs are caused by the changes in the collagen backbone dynamics. We have estimated the backbone librational amplitude Φ to increase from 8° to 15° on increasing the weight % D_2O from 12 to 38%.

A few early studies have shown that dipolar dephasing experiments are useful for estimating motional averaging of dipolar interactions. It was found that for directly bonded ^{1}H-^{13}C pairs the dependence of the signal intensity on the dephasing delay is described using a Gaussian function: $I = I_0 \exp(-t^2 / T_{dd}^2)$, where T_{dd} is the Gaussian dipolar dephasing constant and t is the dephasing delay. Deviations were found for some solids from the Gaussian dependence at longer t values which were tentatively attributed to ^{1}H-^{1}H dipole-dipole interactions. Such inconsistency for the I vs. t dependence has limited the application of the dipolar dephasing experiment and only a handful of reports are known which have employed this technique. From the analysis of data obtained at 850 MHz with high signal-to-noise ratios (Figure 2), we have found that the dipolar dephasing behaviour of protonated carbons is best described using a sum of Gaussian and Lorentzian functions [$I = I_0 \exp(-t / T_{rem})$, where T_{rem} is the dipolar dephasing constant due to remote ^{1}H nuclei], as for any given ^{13}C site there are remote intra- and intermolecular ^{1}H-^{13}C interactions present in organic solids. The addition of the Lorentzian term accounts for the non-Gaussian deviation observed previously at longer t values.

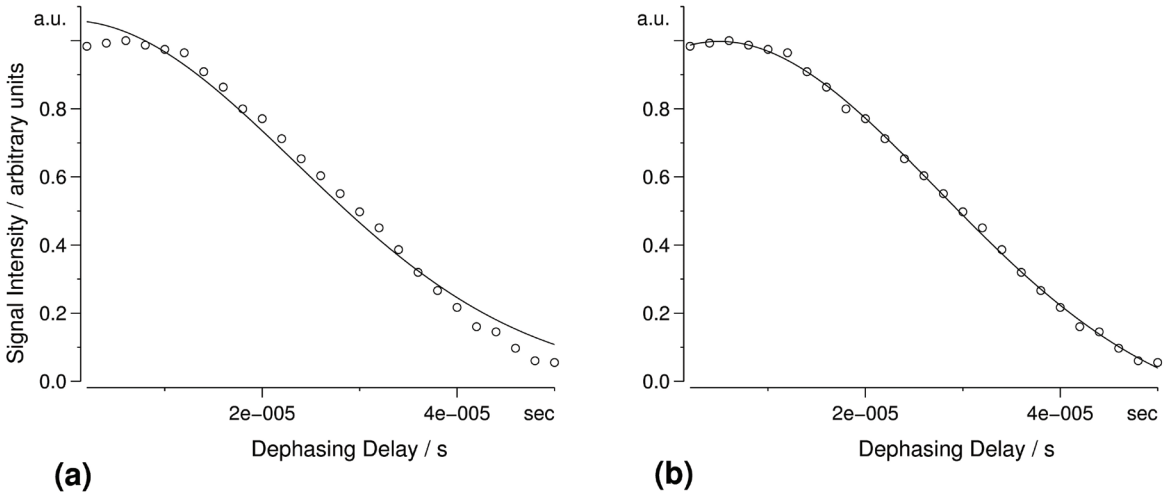

Figure 2. (a) Gaussian and (b) Gaussian+Lorentzian fittings of the methylene ^{13}C intensities of glycine hydrochloride as a function of dipolar dephasing period t at 20 T and ν_R=4.4 kHz.

Using various organic solids and low temperature measurements we have shown that the T_{dd} value for motionally static CH_2 environments is dependent on the MAS frequency (ν_R) and the external field strength: at ν_R=4.4 kHz, the "static" limiting value is ~19 μs at 7.05 T and ~32 μs at 20 T. By dividing the rigid value of T_{dd} for a given C-H bond by motionally averaged values of T_{dd}, we define an order parameter S as a dimensionless measure of the amplitude of the C-H reorientations. This parameter varies between 0 and 1, with higher values corresponding to motionally restricted cases with smaller reorientational amplitudes (e.g., 2Φ in Figure 1). The angle between the reorientation axis (along C-C or C-N bond directions) and the C-H vector is approximately the same (~109°) for the majority of ^{13}C sites in proteins. The obtained values of S at 7.05 and 20 T for the resolved ^{13}C sites in collagen[2] allowed us to estimate uncertainties involved in order parameter estimations and draw following conclusions: (i) the most rigid parts of the collagen molecule include C^{α}–H of Gly and Ala; (ii) backbone C^{α}–H in Pro and Hyp show higher mobility than in Gly and Ala. The C^{γ} site of Pro shows higher motional amplitude than C^{β} and C^{δ} of Pro; (iii) amongst the measured sites, the most mobile acyclic side chains are Glu and Lys; (iv) addition of water leads to significant increase of motional amplitudes of all the measured C-H bond directions in collagen and, within the experimental errors involved, the backbone and side-chain dynamics of collagen are affected to a similar degree by the addition of water.

The correlation times were also estimated using wide-line T_2(^{1}H) measurements. The results suggest that frequencies of motions in collagen increase as the water content is increased. Thus, both the frequency and the amplitude of protein motions increase on increasing the water content. These results were confirmed computationally using MD simulations of a collagen model aggregate in water.

References

1. Baghchi, B. *Chem. Rev.* **2005**, *105*, 3197.
2. Aliev, A. E. *Biopolymers* **2005**, *77*, 230.
3. Aliev, A. E.; Bhandal, S.; Courtier-Murias, D. *J. Phys. Chem. A* **2009**, *113*, 10858.
4. Reichert, D.; Pascui, O.; de Azevedo, E. R.; Bonagamba, T. J.; Arnold, K.; Huster, D. *Magn. Reson. Chem.* **2004**, *42*, 276.

Exploring the Structure of Alzheimer's $A\beta_{(1-42)}C_{21}C_{30}$ Oligomers Using Solid-State NMR

Robert T. Kelly,[1] Andrei V. Filippov,[2] Christofer Lendel,[3] Morten Bjerring,[4] Dinu Iuga,[1] Anatoly Dubnovitsky,[3] Józef R. Lewandowski,[5] Steven P. Brown,[1] Ray Dupree,[1] Niels Chr. Nielsen,[4] Torleif Härd[3] and Oleg N. Antzutkin[1,2]

[1]*Department of Physics, University of Warwick*

[2]*Chemistry of Interfaces, Luleå University of Technology, Sweden*

[3]*Department of Molecular Biology, Swedish University of Agricultural Sciences, Sweden*

[4]*Interdisciplinary Nanoscience Center (iNANO) and Department of Chemistry, Aarhus University, Denmark*

[5]*Department of Chemistry, University of Warwick*

Overview

Small intermediate aggregates (oligomers and protofibrils) of amyloidogenic peptides and proteins have been shown to be neurotoxic *in vitro* and are believed to be the principal toxic species for brain neurons causing Alzheimer's and other neurodegenerative diseases.[1] We recently found that the Arctic mutation of $A\beta_{(1-40)}$ peptide, a mutation causing an early onset (52-57 y. o.) of Alzheimer's disease, gives rise to high levels of well-structured 3.1 nm size oligomers (see Figure 1, right), which are short-lived intermediates for aggregation towards amyloid fibrils.[2] However, cell toxicity and structural studies of oligomers and protofibrils of Aβ using solid-state NMR and microscopy (TEM, STEM and AFM) are challenging, because of the transient nature and structural diversity of oligomers and a high level of polymorphism of protofibrils and amyloid fibrils, usually all coexisting in the same macroscopic sample. Recently, β-sheet-rich oligomers and protofibrils of a model Alzheimer's $A\beta_{(1-42)}$ peptide, $A\beta_{(1-42)}C_{21}C_{30}$, were stabilized by the specific double mutation (A21C and A30C) followed by intramolecular cysteine-cysteine cross-linking.[3] This molecular design of $A\beta_{(1-42)}C_{21}C_{30}$ was based on the spatial proximity of methyl side groups of Ala21 and Ala30 in the β-hairpin structure of monomeric $A\beta_{(1-40)}$ trapped by ZAβ affibodies in aqueous solutions.[4] It is noteworthy that cross-linked $A\beta_{(1-42)}C_{21}C_{30}$ aggregates only to oligomers and protofibrils (with AFM heights of 3.1 nm), shown to exhibit 10^2-10^4 fold higher apoptotic caspase-3/7 activity (neurotoxicity to SH-SY5Y human neuroblastoma cells) compared with $A\beta_{(1-42)}$ and Arctic-$A\beta_{(1-42)}$ amyloid fibrils.[3] We are employing a variety of multi-dimensional ^{13}C-^{13}C and ^{13}C-^{15}N solid-state NMR correlation techniques in addition to $^{15}N\{^{17}O\}$ REAPDOR NMR[5] experiments to obtain important structural constraints in oligomers and protofibrils of cysteine-cysteine cross-linked $A\beta_{(1-42)}C_{21}C_{30}$, ^{13}C,^{15}N and ^{17}O labelled at selective amino acid residues. The 850 MHz NMR spectrometer has proven very useful for these experiments, because of the higher sensitivity and improved resolution in 2D ^{13}C-^{13}C and ^{13}C-^{15}N and, particularly, in $^{15}N\{^{17}O\}$ REAPDOR NMR experiments on amyloid fibrils.[5]

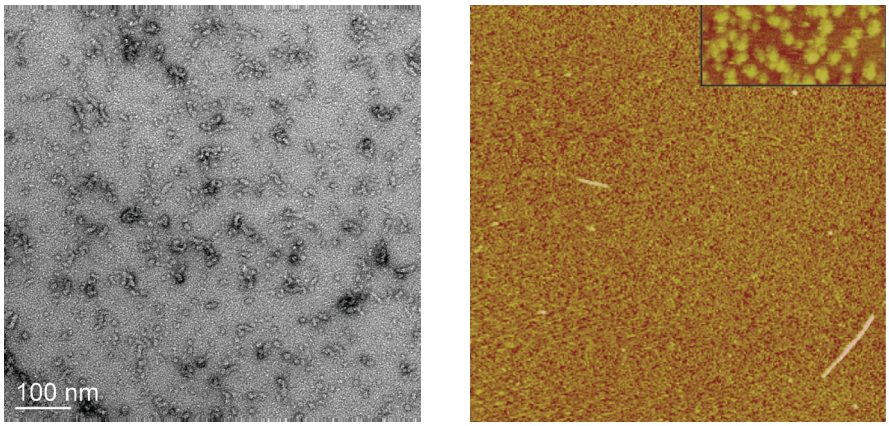

Figure 1. (left) Negatively stained TEM image of oligomers of cysteine-cysteine cross-linked $A\beta_{(1-42)}C_{21}C_{30}$. The peptide was synthesized with U-^{13}C,^{15}N labelling at two amino acid residues, Ile31 and Phe20, to test the intramolecular spatial proximity of side groups in these residues in a putative β-hairpin structural fragment of oligomers near the Cys21-Cys30 cross-linker. The TEM image was obtained by Dr A. A. Sousa, NIH, USA. (right) AFM image of 3.1 nm height oligomers and amyloid fibrils of Arctic-$A\beta_{(1-40)}$.[2] Image size 3200 x 3200 nm (the amplified insert length is 200 nm).

^{13}C-^{13}C DARR NMR Spectra of $A\beta_{(1-42)}C_{21}C_{30}$ Oligomers

A variety of $A\beta_{(1-42)}C_{21}C_{30}$ peptides with selective labelling using U-^{13}C,^{15}N-amino acids (L-Ile, L-Phe, L-Gly, L-Ser, L-Lys, L-Val, L-Asp) and ^{17}O enrichment (L-Gly) were synthesized using Fmoc solid-phase peptide synthesis and purified by HPLC at Luleå University of Technology. $A\beta_{(1-42)}C_{21}C_{30}$ β-sheet oligomers (see Figure 1, left) were prepared following the protocol developed by Sandberg *et al.*[3]

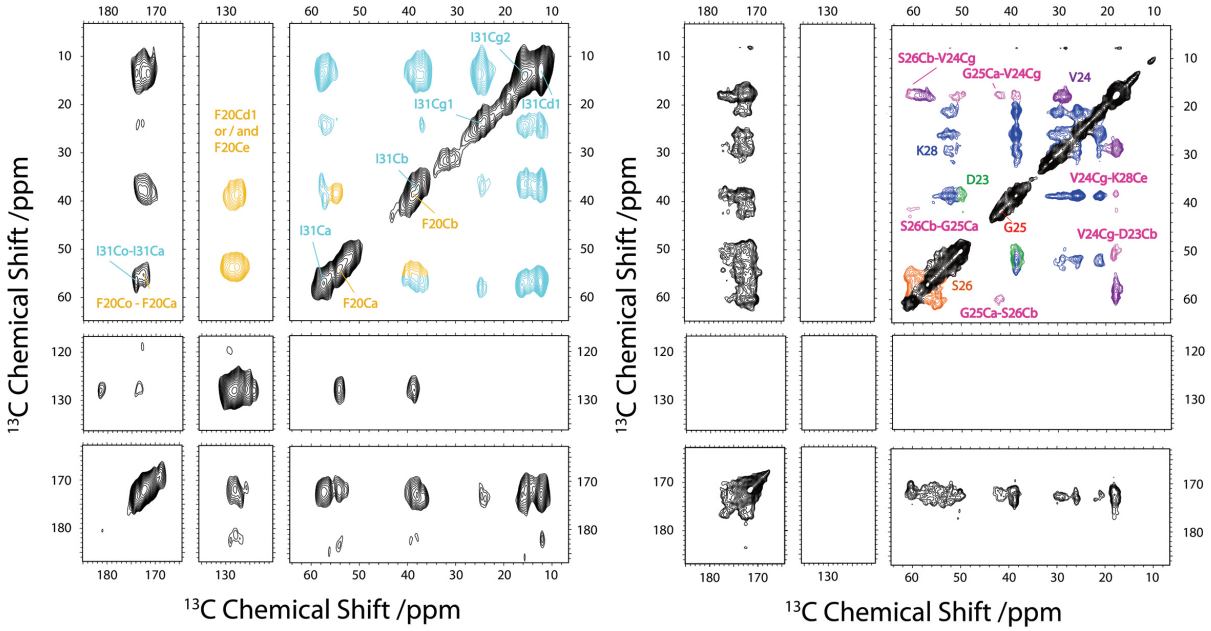

Figure 2. 2D ^{13}C-^{13}C DARR NMR spectra (850 MHz, 2.5 mm MAS probe, dry sample weight 3.5 – 7 mg) of hydrated oligomers of cysteine-cysteine cross-linked [U-^{13}C,^{15}N-I31,F20]-$A\beta_{(1-42)}C_{21}C_{30}$ (left) and [U-^{13}C,^{15}N-D23,V24,G25,S26,K28]-$A\beta_{(1-42)}C_{21}C_{30}$ (right). No inter-residue (Ile31-Phe20) cross-peaks were detected for the first sample, while cross-peaks between carbon sites Cγ and Cε of the side groups of V24 and K28, respectively, in the second sample potentially suggest their spatial proximity. (Experimental conditions for left/right spectra were: 300/400 ms DARR mixing time, 11.5/13 kHz MAS, temperature –15/+20°C, experimental time 23 h).

2D DARR spectra of two samples taken with either 300 or 400 ms mixing time are shown in Figure 2. The detection of DARR V24Cγ-K28Cε cross-peaks together with the Cα and Cβ ^{13}C having chemical shifts characteristic of β-sheet structures in proteins is consistent with a β-hairpin structure in this structural fragment of $A\beta_{(1-42)}C_{21}C_{30}$ oligomers. These data, in addition to structural constraints obtained from 2D ^{13}C-^{13}C and ^{13}C-^{15}N NMR on hydrated oligomers of recombinant cysteine-cysteine cross-linked U-^{13}C,^{15}N-$A\beta_{(1-42)}C_{21}C_{30}$, reveal β-sheet secondary structure features and intermolecular packing in oligomers. The main goal of this project is to obtain a sufficiently large set of structural constraints for unambiguous modelling of the structure of toxic $A\beta_{(1-42)}C_{21}C_{30}$ oligomers to be undertaken.

References

1. Kayed, R.; Head, E.; Thompson, J. L.; McIntire, T. M.; Milton, S. C.; Cotman, C. W.; Glabe, C. G. *Science* **2003**, *300*, 486.
2. Norlin, N.; Hellberg, M.; Filippov, A.; Sousa, A. A.; Gröbner, G.; Leapman, R. D.; Almqvist, N.; Antzutkin, O. N. *J. Struct. Biol.* **2012**, *180*, 174.
3. Sandberg, A.; Luheshi, L. M.; Söllvander, S.; Pereira de Barros, T.; Macao, B.; Knowles, T. P. J.; Biverstål, H.; Lendel, C.; Ekholm-Petterson, F.; Dubnovitsky, A.; Lannfelt, L.; Dobson, C. M.; Härd, T. *Proc. Natl. Acad. Sc. U.S.A.* **2010**, *107*, 15595.
4. Hoyer, W.; Grönwall, C.; Jonsson, A.; Ståhl, S.; Härd, T. *Proc. Natl. Acad. Sc. U.S.A.* **2008**,*105*, 5099.
5. Antzutkin, O. N.; Iuga, D.; Filippov, A. V.; Kelly, R. T.; Becker-Baldus, J.; Brown, S. P.; Dupree, R. *Angew. Chem. Int. Ed.* **2012**, *51*, 10289.

High-Field Solid-State ^{13}C NMR Study of Cu(II)-Based MOFs

Daniel M. Dawson, Russell E. Morris and Sharon E. Ashbrook

School of Chemistry and EaStCHEM, University of St Andrews

Overview

Metal-organic frameworks (MOFs) are microporous materials comprising metal-based units connected by organic "linkers". The large free volume of MOFs may be used for gas storage, catalysis, *etc.* The MOFs themselves can be studied by Bragg diffraction, but this approach is not suitable for frameworks containing disordered or mobile guests. Solid-state NMR is a very sensitive probe of local structure and dynamics, but NMR spectra are complicated by the paramagnetic metal ions present in many MOFs. Here, we build on our previous assignment of the ^{1}H and ^{13}C NMR spectra of the paramagnetic MOFs HKUST-1 and STAM-1,[1] by investigating the temperature dependence of the MOF and guest (H_2O) resonances at 20.0 T.

^{1}H and ^{13}C Variable-Temperature MAS NMR

HKUST-1 contains Cu dimers linked by benzene-1,3,5-tricarboxylate (btc), leading to large (~20 Å) pores. The positions of the ^{1}H and ^{13}C framework resonances have an approximately linear dependence on 1/T (Figure 1), whereas resonances assigned to H_2O display significantly more complicated behaviour, indicative of the formation of an ordered lattice of water molecules within the pores at lower temperature.

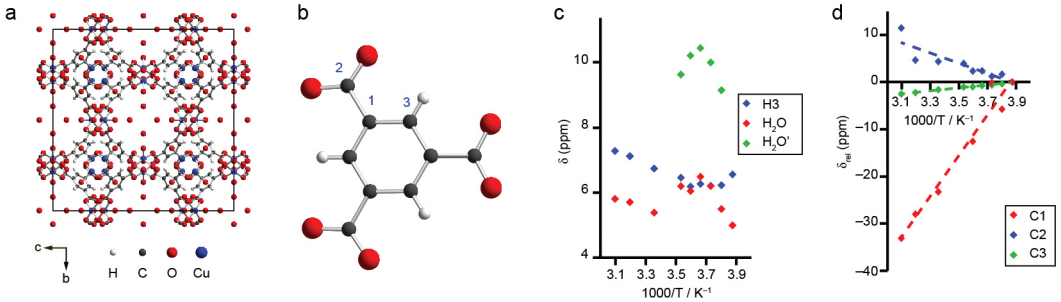

Figure 1. (a) Structure of hydrated HKUST-1 (H atoms of H_2O have not been located). (b) Structure of btc and numbering scheme. Plots of isotropic (c) ^{1}H and (d) ^{13}C shifts as a function of 1/T for HKUST-1. ^{13}C isotropic shifts are reported relative to their values at 258 K.

STAM-1 contains the same dimers as HKUST-1, linked by the methyl ester of btc (mmbtc). The mmbtc leads to the presence of both hydrophobic and hydrophilic pores. In contrast to HKUST-1, there is relatively little temperature dependence observed for any of the ^{1}H or ^{13}C resonances (except C2), indicating a difference in the magnetic behavior of these chemically similar MOFs (Figure 2).

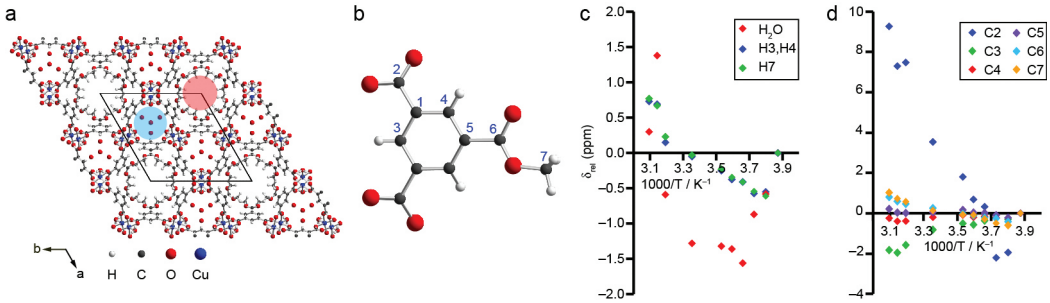

Figure 2. (a) Structure of STAM-1 (H atoms of H_2O have not been located) with hydrophobic and hydrophilic pores coloured pink and blue, respectively. (b) Structure of mmbtc and numbering scheme. Plots of isotropic (c) ^{1}H and (d) ^{13}C shifts as a function of 1/T for STAM-1. ^{1}H and ^{13}C isotropic shifts are reported relative to their values at 258 K.

References

1. Dawson, D. M.; Jamieson, L. E.; Mohideen, M. I. H.; McKinlay, A. C.; Smellie, I. A.; Cadou, R.; Keddie, N. S.; Morris, R. E.; Ashbrook, S. E. *Phys. Chem. Chem. Phys.* **2013**, *15*, 919.

High-Field ^{17}O Solid-State NMR of Ionothermally-Prepared Zeolites

John M. Griffin, Valerie R. Seymour, Russell E. Morris and Sharon E. Ashbrook

School of Chemistry, University of St Andrews

Overview

Microporous materials, including aluminophosphate zeolites (AlPOs) are an important class of material with a variety of industrial applications in catalysis, separation and ion exchange and also in medicine. These solids consist of frameworks that contain pores and channels of molecular dimensions, allowing chemistry to take place at the internal surface of the pores, resulting in a range of interesting properties. Solid-state NMR is a valuable tool for studying the structure of such materials as the basic constituents of the frameworks all have NMR-active isotopes (^{27}Al, ^{31}P and ^{17}O). Whilst ^{27}Al and ^{31}P have been extensively studied, there are comparatively few ^{17}O NMR studies on AlPOs as this nucleus is extremely insensitive owing to its low natural abundance (0.037%) and often large quadrupolar interaction. This is unfortunate as it is the oxygen atoms that line the cavities, and it is at this internal surface that all of the interesting chemistry takes place. We have recently developed a simple, low-cost method for the enrichment in ^{17}O of zeolitic framework materials. Our approach employs the so-called 'ionothermal' synthesis method, which, unlike other synthesis procedures, only uses very small microlitre quantities of water. In this project, we have used ionothermal enrichment to obtain high-quality two-dimensional multiple-quantum (MQ) magic-angle spinning (MAS) NMR and ^{17}O-^{31}P heteronuclear correlation spectra of SIZ-4, a model AlPO with the chabazite topology.

Results

SIZ-4 is an aluminophosphate framework with a structure consisting of double six-membered rings of alternating AlO_4 and PO_4 tetrahedra. We have previously demonstrated that ionothermal synthesis using 35%-^{17}O-enriched H_2O can yield enrichment levels that are sufficient to enable the recording of ^{17}O MAS and double-rotation (DOR) NMR spectra, and a two-dimensional MQMAS NMR spectrum was obtained in 83 hours.[1] Following on from this proof-of-concept work, we have optimised the synthesis procedure further, incorporating 90%-^{17}O-enriched H_2O. As Figure 1a clearly shows, this results in a significant increase in sensitivity, allowing a high-quality ^{17}O MQMAS NMR spectrum to be recorded in only 20 hours. The increased enrichment level also opens up the possibility to perform heteronuclear correlation experiments. A preliminary ^{17}O-^{31}P MAS-J-INEPT correlation spectrum is shown in Figure 1b. This spectrum was recorded in a total experimental time of 12 hours and exhibits correlations between each of the three distinct P sites in the structure and their four directly-bonded O neighbours.

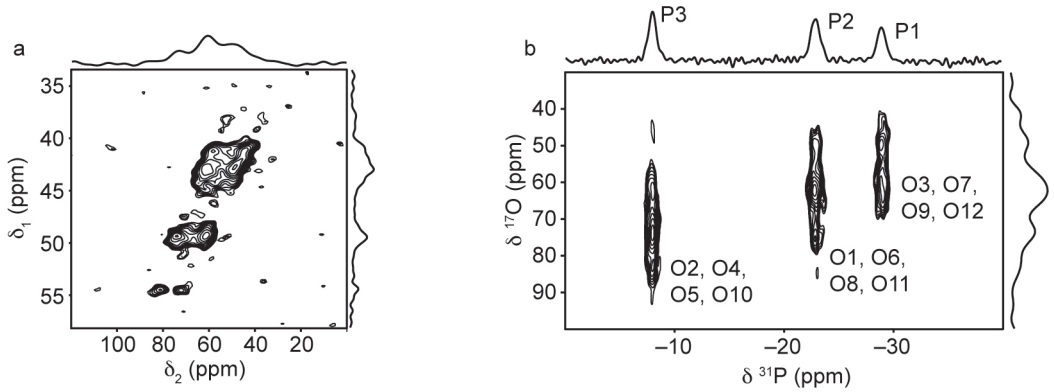

Figure 1. (a) ^{17}O MQMAS NMR and (b) ^{17}O-^{31}P INEPT correlation spectra of ^{17}O-enriched SIZ-4. Experiments were performed at 20.0 T using 80 mg of sample at MAS rates of (a) 14 kHz and (b) 12.5 kHz.

References

1. Griffin, J. M.; Clark, L.; Seymour, V. R.; Aldous, D. W.; Dawson, D. M.; Iuga, D.; Morris, R. E.; Ashbrook, S. E. *Chem. Sci.* **2012**, 3, 2293.

Measuring the ^{31}P CSA of AlPOs Using 2D CSA-Amplified PASS Experiments

Scott Sneddon, Daniel M. Dawson and Sharon E. Ashbrook

School of Chemistry and EaStCHEM, University of St Andrews

Overview

Aluminophosphates[1] (AlPOs) are microporous framework materials that consist of strictly alternating corner-sharing AlO_4 and PO_4 tetrahedra and have a range of potential industrial applications. Solid-state NMR is an excellent probe of local structure and order, and is particularly suited to the study of AlPOs, as the basic components of the framework all have NMR-active nuclei: ^{27}Al, ^{31}P and ^{17}O. ^{31}P is particularly amenable owing to its high receptivity and the high sensitivity of its chemical shift to the local environment. However, in materials with multiple crystallographic sites, spectral assignment can be somewhat challenging, but can be assisted by the measurement of multiple NMR parameters, *e.g.*, the chemical shift anisotropy (CSA), defined in the Herzfeld-Berger convention by the magnitude of the anisotropy, Ω, and its skew, κ.[2] The CSA parameters are usually measured by analytical fitting of spinning sideband patterns obtained from spectra recorded at slow MAS rates. However, this method is challenging in AlPOs, as Ω is typically small, and the slow MAS rates do not always remove interactions such as homo- and heteronuclear dipolar couplings. In addition, in the case of multiple sites, overlapping spinning sideband manifolds can further complicate detailed spectral analysis. The 2D CSA-amplified PASS experiment offers a solution to this problem as the experiment can be performed at higher MAS rates, ω_r, whilst the MAS rate in the indirect dimension is scaled by a factor of ω_r/N_T, where N_T is the total scaling factor.[3]

^{31}P CSAs of As-Prepared and Calcined Aluminophoshates

^{31}P nuclei in as-prepared AlPOs have Ω in the range of 30 to 75 ppm, with higher Ω occasionally observed for a P site with an Al next-nearest neighbour (NNN) with a higher coordination number, *e.g.*, Al^{V} or Al^{VI}. Calcined AlPOs, however, have Ω values much smaller than their as-prepared AlPO counterparts, in the range of 10 to 30 ppm, primarily due to the purely tetrahedral AlPO framework. Using higher field allows more accurate measurement of Ω in calcined AlPOs, owing to the increased chemical shift dispersion (in Hz). Due to the nature of the tetrahedral PO_4 arrangement in as-prepared and calcined AlPOs, it is not possible to correlate any one geometrical parameter, *e.g.*, P-O bond length or Al-O-P bond angle, to Ω.

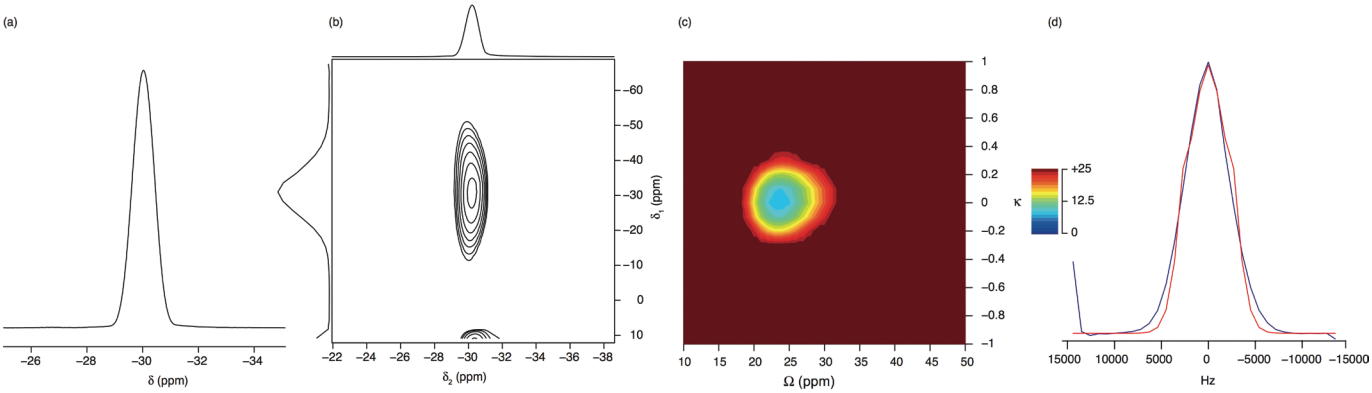

Figure 1: (a) ^{31}P (20.0 T, ω_r = 14 kHz) MAS and (b) ^{31}P (20.0 T, ω_r = 12 kHz, N_T = 13.33) 2D CSA-amplified PASS spectra of calcined SIZ-4. (c) The contour plot of the RMS deviation showing the degree of uncertainty in the Ω and κ from the analytical fit of the extracted sideband manifold in (d).

Figure 1 shows an example of the sideband manifold extracted from the ^{31}P 2D CSA-amplified PASS spectrum of calcined SIZ-4 along with the SIMPSON fit and the contour error plot of the RMS deviation from the analytical fit. The ^{31}P CSA parameters of calcined SIZ-4 are found to be Ω = 23.5 ± 1.5 ppm and κ = 0.0 ± 0.1. To aid interpretation of the ^{31}P MAS and ^{31}P 2D CSA-amplified PASS spectra, NMR parameters were calculated using the periodic planewave DFT CASTEP code.[4] The structures obtained from diffraction were geometry optimised (minimising the forces upon the atoms) with relaxation of the atomic coordinates and lattice parameters. Calculations included Grimme's semi-empirical dispersion correction scheme (G06), to describe the long-range dispersion forces present.[5] For as-prepared AlPOs there is a good agreement between experimental and calculated Ω once the geometry has been optimised, see Figure 2a. For calcined AlPOs, using experimental data acquired at 14.1 T, there is much more scatter in the data and, therefore, less agreement between experimental and calculated Ω, as shown in Figure 2b. However, using experimental data acquired at 20.0 T, there is much better agreement and the scatter in the data is much less, see Figure 2c, and this is due to the more accurate experimental data obtained at high field, owing to the increased magnitude of Ω in Hz.

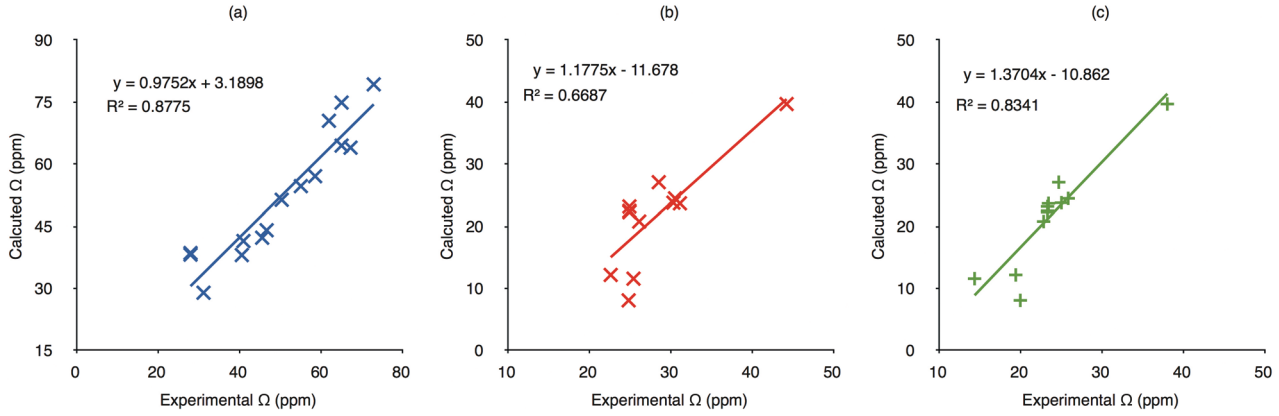

Figure 2: Scatter graphs with a linear regression line fitted to the data. In (a) and (b), calculated vs. experimental Ω acquired at 14.1 T for as-prepared and calcined AlPOs, respectively. In (c), calculated vs. experimental Ω acquired at 20.0 T for calcined AlPOs.

References

1. Wilson, S. T.; Lok, B. M.; Messina, C. A.; Cannan, T. R.; Flanigen, E. M. *J. Am. Chem. Soc.* **1982**, *104,* 1146.
2. Herzfeld, J.; Berger, A. E. *J. Chem. Phys.* **1980**, *73*, 6021.
3. Orr, R. M.; Duer, M. J.; Ashbrook, S. E. *J. Magn. Reson.* **2005**, *174,* 301.
4. Segall, M. D.; Lindan, P. J. D.; Probert, M. J.; Pickard, C. J.; Hasnip, P. J.; Clark, S. J.; Payne, M. C. *J. Phys. Condens. Matter*, **2002**, *14*, 2717.
5. Grimme, S. *J. Comput. Chem.* **2006**, *27*, 1787.

Effects of Fast MAS on ^{13}C Resolution in Membranes – Mersacidin/Lipid II complexes

Judicaël Parisot,[1] Dinu Iuga,[2] David C. Griffin,[1] Gabrielle Bierbaum,[3] Hans-Georg Sahl[3] and Boyan B. Bonev[1]

[1]*School of Biomedical Sciences, University of Nottingham*

[2]*Department of Physics, University of Warwick*

[3]*Institute of Medical Microbiology, University of Bonn, Germany*

Overview

The overall objective of this project is to investigate the antibiotic/target interactions between class B lanthionine antibiotic mersacidin and its molecular target, lipid II. To pursue this we prepared uniformly ^{13}C,^{15}N-labelled mersacidin and ^{13}C,^{15}N-labelled lipid II, which were combined to form molecular complexes, embedded in model lipid membranes of unlabelled phosphatidylcholine/phosphatidylglycerol. The antibiotic/target membranes were then studied by ^{13}C Proton Driven Spin Diffusion in the frozen state. Biological membrane systems typically contain a large number of nuclear species, organised in spectral groups characterised by fairly close chemical shifts. A clear advantage to this was the use of high chemical shift dispersion, offered by the high field of the UK 850 MHz solid state NMR facility.

Effects of MAS on ^{13}C – ^{13}C PDSD spectral resolution

During previous experiments we observed spectra of high resolution and superb quality. Subsequent to experimentation at temperatures between 0 and –60°C and MAS frequencies between 10 and 60 kHz, we observed significant deterioration in spectral resolution (Figure 1), which could not be explained by chemical and compositional degradation of the samples. We hypothesised that the increase in resonance line width is chiefly the result of inhomogeneities in the membrane sample, which arose through sample dehydration and fractional sedimentation under very high centripetal forces within the MAS rotor. Since application of fast MAS NMR to biological studies represent a novel and important field in modern biology, it was considered prudent to investigate the origins of the line broadening we observed during experimentation.

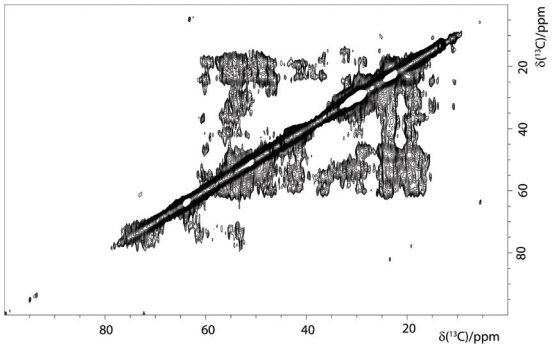

Figure 1: PDSD spectrum from samples after extended fast MAS studies in the 850 MHz spectrometer.

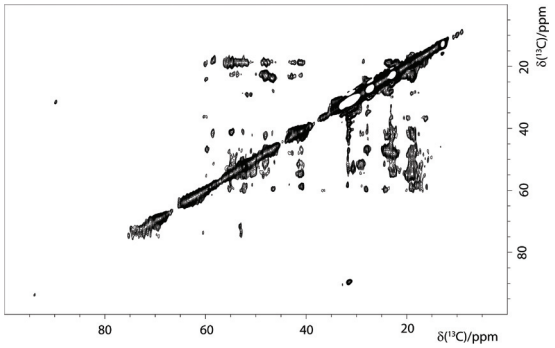

Figure 2: PDSD spectrum from re-processed samples.

Mersacidin/lipid II samples, which gave rise to the ^{13}C PDSD spectrum of Figure 1 were lyophilised and rehydrated. This allowed us to restore the original state of the system to unilamellar vesicles, which were loaded into the MAS rotors and studied under 12.5 kHz MAS at a slightly higher temperature of –40°C.

Observations

Spectral resolution in the reconstituted sample was significantly enhanced (Figure 2). We were able to conclude that sample monodispersity is essential to the acquisition of high resolution spectra. In addition, we noticed at the higher temperature of –40°C the loss of some spectral features by comparison to –60°C, particularly those involving methyl groups. This suggests the presence of residual mobility at the higher temperature.

In summary, the behaviour of membrane systems under fast MAS, even below the water freezing point, is complex and requires a systematic analysis to create methodology for reliable and reproducible structural analysis of protein and peptide systems in hydrated lipid bilayers membrane models.

What is the Detection Limit of a Minority Solid-State Form of a Pharmaceutical by ^{1}H Double-Quantum MAS NMR?

Keisuke Maruyoshi,[1,2] Dinu Iuga[1] and Steven P. Brown[1]

[1]*Department of Physics, University of Warwick*
[2]*Daiichi Sankyo Co. Ltd., Kanagawa, Japan*

Overview

^{1}H double-quantum (DQ) 2D solid-state NMR spectra constitute "fingerprints" and can be used to distinguish different solid-state forms, e.g., the anydrate and hydrate forms of an active pharmaceutical ingredient.[1,2] We investigate here the lower detection limit of a minority amount of cimetidine (polymorphic form A) in a physical mixture with its HCl salt by ^{1}H DQ MAS NMR at 850 MHz.

^{1}H DQ MAS Spectra

Figure 1 shows that the detection limit using ^{1}H (850 MHz) DQ MAS at 30 kHz MAS (~10 mg of sample) is approximately 1% for a physical mixture of the free and salt form of cimetidine.

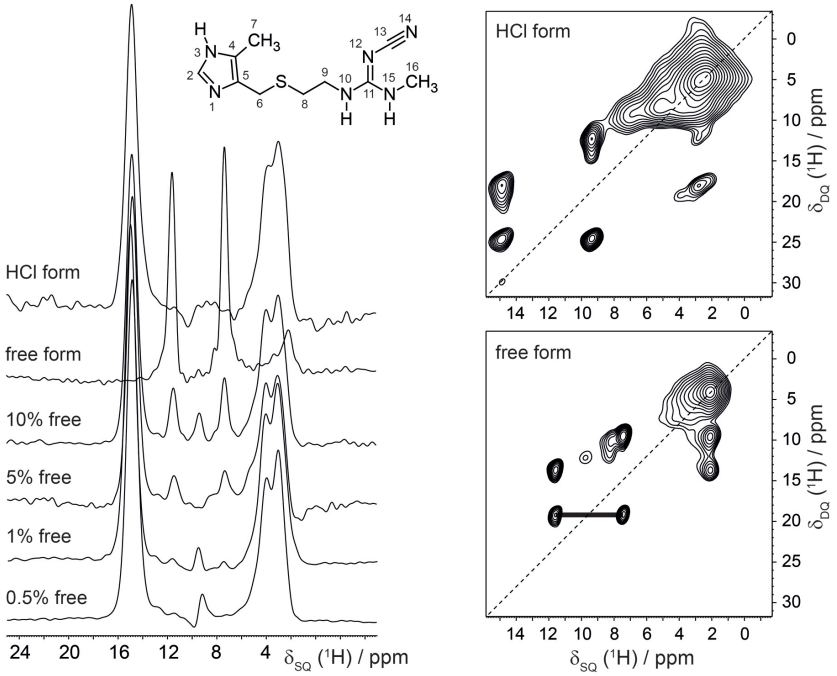

Figure 1. Right: ^{1}H DQ MAS (850 MHz, 30 kHz MAS) spectra of the HCl salt (top) and free (bottom) solid-state forms of cimetidine. Left: Rows extracted from ^{1}H DQ MAS spectra of different mixtures of the free and salt forms at the ^{1}H DQ frequency of 19.0 ppm, corresponding to the 7.4 + 11.6 ppm pair of ^{1}H DQ cross peaks for the free form.

References

1. Griffin, J. M.; Martin, D. R.; Brown, S. P. *Angew. Chem. Int. Ed. Engl.* **2007**, *46*, 8036.
2. Brown, S. P. *Solid State Nucl. Magn. Reson.* **2012**, *41*, 1.

Probing Intra- and Intermolecular Proximities: ^{14}N-^{1}H Correlation Spectra

Andrew Tatton,[1] Keisuke Maruyoshi,[1,2] Dinu Iuga,[1] Oleg N. Antzutkin,[1,3] Amjad Alhalaweh,[4] Sitaram P. Velaga[4] and Steven P. Brown[1]

[1]*Department of Physics, University of Warwick*

[2]*Daiichi Sankyo Co. Ltd., Kanagawa, Japan*

[3]*Chemistry of Interfaces, Luleå University of Technology, Sweden*

[4]*Department of Health Science, Luleå University of Technology, Sweden*

Overview

^{14}N-^{1}H solid-state NMR experiments offer the opportunity to probe N-H correlations for organic solids without recourse to isotopic labelling.[1,2] Brown and co-workers have recently shown, for the case of a synthetic guanosine derivative and a pharmaceutical molecule, how ^{14}N-^{1}H spectra identify N...H contacts across intermolecular hydrogen bonds.[3,4] We show here further applications of the ^{14}N-^{1}H method to a depeptide[5] and a co-crystal.[6] ^{14}N-^{1}H experiments were recorded using a HMQC pulse sequence with R^3 recoupling of the ^{14}N-^{1}H dipolar coupling,[1] employing the UK 850 MHz solid-state NMR facility's 1.3 mm probe that allows MAS at 60 kHz and a ^{14}N nutation frequency of 120 kHz.

^{14}N-^{1}H Spectra

Figure 1 illustrates how NH cross peak intensity builds up as a function of the R^3 recoupling time for the dipeptide β-AspAla.[5] For the shortest recoupling time (top row, τ_{RCPL} = 67 μs), only one-bond NH correlation peaks are observed for the NH and NH_3 moieties. For longer recoupling times (middle and bottom row, τ_{RCPL} = 333 & 500 μs), longer-range NH correlation peaks are additionally observed, e.g., to the neighbouring Cα proton as well as an intermolecular proximity between the NH_3 and COOH protons.

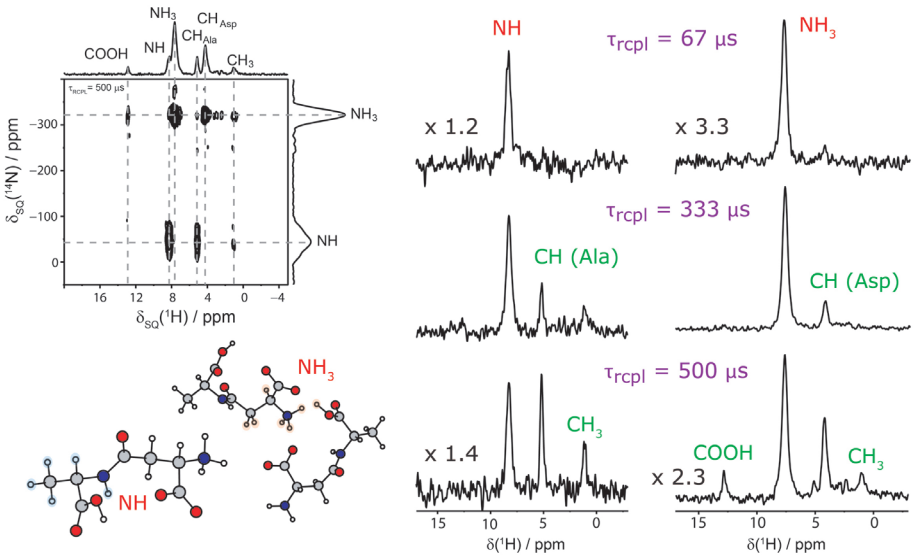

Figure 1. The build-up of peak intensity in ^{14}N-^{1}H HMQC (850 MHz, 60 kHz MAS) spectra of the dipeptide β-AspAla for experiments performed using n = 2 rotary resonance (R^3) recoupling of ^{14}N-^{1}H heteronuclear dipolar couplings.[5] Top left: a 2D spectrum recorded with τ_{RCPL} = 500 μs. Bottom left: representations of the crystal structure showing the seven nearest protons around the NH and NH_3 nitrogen atoms. Right: rows extracted at the NH and NH_3 resonances for spectra with increasing τ_{RCPL}.

Figure 2 presents ^{14}N-^{1}H spectra of a co-crystal formed between indomethacin (IND) and nicotinamide (NIC).[6] In the top spectrum, for a short τ_{RCPL} = 133 μs, NH peaks are only observed for the one-bond connectivity of the NIC NH_2 nitrogen to the two hydrogen atoms that have different ^{1}H chemical shifts. For the bottom spectrum corresponding to a long τ_{RCPL} = 667 μs, of particular note is the peak corresponding to an intermolecular proximity between the non-protonated nitrogen of NIC and the carboxylic acid proton of IND that proves an intimate molecular level mixing of the two constituents of the co-crystal as well as identifying the specific mode of intermolecular hydrogen bonding.

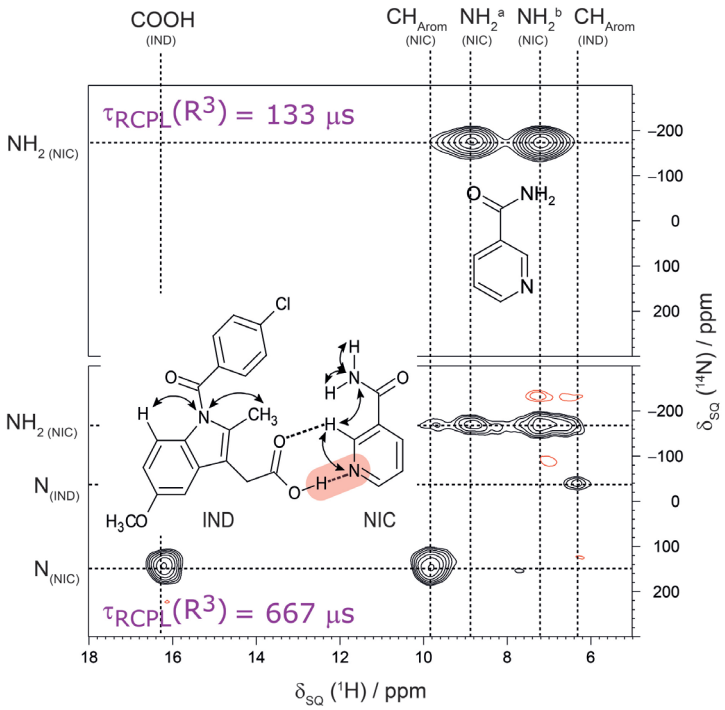

Figure 2. ^{14}N-^{1}H HMQC (850 MHz, 60 kHz MAS) spectra of an indomethacin-nicotinamide (IND-NIC) co-crystal, recorded using n = 2 R^3 durations of 133 (top) and (bottom) 667 μs.[6]

References

1. Gan, Z. H.; Amoureux, J. P.; Trebosc, J. *Chem. Phys. Lett.* **2007**, *435*, 163.
2. Cavadini, S.; Abraham, A.; Bodenhausen, G. *Chem. Phys. Lett.* **2007**, *445*, 1.
3. Webber, A. L.; Masiero, S.; Pieraccini, S.; Burley, J. C.; Tatton, A. S.; Iuga, D.; Pham, T. N.; Spada G. P.; Brown, S. P. *J. Am. Chem. Soc.* **2011**, *133*, 19777.
4. Tatton, A. S.; Pham, T. N.; Vogt, F. G.; Iuga, D.; Edwards, A. J.; Brown, S. P. *CrystEngComm* **2012**, *14*, 2654.
5. Tatton, A. S.; Bradley, J. P.; Iuga, D.; Brown, S. P. *Z. Phys. Chem.* **2012**, *226*, 1187.
6. Maruyoshi, K. ; Iuga, D.; Antzutkin, O. N.; Alhalaweh, A.; Velaga, S. P.; Brown, S. P. *Chem. Commun.* **2012**, *48*, 10844.

^{17}O NMR of Bone and Biomimetic Materials

Sharon E. Ashbrook,[1] Erika Davies,[2] Melinda J. Duer[2] and David G. Reid[2]

[1]*School of Chemistry and EaStCHEM, University of St Andrews*

[2]*Department of Chemistry, University of Cambridge*

Overview

Bone is a complex organic-inorganic composite, consisting primarily of a protein network (collagen type I) into which nanocrystalline mineral platelets deposit. Bone mineral forms in tube-like spaces in the collagen matrix of order 50 nm in diameter. Thus, the process of mineral formation is intriguing because it effectively occurs in a closed vessel and begins with the relatively disordered aqueous component ions of the mineral phase and results in a much more ordered solid phase. The process is thus accompanied by a significant decrease in entropy, which must be compensated for by (at least) an equivalent entropy change elsewhere. The collagen matrix, i.e., the wall of the mineralisation vessel, is the primary component in thermal contact with the mineral phase, so it is this component which must gain entropy, i.e., become more disordered. However, the collagen matrix is previously ordered in such a way that cells and the rest of the extracellular matrix can interact with it optimally, so the extent to which it is disordered by mineralisation occurring around it must be carefully controlled. Our hypothesis is that the extent of ordering in the mineral phase (and thus the extent of disordering of the collagen matrix by mineralisation) is controlled by the incorporation of species into the mineral phase which prevent completely ordered structures from forming, in particular, species which lack symmetry and which can be incorporated in a variety of ways into the mineral structure.

While the mineral phase in bone can be described as a non-stoichiometric carbonatoapatite, it contains an abundance of both hydrogen phosphate and strongly-bound water, neither of which are present in a apatite structure. Previous solid-state NMR work by us and others has demonstrated that the hydrogen phosphate and water species occur in a layer around an apatitic structure. Octacalcium phosphate (OCP) has a layered structure in which apatitic layers alternate with hydrated layers containing hydrogen phosphate and for this reason, has been proposed as a possible model for at least some regions of bone mineral.

We further suggest that OCP is a useful model of bone mineral, not only in describing the hydrated layers of this material, but because of its ability to incorporate other species into its hydrated layer, species which may confer intrinsic disorder into the mineral phase. Thus we have been investigating the range of structures available to OCP double salts. In all cases, the materials are not amenable to structure determination via conventional diffraction methods, so we have been exploring their structures via a combination of first-principles electronic structure calculations, solid-state NMR and powder X-ray diffraction.

New Insights from ^{17}O NMR at 850 MHz

Density functional theory (DFT) calculations performed using CASTEP[1,2] for the published crystal structure of OCP yields NMR parameters for ^{1}H, ^{31}P and ^{17}O that are wildly inconsistent with experiment. Accordingly, we optimised the published structure of OCP[3] until a structure which gave NMR parameters and a powder X-ray diffraction pattern in good agreement with the experiment was obtained (Figure 1) which led to the publication in ref 4. Key is the fact that in our new structure, the hydrated layer is held together by an extensive hydrogen-bonding network not present in the original structure. Incorporation of ions within the hydrated layer will disrupt this and thus destabilise the structure unless the incorporated ion can bridge across the hydrated layer; hence only complex ions capable of coordinating to calcium ions either side of the hydrated layer are likely to be incorporated successfully.

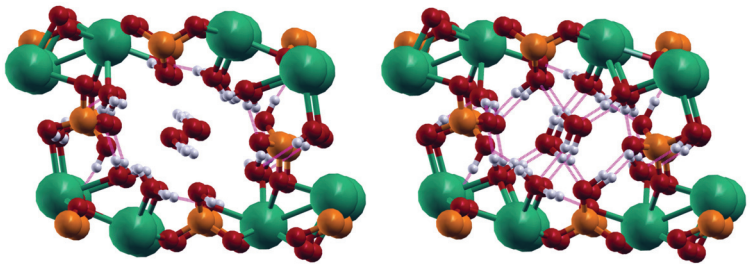

Figure 1. Left: the original published structure for the hydrated layer in OCP[3]. Right the optimised structure of the OCP hydrated layer found in this work[4]. Dotted pink lines indicate strong or medium-strength hydrogen bonds

We have previously shown (see Annual Report 2011) that the OCP-citrate double salt gives a ^{17}O NMR spectrum in close agreement to that of bone mineral in intact bone. Further investigations with other OCP and hydroxyapatite (HA) composites showed that OCP-citrate is the most bone mineral-like in terms of its ^{17}O NMR spectrum (Figure 2).

Accordingly, we have concentrated most recently on deriving a model structure for this double salt using the OCP structure as a starting point, introducing a single citrate ion into the hydrated region of the unit cell and allowing the structure to relax. To date, we have determined nine similar energy structures for this material (an example is shown in Figure 2) which give NMR parameters that are consistent with the (relatively broad) experimental NMR signals and powder X-ray diffraction pattern. The nine structures all appear quite different with the citrate coordinated via various of its three COOH groups and hydroxyl group to different calcium ions in the unit cell and hydrogen bonded in a range of patterns to water and hydrogen phosphates.

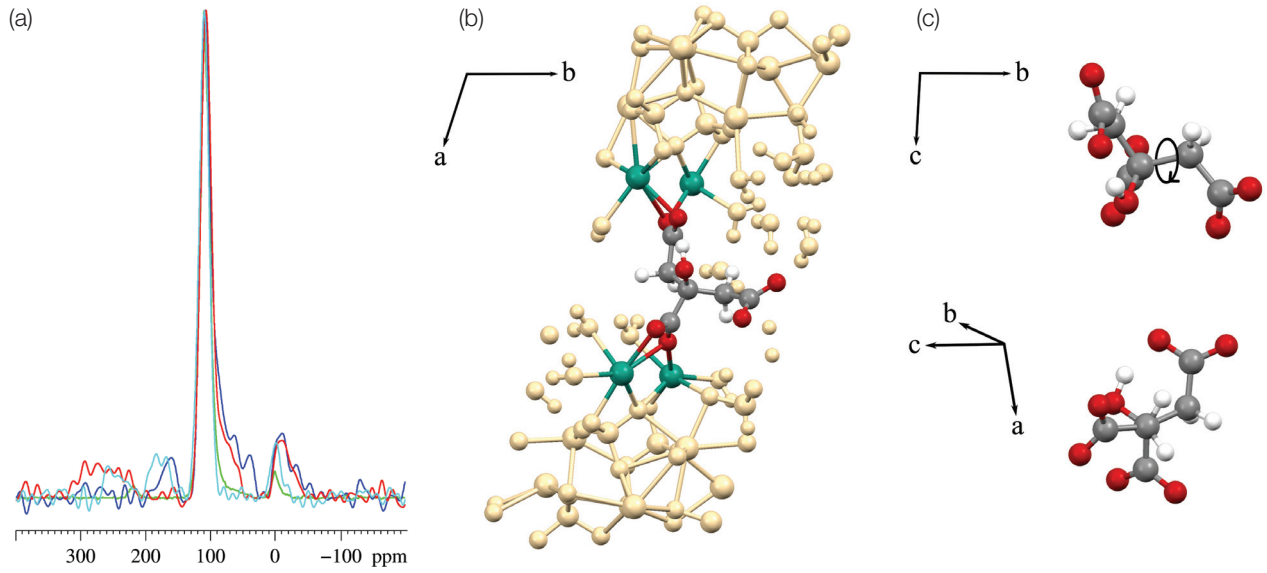

Figure 2. (a) ^{17}O double-frequency sweep (DFS) spectra of (fresh) sheep bone (blue, 69,632 transients), OCP-CIT (red, 67,390 transients), 5% ^{17}O -enriched hydroxyapatite (green, 18,432 transients) and bone mineral soaked in citric acid (cyan, 58,392 transients). (b) one of the models of the OCP-citrate structure produced in this work. The OCP structure is shown in cream except for the calcium ions involved in coordinating to the citrate ion (shown in full colour). (c) Top: The citrate ion in the structure viewed from above, showing that the C_{quat}-CH_2 bond of the 'dangling' branch of the citrate ion can exist in different rotational conformations, giving disorder in the structure. Bottom: The citrate molecule viewed along this C_{quat}-CH_2 bond, showing the staggered arrangement of the methylene C-H bonds.

Summary

Bone contains 1 – 2% by weight of citrate and our work suggests that it may provide an essential source of entropy in the mineral structure, preventing a completely ordered mineral structure from forming. A completely ordered mineral structure would be mechanically brittle, and therefore unsuitable in a material that must have some flexibility to function. Moreover as described here, the more ordered the mineral structure, the more disordered the surrounding organic matrix in bone must become, to the detriment of the biological functioning of that matrix. Crucial in this work has been the determination of plausible structures for the OCP-citrate composite material that models bone mineral. Crystals of the OCP-citrate double salt are too small for conventional diffraction techniques to be useful; moreover, our whole interest in this material is its intrinsic disorder, which diffraction methods do not describe well. Our approach to structure determination has been the combined use of solid-state NMR and first-principles electronic structure calculations and for this to yield unambiguous results, NMR parameters from as many nuclear species in the structure as possible are needed; oxygen is the most abundant species in bone mineral and ^{17}O NMR, requiring the use of high magnetic fields, is therefore essential to this work.

References

1. Clark, S. J.; Segall, M. D.; Pickard, C. J.; Hasnip, P. J.; Probert, M. I.; Refson, K.; Payne, M. C. *Z. Kristallogr.* **2005**, *220*, 567.
2. Pickard, C.; Mauri, F. *Phys. Rev. B* **2001**, *63*, 1.
3. Mathew, M.; Brown, W. E.; Schroeder, L. W.; Dickens, B. *J. Cryst. Spectrosc. Res.* **1988**, *18*, 235.
4. Davies, E.; Duer, M. J.; Ashbrook, S. E.; Griffin, J. M. *J. Am. Chem. Soc.* **2012**, *134*, 12508.

2D and 3D ^{13}C NMR Studies of Whole Plant Stems

Paul Dupree,[1] Jennifer C. Mortimer,[1] Steven P. Brown[2] and Ray Dupree[2]

[1]*Department of Biochemistry, University of Cambridge*
[2]*Department of Physics, University of Warwick*

Overview

A major technological challenge in using plant biomass for renewable energy is to release the sugars from cellulose and other polysaccharides effectively and cheaply. Pilot biofuel production processes involve the use of energy-intensive harsh biomass pretreatments, and also requires the addition of high quantities of enzymes to break down the biomass. Progress in improving these steps is restrained by the limited understanding of the molecular basis of plant cell wall 'recalcitrance' - the difficulty in deconstructing lignocellulose into fermentable sugars. The main carbohydrate components in the cell walls are xylan, a polymer of 5-carbon xylose, and cellulose, a polymer of 6-carbon glucose. The molecular arrangement of these in secondary plant cell walls (woody materials) is poorly understood. Whilst ^{13}C NMR should be a good probe of the local environment, almost all NMR experiments on plants have necessarily been 1D so that there is considerable overlap of signals from the different components which makes it very difficult to fully interpret the spectrum. Recently Dick-Perez et al.[1] used enriched ^{13}C to study the *primary* cell walls of plants germinated and grown in the dark in a liquid culture with uniformly ^{13}C labelled glucose as the carbon source. Whole seedlings including roots were powdered and had extensive chemical treatment before NMR. Our aim is to study the *secondary* cell walls important for bioenergy and we have grown *Arabidopsis* plants in air enriched with $^{13}CO_2$ as the carbon source. The stems of these plants were inserted into MAS rotors with minimal pre-treatment and no chemical treatment or ball milling. Experiments at 500 MHz showed that the enrichment (although only ~ 25%) was sufficient to allow 2D ^{13}C -^{13}C experiments to be undertaken and time was requested at 850 MHz to allow investigation of the possible resolution obtainable in 3D ^{13}C - ^{13}C - ^{13}C experiments.

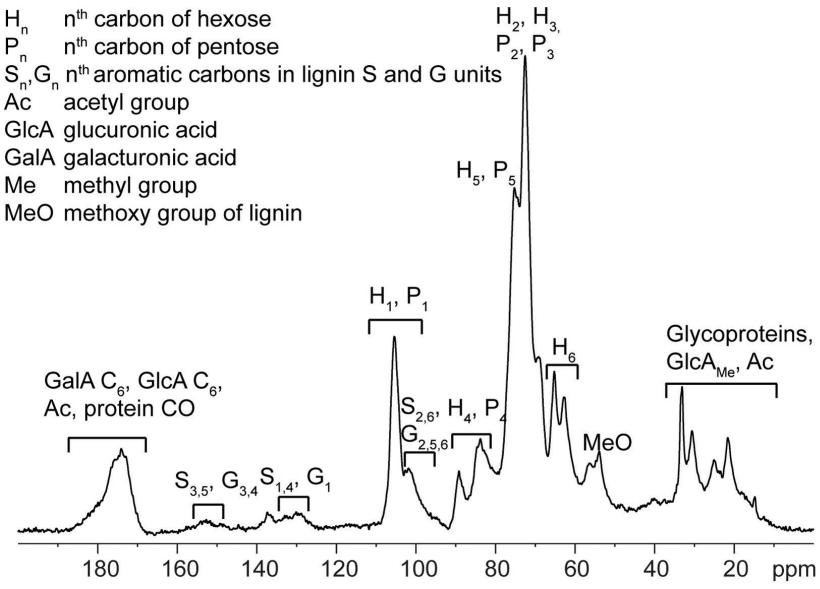

Figure 1. 1D ^{13}C CP MAS spectrum of WT Arabidopsis stems, illustrating the overlapping signals from the many cell wall components. Assignments based on the literature.

Results

The spectra were acquired in a 4 mm MAS probe as the samples were already packed for lower field measurements. A 1D ^{13}C spectrum of WT *Arabidopsis* is shown in Figure 1 where the many overlapping peaks from xylose and cellulose are seen as well as peaks from lignin (assignments based on literature). In a 3D ^{13}C - ^{13}C - ^{13}C DARR experiment there are two mixing times t_{m1} and t_{m2} and, as there was sufficient time for only one 3D experiment on this partially enriched sample, it was decided to have t_{m1} short, 10 ms, and t_{m2} long, 300 ms. This combination should allow the observation of both intermolecular and intramolecular peaks.[2] Figure 2 shows the sugar ring region for some selected planes from the 3D spectrum together with a tentative assignment.

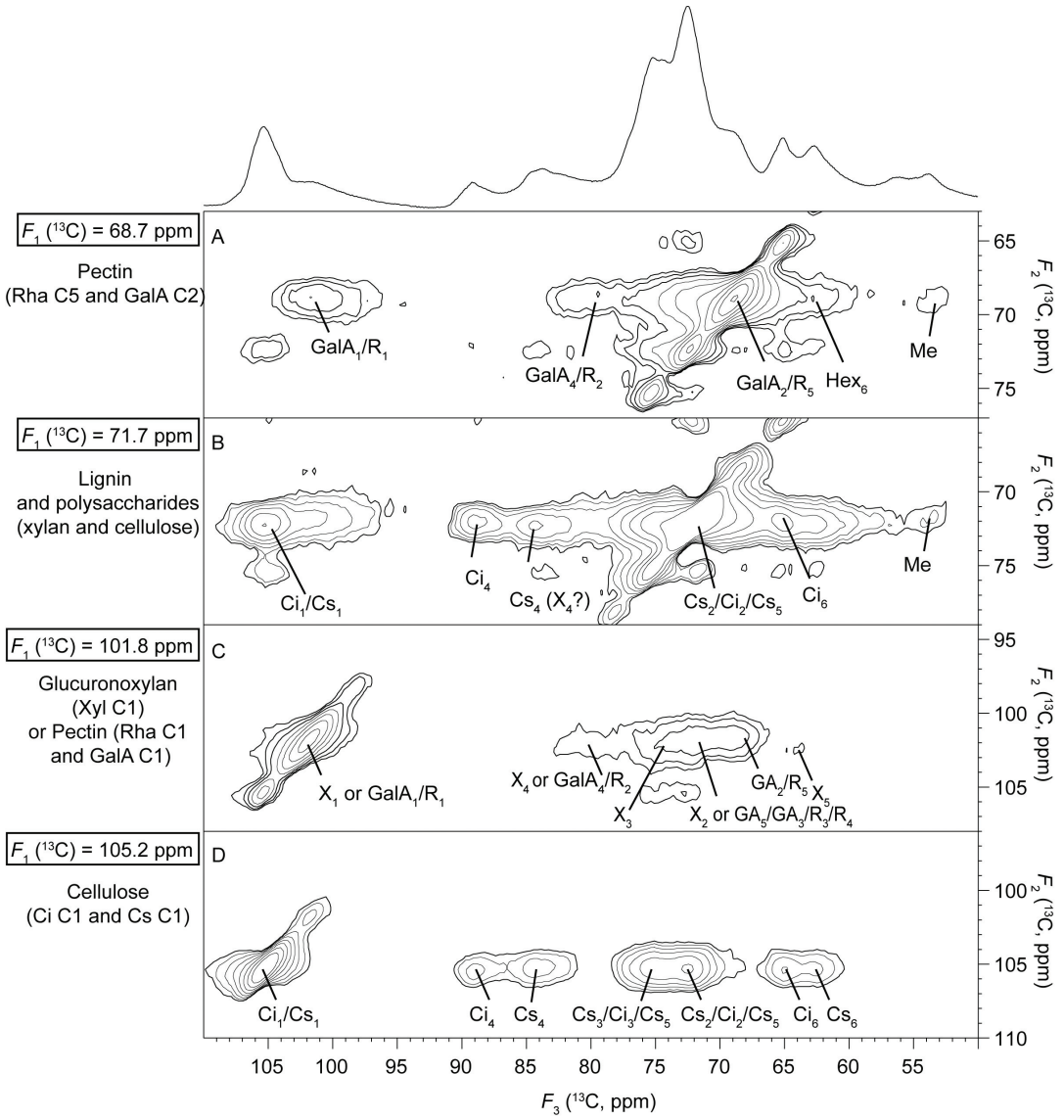

Figure 2. The sugar region of selected planes for a 3D ^{13}C-^{13}C-^{13}C DARR mixing experiment of WT Arabidopsis stems with spin diffusion mixing times of 10 ms and 300 ms. A 1D spectrum is shown above. Tentative assignments are given. GalA, galacturonic acid; R, rhamnose; Hex, unknown hexose; Me, methyl group; Ci, interior cellulose; Cs, surface cellulose; X, xylose.

The resolution is clearly greatly enhanced, for instance the cellulose signals, both interior, Ci, and surface, Cs, can confidently be assigned (see the F_1 = 105.2 ppm plane) and xylose (not previously resolvable from cellulose) (F_1 = 101.8 ppm plane) connections clearly seen. In addition, the long mixing time has revealed cross peaks between polysaccharides and non-cellulosic cell wall components (primarily the phenolic polymer lignin). These initial results clearly demonstrate the promise of multidimensional ^{13}C NMR for investigating plant biomass and further work is currently underway to improve the ^{13}C enrichment. This new plant material will allow collection of still better quality data allowing, in combination with the data already collected, more complete assignment of the secondary cell wall spectrum.

References

1. Dick-Perez, M.*;* Zhang, Y.; Hayes, J.; Salazar, A., Zabotina, O. A.; Hong, M. *Biochemistry* **2011,** *50* 989.
2. Li, S.; Zhang, Y.; Hong, M. *J. Magn. Reson.* **2010**, *202*, 203.

Double Rotation (DOR) NMR and Dipolar Coupling between Quadrupolar ^{11}B Nuclei in Crystalline Borates

Ray Dupree, Diane Holland and Oliver L. G. Alderman

Department of Physics, University of Warwick

Overview

We have a programme of work investigating the superstructural units in borate crystals. These are single or fused rings, containing 3-coordinated, B(III), and 4-coordinated, B(IV), boron atoms which give rise to unusually extensive medium-range order in boron-containing glasses – of considerable interest to glass structure modelling. As an aide in assigning the spectra, we are particularly interested in the way in which magnetisation is exchanged between the quadrupolar ^{11}B nuclei within these units and specifically under double rotation (DOR) acquisition. Experiments have been conducted during 2012 to assess various methods of improving the resolution of the magnetisation exchange within the B(III) and B(IV) manifolds such as isotope dilution. Further data were obtained on the single-quantum, spin-diffusion (SD) build-up curves of CsB_3O_5 and $K_2B_4O_7$.

Use of DOR ^{11}B NMR to reveal dipolar couplings between similar sites in borates

SD DOR spectra of CsB_3O_5 were obtained for various mixing times, τ_{mix}, at 1350 Hz outer rotor spinning frequency, ν_r, to give information on the build up of the signal, and hence the dipole coupling, and to compare with data obtained at a ν_r of 1550 Hz (Figure 1). At 1350 Hz, the B3-B1 build-up rate is enhanced by 3rd order rotational resonance ($\Delta\delta$ = 4050 Hz ≈ 3 ν_r). The rate of build-up is also complicated by the direction of the various EFGs relative to the dipole interaction and the presence of multiple boron contacts.

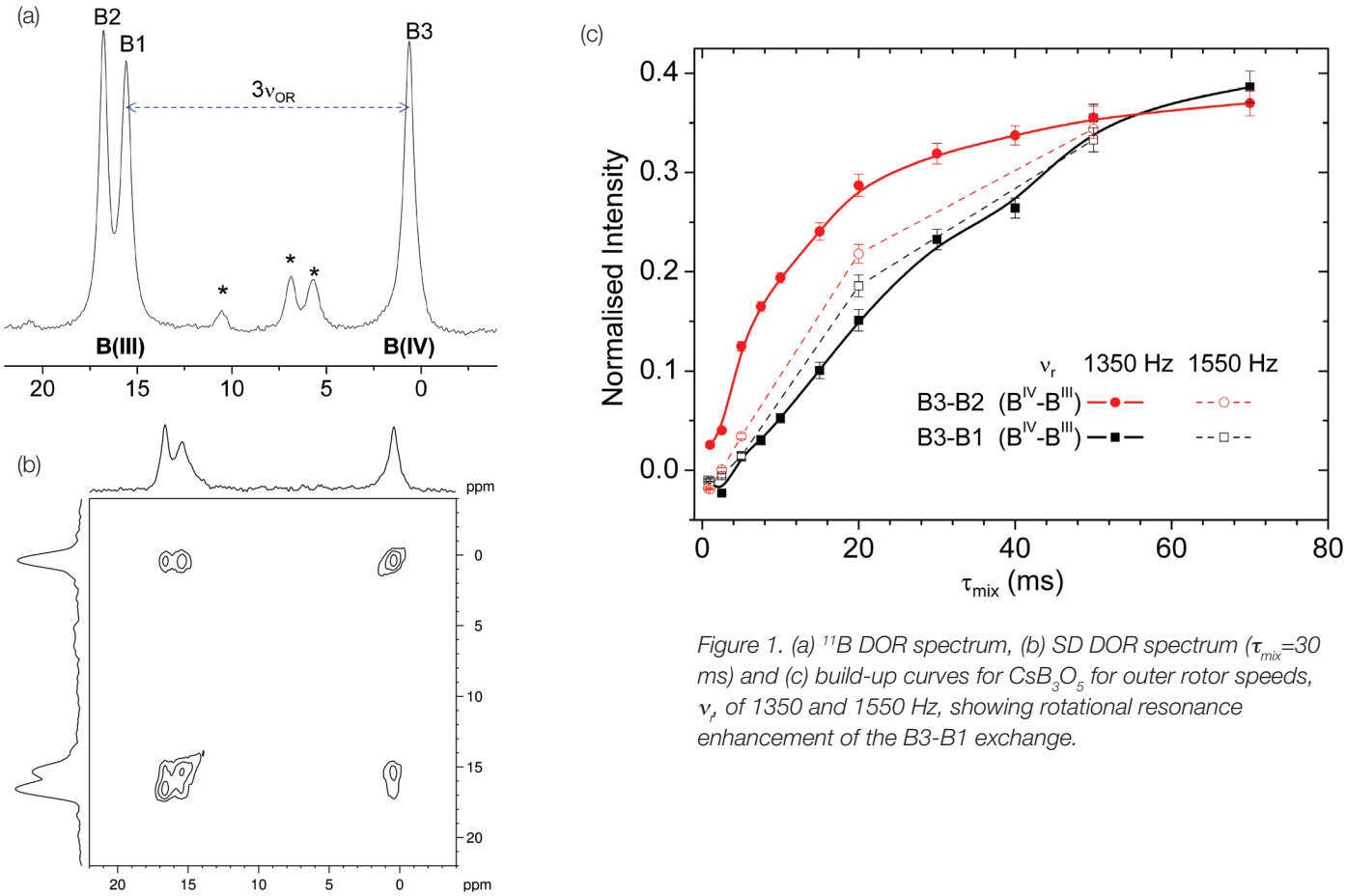

Figure 1. (a) ^{11}B DOR spectrum, (b) SD DOR spectrum (τ_{mix}=30 ms) and (c) build-up curves for CsB_3O_5 for outer rotor speeds, ν_r, of 1350 and 1550 Hz, showing rotational resonance enhancement of the B3-B1 exchange.

To reduce the complexity of dipolar coupling between more than two boron nuclei, samples were prepared which were isotopically diluted to 25% ^{11}B. Statistically, this should reduce the number of ^{11}B with two or more ^{11}B neighbours to ≤ 20% leaving approximately 42% with only one ^{11}B neighbour with which to exchange magnetisation. It does not however prevent the complication of inter-ring rather than intra-ring interactions between boron nuclei in a given superstructural unit and the low level of ^{11}B -^{11}B connections means that S/N is significantly reduced in a spin-diffusion experiment.

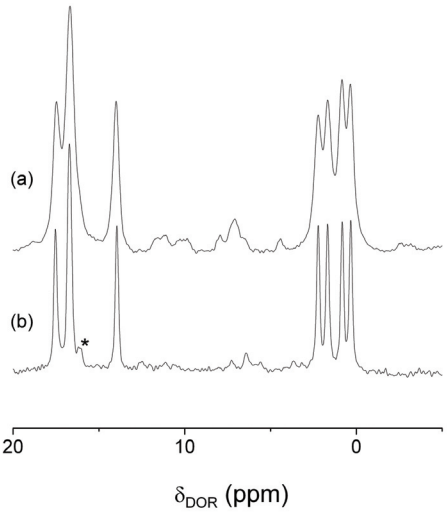

Figure 2. ^{11}B DOR NMR spectra from $K_2B_4O_7$: (a) 99.95% ^{11}B; (b) 25% ^{11}B.

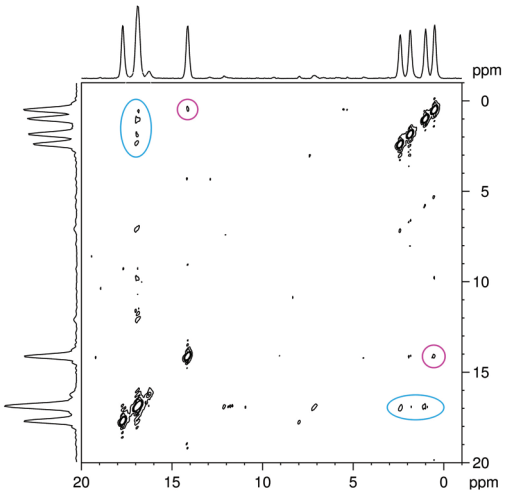

Figure 3. SD DOR spectrum from isotopically dilute (25% ^{11}B) $K_2B_4O_7$ with a 40 ms mixing time.

Figure 2 shows the dramatic effect of isotopic dilution on the resolution of the DOR spectrum from $K_2B_4O_7$ which has 4 B(IV) lines within 2 ppm. The linewidths are ~ 0.15 ppm which is, to the best of our knowledge, the narrowest yet observed for a quadrupolar nucleus at a site with a significant electric field gradient. Thus peaks separated by only 0.5 ppm can now be fully resolved, which gives the possibility that cross peaks in a SD experiment arising from exchange within the B(III) or B(IV) manifold could now be clearly separated from the on-diagonal, self-correlation peaks. However the T_1 is rather long, being > 1800 s for this 25% ^{11}B $K_2B_4O_7$ sample. Attempts to reduce T_1 were made by introducing 0.1 and 0.2 mol% MnO into the isotopically dilute samples and the 0.1% addition reduced T_1 to ~ 450 s. Addition of further MnO begins to compromise resolution due to paramagnetic broadening. This long T_1 makes 2D experiments rather time-consuming – particularly since the signal now dies away very slowly in the t_1 direction and thus many slices are required to take full advantage of the increased resolution.

Figure 3 shows the results of a SD experiment with mixing time of 40 ms. Both positive and negative B(III)-B(IV) cross-peaks are apparently present between the B(III) at ~ 17 ppm and the B(IV) peaks and also possibly between the 13 ppm B(III) peak and the B(IV) peak at 0.5 ppm. However, no B(III)-B(III) or B(IV)-B(IV) cross-peaks (if present) could be resolved because of the remaining termination ripples arising from the truncation in t_1.

Static ^{65}Cu NMR Spectra of Copper(I)-"Ladder" Catalysts

Mark Edgar,[1] Dinu Iuga[2] and Sandie Dann[1]

[1]*Department of Chemistry, Loughborough University*

[2]*Department of Physics, University of Warwick*

Overview

Dinuclear alkynylcopper(I) complexes have been found to be the active pre-catalysts in copper-catalysed cycloaddition of azides and terminal alkynes (CuAcc). Recent NMR and Raman results have shown that the formation of the Cu-alkyne may be linked to solvent inclusion and that information on the nature of the Cu-alkyne bonds is available from the ^{13}C CP-MAS spectra. The metal-organic catalyst[1] Cu(I)--C≡C-Ph displays an unusual one-dimensional arrangement of copper(I) in a "ladder" arrangement.[2] Of interest here is the influence of ortho, meta and para substituted aromatics on the Cu-CC-Ph-CH_3 (ortho, meta, para) structures, as the catalytic chemistry differs significantly.

Static ^{65}Cu spectra

Our ^{13}C CP-MAS NMR data (500 MHz for ^{1}H) highlighted the distorted hybrid alkyne/alkene nature of the organic group and differences in dynamics of the two unique phenyl groups in the unit cell. As the powder-X-ray structure produced short Cu-Cu bonds (2.49 Å) and long Cu-C bonds (2.63 Å), it was of interest to record the ^{65}Cu NMR spectra of this material and a family of similar catalysts for which X-ray structures have not yet been determined: Cu(I)--C≡C-Ph-CH_3 (ortho, meta, para). Static echoes were recorded, frequency-stepped to acquire the whole spectral width. The NMR spectra and fits from DM-FIT are shown in Figure 1, the best fit was obtained using two individual copper nuclei and the quadrupolar coupling and site occupancy (%) is presented in Table 1.

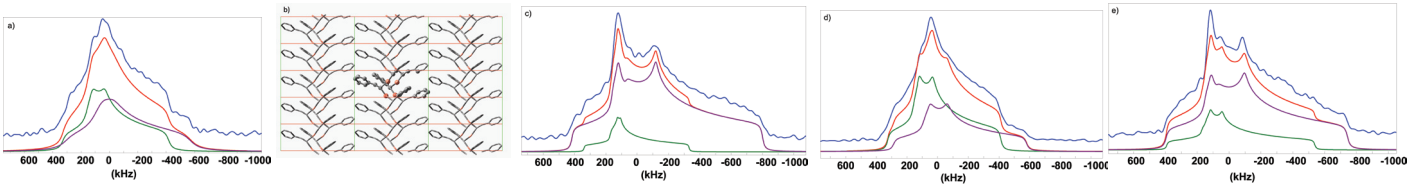

Figure 1. Static ^{65}Cu echo spectra, obtained as a summation of 10 individual frequency-stepped spectra (at 850 MHz for ^{1}H). (a): Cu(I)--C≡C-Ph, (b): powder X-ray structure, (c): Cu(I)--C≡C-Ph-CH_3 (ortho), (d): Cu(I)--C≡C-Ph-CH_3 (meta), (e): Cu(I)--C≡C-Ph-CH_3 (para). Fits were performed using TOPSPIN, QUEST and DM-FIT.

Table 1. The quadrupolar parameters used for fitting the spectra.

	Cu-CC-Ph		Cu-CC-Ph-CH_3 (o)		Cu-CC-Ph-CH_3 (m)		Cu-CC-Ph-CH_3 (p)	
	Site 1	Site 2	Site 1	Site 2	Site 1	Site 2	Site 1	Site 2
%	50%	50%	75%	25%	60%	40%	70%	30%
C_Q (MHz)	28.0	30.0	36.8	25.7	27.9	30.4	35.5	30.8
η_Q	0.83	0.87	0.73	0.96	0.83	0.81	0.74	0.89

References

1. Buckley, B. R.; Dann, S. E.; Harris, D. P. Heaney, H. *Chem. Eur. J.* **2012**, *16*, 6278.
2. Chui, S. S. Y.; Ng, M. F. Y.; Che, C. *Chem. Eur. J.* **2005**, *11*, 1739.

^{27}Al NMR Study of the Aluminium Environment in Levitation-Melted Al_2O_3-SiO_2 Glasses

Alex C. Hannon,[1] Masayuki Nogami,[2] Yasutomo Arai,[3] Shinji Kohara,[4] Diane Holland[5] and Ray Dupree[5]

[1]*ISIS, STFC, Rutherford Appleton Laboratory*
[2]*Nagoya Institute of Technology, Japan*
[3]*Japan Aerospace Exploration Agency, Japan*
[4]*Japan Synchrotron Radiation Research Institute/SPring-8, Japan*
[5]*Department of Physics, University of Warwick*

Overview

Vitreous Al_2O_3-SiO_2 is an important binary system, found in rapidly cooled magmas and at grain boundaries in many refractory materials. The glasses are difficult to make in the laboratory, requiring containerless melting at very high temperatures followed by rapid cooling. Previous studies produced conflicting ideas about the occurrence of phase separation, the presence of various [AlO_n] species, average Al coordination number and the existence of edge-sharing as well as corner-sharing polyhedra. We are carrying out the first study combining not only high-energy X-ray diffraction (HEXRD), neutron diffraction (ND) and Reverse Monte Carlo (RMC) modelling, but also ^{29}Si and ^{27}Al NMR. The NMR data are essential to provide the number and type of polyhedra present, which are used to constrain the fitting of the diffraction data.

Results

The samples studied were levitation-melted $xAl_2O_3 \bullet (100\text{-}x)SiO_2$ glasses (x = 20, 30, 40, 50) in the form of solid beads. ^{27}Al MAS spectra were taken at 20 T to provide the resolution necessary to obtain Al-O coordination information of sufficient accuracy for the fitting of neutron diffraction data taken at ISIS. The majority of spectra were from *powdered* beads but an identical MAS spectrum was also obtained from a single (x = 50) glass bead under the same conditions, demonstrating that no structural changes were induced by mechanical grinding (Figure 1). The ^{27}Al spectra are independent of sample composition, with ~ 5% 6-coordinated Al and approximately equal amounts of 4- and 5-coordinated Al. This indicates that the glasses are phase separated and this is supported by low-field (7 T) ^{29}Si spectra which show two sites: [$Si(OSi)_4$] units from near-pure SiO_2 and [$Si(OSi)(OAl)_3$] units from near-pure 3:2 "mullite". Their relative amounts change ~ linearly with x as expected. The major finding is that this amorphous 3:2 "mullite" contains [AlO_4] and [AlO_5] instead of [AlO_4] and [AlO_6] units in addition to [SiO_4]; observations of great significance in trying to understand which structural units can stabilise the amorphous state. Figure 2 shows how the NMR data are used successfully to simulate the neutron diffraction data. Since the 850 MHz experiments took place, high Q-range neutron diffraction data taken at ISIS have shown small-angle neutron scattering from these samples, consistent with there being phase separation into regions significantly larger than ~60 Å. Small amounts of an x = 60 sample (mullite stoichiometry) have been prepared and HEXRD data have been obtained but these have yet to be analysed.

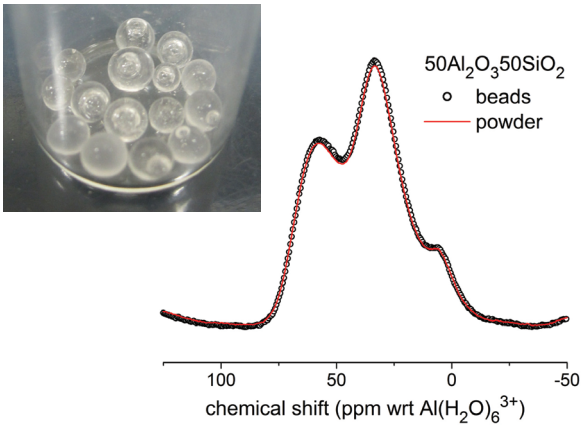

Figure 1. ^{27}Al MAS NMR spectra of x = 50 in both powder and bead form (3.2 mm probe; ν_r = 20 kHz; 1 μs (π/6) pulse; 2 s recycle delay). The broad peaks indicate the large distribution of shift and quadrupole parameters. (inset shows typical beads)

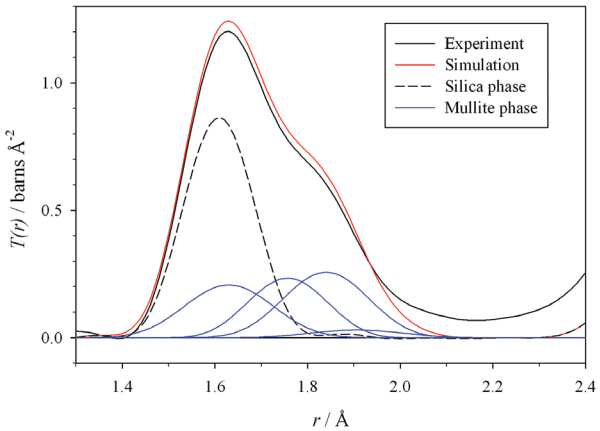

Figure 2. Neutron total correlation function, T(r) (black line), compared with simulated (red) curve based on contributions from different environments identified from ^{27}Al and ^{29}Si NMR. Dashed: silica phase; blue: "mullite" phase.

Identifying Electrochemical Products and Processes in the Lithium-Oxygen Battery by ^{17}O Solid State NMR

Michal Leskes,[1] Gillian R. Goward[2] and Clare P. Grey[1]

[1]*Department of Chemistry, University of Cambridge*

[2]*Department of Chemistry, McMaster University, Canada*

Overview

The lithium-oxygen battery is a promising energy storage device due to its potentially high energy density.[1,2] However, to fulfil its promise several challenges must be addressed - among these are the identification of stable electrolyte systems that will accommodate a reversible reaction between lithium and oxygen forming lithium peroxide.[3] Monitoring the formation of electrochemical products in working cells is a crucial step in the development of a viable battery. Using solid-state NMR, mainly of the ^{17}O isotope, we have recently demonstrated how the desired product, lithium peroxide, can be distinguished from lithium carbonate, the main product of parasitic electrolyte decomposition reactions.[4] High field measurements at the 850 MHz facility have allowed us to extend the library of spectra from possible decomposition products and using fast MAS (60 kHz) benefiting from the high sensitivity offered by the 1.3 mm probe, we were able to identify the electrochemical products formed in several candidates for electrolytes solvents and monitor their evolution as a function of the battery's cycle.

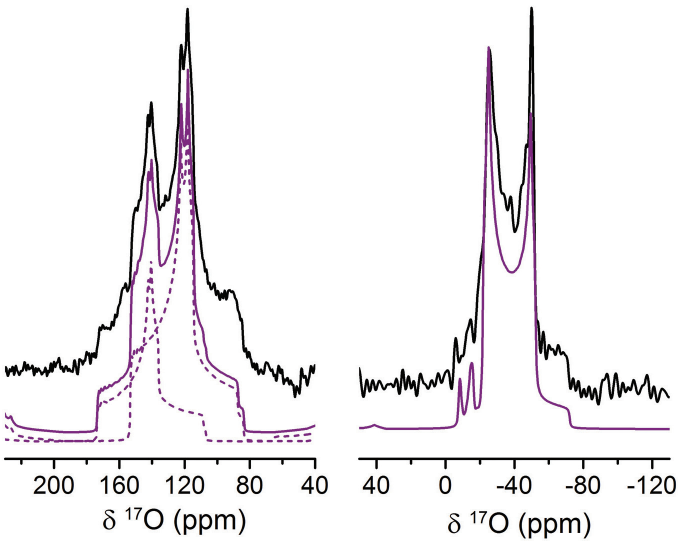

Figure 1. ^{17}O spectrum of lithium carbonate (10% ^{17}O enriched) acquired at 12.5 kHz MAS (left) fitted with two ^{17}O sites with $C_{q,1}$=7.2 MHz, $\eta_{q,1}$=0.94, $\delta_{iso,1}$=174 ppm and $C_{q,2}$=7.4 MHz, $\eta_{q,2}$=0.88, $\delta_{iso,2}$=153.5 ppm. The ^{17}O spectrum of lithium hydroxide acquired at 60 kHz MAS (right) was fitted with a single ^{17}O site with C_q=7.1 MHz, $\eta_{q,1}$=0.1, $\delta_{iso,1}$=-15 ppm. Line shape simulations were performed using Topspin3.0.

^{17}O spectra of model compounds

Figure 1 presents the ^{17}O spectra of lithium hydroxide and lithium carbonate. These compounds are commonly formed in cathodes when electrolyte decomposition is occurring. The carbonate spectrum was fitted with two oxygen sites as expected from the crystal structure, and the hydroxide with a single site. The quadrupole parameters and the isotropic chemical shift were then used to identify formation of these products in operating batteries.

^{17}O spectra of products formed in discharged cathodes

In order to identify suitable electrolyte systems three possible aprotic solvents were compared: 1,2-dimethoxyethane (DME), dimethyl sulfoxide (DMSO) and tetraethylene glycol diethyl ether (TEGDME). Lithium-oxygen cells were assembled with electrolyte made of 1 M lithium bis-trifluoromethanesulfonyl imide (LiTFSI) in each of these solvents and cycled under ^{17}O oxygen enriched atmosphere (about 20% enrichment). The cells were discharged to 2 V, disassembled and the cathodes, containing the discharge products, were extracted and packed in the MAS rotor. The ^{17}O spectra acquired from the cathodes are plotted in Figure 2 along with the fit based on the library of ^{17}O spectra of possible products. All solvents show some tendency towards decomposition in the order DME<DMSO<TEGDME. Only DME is stable enough so that a significant amount of lithium peroxide is formed in the cathode and is thus a more suitable candidate as an electrolyte solvent.

To gain insight into the electrochemical reactions in DME we have acquired ^{17}O spectra from the products accumulated in the cathode at different stages in the electrochemical cycle. Representative spectra are shown in Figure 3 from the cathode discharged to 1000 mAh/g (Figure 3a), fully discharged (Figure 3b) and partially charged (Figure 3c). These results demonstrate that initially lithium peroxide is formed as well as lithium carbonate, hydroxide and formate. Deeper discharge leads to predominantly formation of peroxide which is the first product to decompose upon charging while more carbonate is formed at increased charging voltages, presumably from the reaction of lithium peroxide and the carbon cathode.

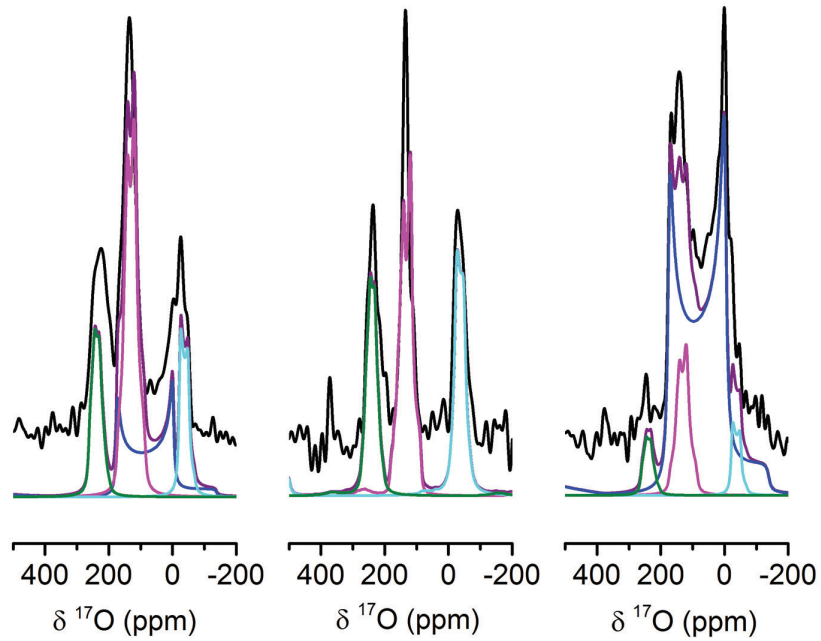

Figure 2. ^{17}O Hahn echo spectra acquired at 60 kHz MAS from cathodes that were discharged to 2 V in 1 M LiTFSI in DMSO (left), TEGDME (middle) and DME (right). Four discharge products were identified: lithium peroxide (blue) and electrolyte decomposition products such as lithium formate (green), lithium carbonate (magenta) and lithium hydroxide (cyan). The additional resonance at 380 ppm is assigned to the ^{17}O natural abundance signal of the zirconia rotor.

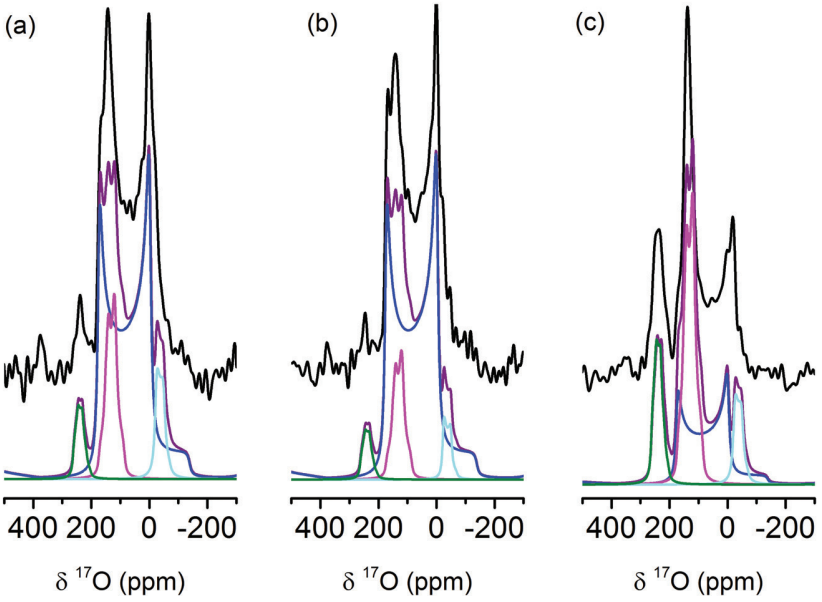

Figure 3. ^{17}O Hahn echo spectra acquired at 60 kHz MAS from cathodes that were (a) discharged to 1000 mAh/g (b) fully discharge to a voltage limit of 2 V and (c) charged to 4.5 V. Spectra were fitted with lithium peroxide (blue), lithium carbonate (pink), lithium formate (green) and lithium hydroxide (cyan).

References

1. Bruce, P. G.; Freunberger, F. A.; Hardwick, L. J.; Tarascon, J.-M. *Nat. Mater*. **2012**, *11*, 19.
2. Bruce, P. G.; Hardwick, L. J.; Abraham, K. M. *MRS Bull*. **2011**, *36*, 506.
3. Grishkumar, G.; McCloskey, B.; Luntz, A. C.; Swanson, S.; Wilcke, W. *J. Phys. Chem. Lett*. **2010**, *1*, 2193.
4. Leskes, M.; Drewett, N. E.; Hardwick, L. J.; Bruce, P. G.; Goward, G. R.; Grey, C. P. *Angew. Chem. Int. Ed.* **2012**, *51*, 8560.

Hydroxyl Defects and Fast Ion Conduction in Perovskites

Frédéric Blanc,[1] Luke Sperrin[1] and Clare P. Grey[1,2]

[1]*Department of Chemistry, University of Cambridge*

[2]*Department of Chemistry, Stony Brook University, United States*

Overview

Solid-state NMR experiments on challenging nuclei like ^{89}Y and ^{17}O provide structural characterization and dynamical insight into solid oxide fuel cell ceramic electrolytes. Multinuclear solid-state NMR spectroscopy was used, first, to observe the proton charge carrier and identify the spatial proximity of this proton with the dopant or host in fast protonic conductors and, second, to monitor O^{2-} ionic motion in fast anionic conductors. Using ^{1}H-^{89}Y CP Heteronuclear Correlation (HETCOR) experiments, we located the H site in close proximity with the Y dopant in Y doped $BaZrO_3$[1] identifying the presence of a YOH group. By recording highly resolved ^{17}O NMR spectra at the UK 850 MHz Solid-State NMR Facility, we observed O^{2-} ionic motion by ^{17}O variable temperature and exchange spectroscopy in Mg doped $LaGaO_3$[2] fast anionic conductors.

Hydroxyl Defects in Y Doped $BaZrO_3$ Perovskites

Figure 1a presents ^{1}H-^{89}Y CP[3] MAS spectra of $BaY_xZr_{1-x}O_{3-x/2-y}(OH)_{2y}$ for a range of compositions (x = 0.1, 0.3, 0.5) recorded at a MAS frequency of 3 kHz and at –80 °C. The 850 MHz Facility enabled these challenging spectra to be recorded with good signal to noise after only five hours of acquisition. Two ^{89}Y resonances were detected at 360 and 414 ppm, respectively, the latter being assigned to the 6 coordinate yttrium site in agreement with Y doping on the 6 coordinate Zr site of $BaZrO_3$. We tentatively assign the peak at 360 ppm to yttrium that is located on the 12 coordinate Ba site of $BaZrO_3$, with this leading to stoichiometries of the type $Ba_{1-x}Y_xZrO_{3-x/2}$. This is particularly important as this is the first spectroscopic observation of such substitution on the Ba site; this substitution acts to reduce the concentration of oxygen vacancies, and is associated with BaO loss during sample preparation.[1]

Figure 1b shows a ^{1}H-^{89}Y CP HETCOR spectrum of $BaY_{0.3}Zr_{0.7}O_{2.85}(OH)_{2y}$ recorded with Frequency Switched Lee Goldburg (FSLG)[4] proton decoupling during t_1 in order to increase the ^{1}H T_2' (very short due to the slow spinning frequencies required to obtain efficient CP transfer between ^{1}H and ^{89}Y), improving resolution in the proton dimension (Figure 1c) and allowing editing of the broad ^{1}H MAS spectrum (Figure 1d). Two ^{1}H sites at about 2.4 and 3.5 ppm (Figure 1c) are correlated with ^{89}Y at 414 ppm and correspond to proton sites trapped near the yttrium dopant. This is an important result as these results illustrate for the first time the presence of hydroxyl groups on the dopant (yttrium) site rather than solely on the guest (zirconium) site in Y doped $BaZrO_3$.

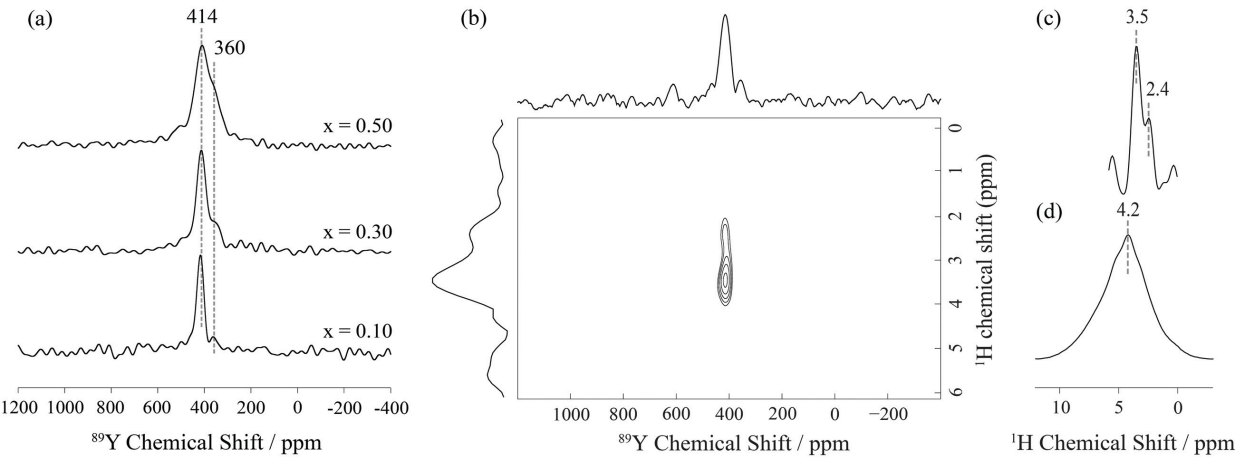

Figure 1. ^{89}Y and ^{1}H NMR spectra obtained at 850 MHz at a MAS frequency of 3 kHz at –80 °C. (a) ^{1}H-^{89}Y CP NMR spectra of $BaY_xZr_{1-x}O_{3-x/2-y}(OH)_{2y}$ (x = 0.1, 0.3, 0.5) – each spectrum was obtained in 5 hours (2048 transients), (b) ^{1}H-^{89}Y FSLG HETCOR spectrum of $BaY_{0.30}Zr_{0.70}O_{2.85-y}(OH)_y$ – obtained in 20 hours, (c) Projection of the ^{1}H dimension from the ^{1}H-^{89}Y HETCOR spectrum, (d) ^{1}H Hahn-echo spectrum recorded at 12.5 kHz MAS frequency.

Fast Ionic Motion in Mg Doped $LaGaO_3$ Perovskite

Figure 2 shows variable temperature ^{17}O MAS NMR spectra of ^{17}O enriched $La_{0.8}Sr_{0.2}Ga_{0.8}Mg_{0.2}O_{2.8}$ perovskites. The room and below room temperature ^{17}O MAS spectra of this compound exhibit resonances at isotropic chemical shifts of 244 and182 ppm, assigned to oxygen occupying equatorial (O_{eq}) and axial (O_{ax}) positions, respectively, with respect to the five fold Ga – vacancy axis, and 223 ppm corresponding to oxygen coordinated to Ga or Mg in a six-fold environment (O_{poly}).[5] This is an indication that little oxygen motion is observed at low temperature. However, clear evidence of motion is observed at 130 °C and above where only one resonance could be identified indicating that all three resonances coalescence into a single lineshape, with a motional rate given by $k = 2^{-1/2}\pi\Delta\nu$, i.e., ~ 13 kHz. We propose that motion occurs via anion vacancy jumps between O_{eq} and O_{lin}. A series of two-dimensional ^{17}O EXSY spectra as a function of mixing time and temperature were also recorded and show exchange peaks between all three different oxygen sites.

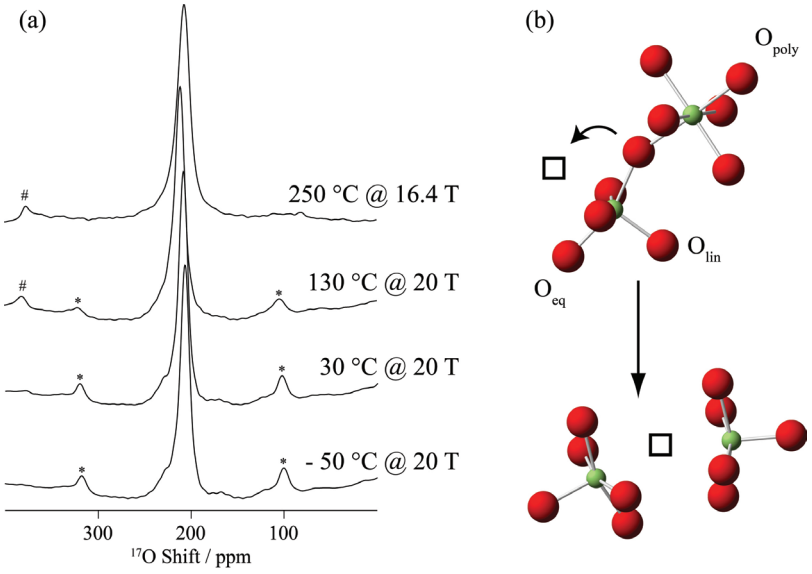

Figure 2. (a) Variable temperature ^{17}O NMR Hahn echo spectra (850 MHz and 700 MHz, 12.5 kHz MAS) of ^{17}O enriched $La_{0.8}Sr_{0.2}Ga_{0.8}Mg_{0.2}O_{2.8}$. Spectra were recorded with a 90° selective pulse of 2.3 μs at a rf field amplitude of 36 kHz and a 2 ms DFS population transfer pulse[6] at a rf field amplitude of 5 kHz. The ^{17}O signal of the ZrO_2 rotor and caps (#) is seen at 380 ppm. (b) Proposed mechanism of motion using representative DFT optimized local structures showing O_{eq}, O_{lin} and O_{poly}.[5] Green and red spheres represent Ga and O ions, respectively, while the square denotes the O vacancy.

References

1. Yamazaki, Y.; Babilo, P.; Haile, S. M. *Chem. Mater.* **2008**, *20*, 6352.
2. Ishihara, T.; Matsuda, H.; Takita, Y. *J. Am. Chem. Soc.* **1994**, *116*, 3801.
3. Wu, J.; Boyle, T. J.; Shreeve, J. L.; Ziller, J. W.; Evans, W. J. *Inorg. Chem.* **1993**, *32*, 1130.
4. Bielecki, A.; Kolbert, A. C.; Levitt, M. H. *Chem. Phys. Lett.* **1989**, *155*, 341.
5. Blanc, F.; Middlemiss, D. S.; Gan, Z.; Grey, C. P. *J. Am. Chem. Soc.* **2011**, *133* 17662.
6. Iuga, D.; Schäfer, H.; Verhagen, R.; Kentgens, A. P. M. *J. Magn. Reson.* **2000**, *147*, 192.

^{71}Ga Fast MAS Experiments on Gallium Doped Calcium Phosphate and Calcium Gallate Based Bioactive Glasses

Scott P. King,[1] Jodie M. Smith,[2] Robert J. Newport,[2] Jonathan C. Knowles[3] and John V. Hanna[1]

[1]*Department of Physics, University of Warwick*

[2]*School of Physical Sciences, University of Kent*

[3]*Division of Biomaterials and Tissue Engineering, University College London*

Overview

Calcium phosphates and calcium gallate glasses are important and interesting materials in the field of tissue engineering as their compositions are similar to that of the mineral component of bone. It has widely been reported that the materials such as glassy calcium phosphates exhibit great potential for use as bioactive implants, owing to their ability to provide the relevant ions required to help stimulate bone regrowth upon the *in situ* breakdown of the glass.[1] Glassy rather than crystalline materials are preferred in these situations as they have an ability to incorporate and exchange a wide range of different cations within the structure while still retaining a similar structure to the initially disordered phase. Recently, the addition of gallium ions to the calcium phosphate glass network has been shown to promote antibacterial activity, due to the release of Ga^{3+} ions, producing a promising alternative technique in tackling antibiotic resistant bacteria such as MRSA.[2]

The structural detail on the atomic level is crucial to our understanding of these materials since the structure-function relationship defining them bears a major influence on their bioactivity. However, inherent disorder (which essentially removes any long range order) within the structure of calcium phosphate glass systems renders diffraction techniques of limited value when a detailed structural characterisation is desired. Solid-state NMR is a powerful alternative due to its atomic specificity enabling the user to probe specific nuclei to determine the local (short range) atomic structure that defines that specific position. Many studies in recent years have used solid-state NMR to help characterise the structure of calcium phosphate glasses. However this has been predominantly restricted to studies involving spin-½ nuclei such as ^{31}P, and some work on relatively accessible quadrupolar nuclei such as ^{23}Na (and ^{27}Al, depending on composition). ^{71}Ga MAS NMR studies on calcium phosphate glasses have not been widely attempted, with only one such paper having been reported.[2] This is due to the difficulty in acquiring useful ^{71}Ga MAS NMR data as the large second-order quadrupolar interaction influencing the spin-3/2 ^{71}Ga nucleus requires a combination of high magnetic fields and fast MAS frequencies to effectively remove this broadening.

^{71}Ga One Pulse and ^{31}P-^{71}Ga *J*-HMQC Spectra

The calcium phosphate glasses that were investigated using the UK 850 MHz Solid-State NMR Facility were:

(a) 45(P_2O_5) 30(CaO) 25-x(Na_2O) x(Ga_2O_3) with x = 1 , 3 , 5 , 10, 15.

(b) 50(P_2O_5) 30(CaO) 20-x(Na_2O) x(Ga_2O_3) with x = 1 , 3 , 5 , 10, 15.

(c) 55(P_2O_5) 30(CaO) 15-x(Na_2O) x(Ga_2O_3) with x = 1 , 3 , 5 , 10.

Figure 1 shows the ^{71}Ga MAS NMR data acquired at 20 T for the glass series outlined above. These data are characterised by three clearly resolved resonances which are attributed to Ga assuming 4 (~130 ppm), 5 (~20 ppm) and 6 fold (~-70 ppm) coordination in the glass network. The observed lineshapes are broad with extended tailing towards higher frequencies, as expected for a distribution of chemical shifts and quadrupole parameters emanating from the disordered nature of the Ga speciation in each glass system. The use of the high B_0 field has enabled maximum resolution to be obtained owing to the reduction of the MAS linewidth in comparison to that acquired at lower field strengths, due to the inverse relationship between the second order quadrupole interaction and the external magnetic field strength. This has been used in combination with fast MAS frequencies of ~60 kHz which has contributed significantly to the line narrowing, and it has been successful in removing the much-reduced spinning sidebands to regions well outside the centreband intensities.

It can be observed for all three glass series that as Ga initially enters the network in low concentrations it assumes a predominantly octahedral (network modifying) coordination. Upon further increase in Ga content more tetrahedrally coordinated speciation is assumed, most likely inducing network formation and crosslinking between the phosphate chains. This is most obvious for the 15 mol% Ga_2O_3 glasses, where the majority of the Ga is now occupying these tetrahedral positions. Such Ga speciation behaviour is similar to that previously reported for Al speciation within phosphate glass networks,[3,4] thus indicating that Ga and Al perform very similar roles within phosphate glass networks. This is not surprising as both elements are trivalent species residing in the same group of the Periodic Table (Group III), and they possess similar ionic radii.

Figure 1d shows the result of a ^{31}P - ^{71}Ga *J*-HMQC experiment on a 45 mol% P_2O_5 glass with the highest (15 mol%) Ga_2O_3 content. The difficulty of this experiment lies in the weak two-bond *J* coupling that is present between the ^{71}Ga and ^{31}P nuclei, the large ^{71}Ga and ^{31}P linewidths, the relatively small amounts of Ga present in the sample, and the small 1.3 mm probe sample volume, consequently invoking the necessity for a long experimental acquisition time. Due to the length of the experiment, limited resolution is obtained in the indirect ^{31}P (F_1) dimension. However, it is clear that signal is present showing that all three Ga species are correlated to a P site, thus indicating P-O-Ga bonds are present for all Ga coordination environments. It should be noted that the intensity of the correlation associated with the tetrahedral Ga is the most intense, as might be expected with the network forming GaO_4 moieties forming more tetrahedral linkages between phosphate chains.

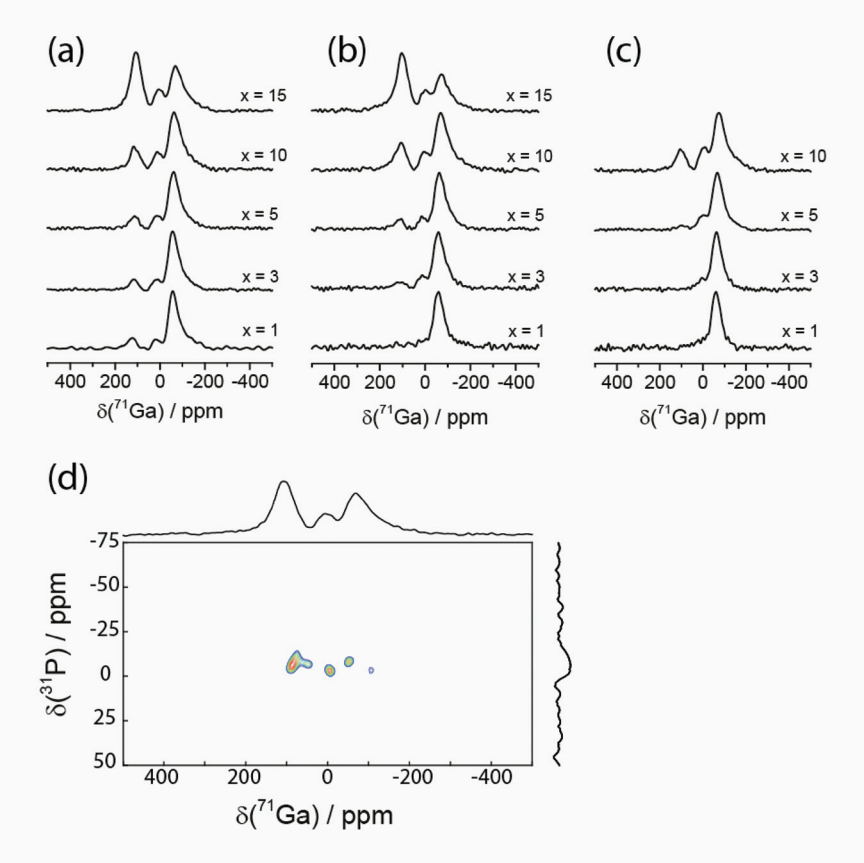

Figure 1: ^{71}Ga single pulse measurements of, (a) 45 mol% P_2O_5, (b) 50 mol% P_2O_5, (c) 55 mol% P_2O_5 containing glass series (B_0 = 20 T, ν_r = 60 kHz), and (d) 2D ^{31}P-^{71}Ga J-HMQC experiment of 45 mol% P_2O_5/15 mol% Ga_2O_3 glass (B_0 = 20 T, ν_r = 60 kHz, $\tau/2$ = 3.3 ms).

References

1. Knowles, J. C. *J. Mater. Chem.* **2003**, *13, 2395.*
2. Valappil, S. P.; Ready, D.; Abou Neel, E. A.; Pickup, D. M.; Chrzanowski, W.; O'Dell, L. A.; Newport, R. J.; Smith, M. E.; Wilson, M.; Knowles J.C. *Adv. Funct. Mater.* **2008**, *18*, 732.
3. Brow, R. K.; Kirkpatrick, R. J.; Turner, G. L. *J. Am. Ceram. Soc.* **1990**, *73*, 2293.
4. Brow, R. K.; Kirkpatrick, R. J.; Turner, G. L. *J. Am. Ceram. Soc.* **1993**, *76*, 919.

Discovering Polymorphism Among Phosphine Oxides by *In-Situ* Solid-State NMR Studies of Crystallization Processes

Colan E. Hughes, P. Andrew Williams and Kenneth D. M. Harris

School of Chemistry, Cardiff University

Overview

We have developed a new technique for studying crystallization processes using *in-situ* observation by solid-state NMR,[1,2] with particular interest in monitoring the evolution of different polymorphic forms of the solid phase produced during the crystallization process. In the present project, this technique has been applied to study the crystallization of several different phosphine oxides, yielding significant new insights into the polymorphic evolution during crystallization of these materials.

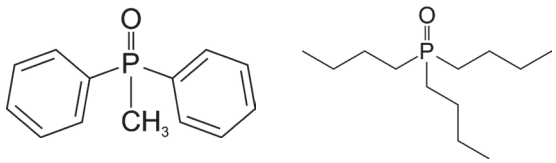

MDPPO TBPO

In earlier work, we demonstrated the existence of several hitherto unknown solid forms of triphenylphosphine oxide (TPPO). During 2012, this work was extended to include the following compounds: diphenylphosphine oxide (DPPO), methyldiphenylphosphine oxide (MDPPO),[3] ethyldiphenylphosphine oxide (EDPPO), (methoxymethyl)diphenylphosphine oxide (MOMDPPO), trimethylphosphine oxide (TMPO) and tributylphosphine oxide (TBPO). Of these six compounds, evidence of polymorphism was found in two cases, MDPPO and TBPO, each of which has had only one crystal structure published previously.[4,5] For the other four compounds, no evidence of polymorphism was found, although other interesting aspects of the crystallization processes were observed. However, in the present report, we focus on the new insights on polymorphism observed for MDPPO and TBPO.

Methyldiphenylphosphine Oxide (MDPPO)

Crystallization of MDPPO was carried out from methanol, with $^{1}H \rightarrow ^{31}P$ CPMAS NMR spectra recorded *in situ* as a function of time over a total of 11.4 hours during the crystallization process. Figure 1 shows the evolution of the region of the spectrum between 60 ppm and 70 ppm as a function of time during the first 50 minutes of the experiment. This spectral region corresponds to the first spinning sidebands at higher chemical shift than the isotropic ^{31}P peak (which is the most intense peak in the manifold of spinning sidebands). At the earliest stages of the crystallization experiment, three peaks are observed in this region. The most intense peak (at 65.6 ppm) corresponds to the known solid phase of MDPPO (for which the isotropic peak is at 30.8 ppm). Significantly, however, two much weaker peaks are also observed at 63.7 and 64.5 ppm (corresponding to isotropic peaks at 28.8 and 29.6 ppm). The peak at 63.7 ppm is discernible for only about 16 minutes after commencing the crystallization process, whereas the peak at 64.5 ppm survives for about six hours after the beginning of the experiment. As the high intensity peak at 65.6 ppm is known to correspond to the one solid form of MDPPO reported previously, it is clear that the two additional peaks observed during the early stages of the crystallization process must represent new solid forms of MDPPO.

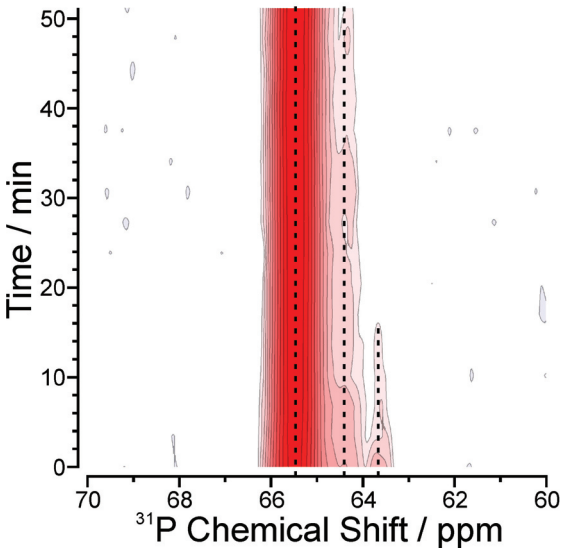

Figure 1. In-situ ^{1}H-^{31}P CPMAS NMR spectra recorded during crystallization of MDPPO from toluene, showing the region of the first spinning sideband. Spinning frequency 12 kHz.

Owing to the low concentration and short lifetime of the two new solid forms under these conditions, attempts to isolate them for further study (including structure determination) have so far been unsuccessful. We therefore intend to carry out new experiments on the UK 850 MHz solid-state NMR facility to study the effects of various experimental parameters on the crystallization process in order to identify conditions under which these short-lived forms may be trapped as pure solid phases.

Tributylphosphine Oxide (TBPO)

Crystallization of TBPO was studied in two separate experiments, using cyclohexane and ethyl acetate as the solvent respectively, again focusing on the *in-situ* measurement of $^{1}H \rightarrow ^{31}P$ CPMAS NMR spectra as a function of time during the crystallization experiment. For each solvent, crystallization was initiated immediately, as observed from the ^{31}P NMR spectra. In these spectra, two distinct ^{31}P resonances are observed in the centreband and spinning sidebands, corresponding to two different ^{31}P isotropic chemical shifts. Importantly, the relative intensities of these two peaks are different in the crystallization experiments from the different solvents (Figure 2), which strongly suggests that the two peaks represent different solid forms of TBPO (rather than arising from crystallographically-distinct molecules of TBPO in a given polymorph).

As shown in Figure 2, the same chemical shifts are observed in the crystallization experiments carried out from cyclohexane and ethyl acetate, suggesting that the same solid forms are produced in each case; hence, it is unlikely that these solid forms are solvates. We therefore conclude that TBPO is polymorphic and we are now in the process of isolating these polymorphs and determining their crystal structures.

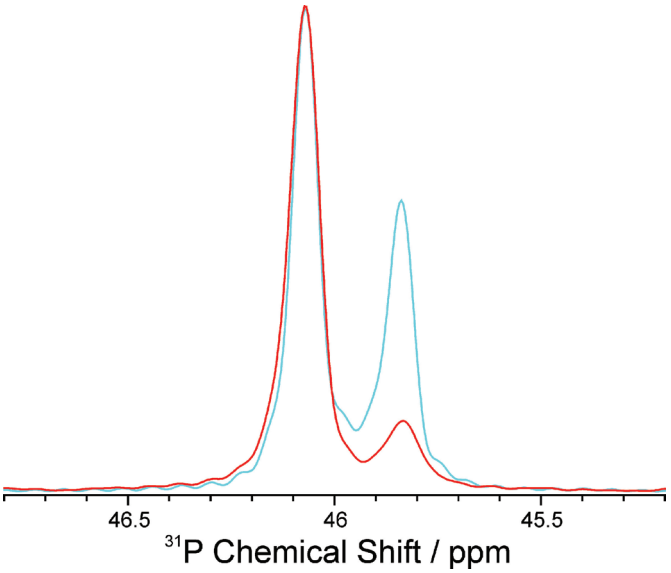

Figure 2. In-situ ^{1}H-^{31}P CPMAS NMR spectra recorded during crystallization of TBPO from cyclohexane (blue) and ethyl acetate (red). Spinning frequency 12 kHz.

Concluding Remarks

The *in-situ* solid-state NMR technique employed in this work provides new opportunities for directly monitoring the evolution of solid forms during crystallization processes and our results demonstrate that this technique can play a crucial role in the discovery of new polymorphs and other solid forms that may not be evident from *ex-situ* analysis of the final solid products recovered from crystallization experiments. This technique thus delivers a new tool to the field of polymorph discovery, allowing the identification of new solid forms which, although they may only appear as transient intermediates under a given set of crystallization conditions, may be isolated by other methods. Importantly, we emphasize that the *in-situ* solid-state NMR technique gives insights not only on the crystallization conditions required to produce new solid forms, but also yields knowledge of the specific time-window during which the new solid forms are present during the crystallization process.

References

1. Hughes, C. E.; Harris, K. D. M. *J. Phys. Chem. A* **2008**, *112*, 6808.
2. Hughes, C.E.; Harris, K. D. M. *Chem. Comm.* **2010**, *46*, 4982.
3. Hughes, C. E.; Williams, P. A.; Peskett, T. R.; Harris, K. D. M. *J. Phys. Chem. Lett.* **2012**, *3*, 3176.
4. Dornhaus, F.; Bolte, M.; Lerner, H. W.; Wagner, M. *Eur. J. Inorg. Chem.* **2006**, 5138.
5. Hilliard, C. R.; Bhuvanesh, N.; Gladysz, N. A.; Blümel, J. *Dalton Trans.* **2012**, *41*, 1742.

Insights into Pre-Nucleation Behaviour from *In-Situ* NMR Studies

Colan E. Hughes, P. Andrew Williams and Kenneth D. M. Harris

School of Chemistry, Cardiff University

Overview

We have studied a wide range of different crystallization systems during our visits to the UK 850 MHz Facility in 2012, with the aim of exploiting the *in-situ* NMR strategy that we have developed for monitoring the time-evolution of crystallization processes.[1,2] In addition to carrying out a systematic study of polymorphism in phosphine oxides,[3] we have also investigated several other crystallization processes. One question which we have sought to answer is whether our strategy of studying crystallization by simultaneous solid-state and solution-state NMR measurements can provide new insights into pre-nucleation behaviour. In particular, we are interested to understand changes in the solution-state chemical shifts that occur before and during the crystallization process. This approach is particularly suitable for studying unstable, super-saturated solutions, recognizing that as the crystallization process evolves, these super-saturated solutions decrease in concentration towards saturation.

In our previous work on pre-nucleation behaviour, which was focused on studies of *m*-aminobenzoic acid crystallizing from different solvents (manuscript in preparation), the chemical shifts for different ^{13}C nuclei in both the solute (*m*-aminobenzoic acid) and solvent molecules were found to change in well-defined and characteristic ways as a function of time during crystallization. However, as several different factors may influence the chemical shifts in this system (for example, possible changes in protonation state and hydrogen bonding environment), it is challenging to decipher the primary factor underlying the observed evolution of the chemical shifts. For this reason, our subsequent studies, reported here, were focused specifically on a much simpler system (benzoic acid) and on a system (inosine) for which the crystallization process has been studied previously by other methods.

Benzoic Acid

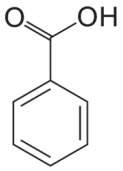

Benzoic acid

Benzoic acid is known to aggregate as hydrogen-bonded dimers in some solvents (e.g., chloroform or carbon tetrachloride); however, for other solvents, dimer formation in under-saturated solutions has been ruled out.[4] In the only known crystalline form of benzoic acid, the molecules adopt the double hydrogen-bonded dimer arrangement. In the present work, we have applied our *in-situ* NMR strategy to explore the crystallization of benzoic acid from acetone. Clearly, a focal point of this work was to identify the specific stage of the crystallization process at which solution-state dimerization is observed to occur.

Several crystallization experiments were carried out involving *in-situ* measurement of solution-state ^{1}H NMR and solid-state ^{13}C NMR spectra. The solid-state ^{13}C NMR spectra indicate clearly that crystallization is initiated within the first nine minutes of the experiment (the time to record an individual spectrum was nine minutes and a signal was observed in the first spectrum recorded).

Figure 1 shows a series of solution-state ^{1}H NMR spectra recorded as a function of time during crystallization of benzoic acid from acetone. It is clear that the ^{1}H chemical shifts in solution undergo rapid changes in the first few minutes of the experiment, during which it is known from the solid-state ^{13}C NMR measurements that crystallization is occurring. Of great interest is the fact that the ^{1}H chemical shift for the carboxylic acid group (green) moves to lower ppm whereas the chemical shifts of the other ^{1}H nuclei in both the benzoic acid solute and the acetone solvent (red) move to higher ppm over the same period.

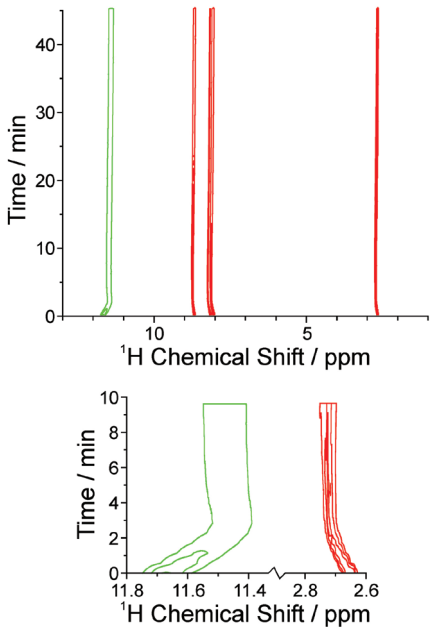

Figure 1. In-situ solution-state ^{1}H NMR spectra recorded during crystallization of benzoic acid from acetone.

During crystallization, the key change in the solution state is a reduction in concentration. The distinct behaviour observed for the ^{1}H chemical shift of the carboxylic acid group indicates that the change in solution concentration has a different effect on this moiety than on the rest of the benzoic acid molecule and can be interpreted in terms of aggregation of the benzoic acid molecules via hydrogen bonding between the carboxylic acid moieties occurring in the supersaturated solution during crystallization. In contrast, for an undersaturated solution of benzoic acid in acetone, association (dimerization) of the carboxylic acid moieties is not observed.

Inosine

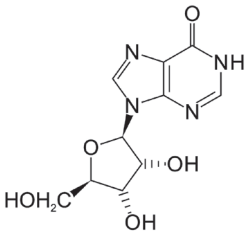

Inosine

The pre-nucleation behaviour of inosine has been studied previously[5] by solution-state ^{1}H NMR, involving comparison of experimental chemical shifts with those determined by computational techniques for isolated dimers of inosine. The study concluded that inosine molecules associate in aqueous solution by the formation of stacks.

In the present work, we have applied our *in-situ* NMR strategy to study the crystallization of inosine from D_2O. From our solid-state ^{13}C NMR spectra, it is known that crystallization occurs within the first 40 minutes of the experiment. Figure 2 shows *in-situ* solution-state ^{1}H NMR spectra recorded as a function of time during a separate crystallization of inosine from D_2O. Throughout the experiment, all resonances exhibit a gradual shift to lower ppm, which is a well-understood effect due to slow cooling of the shims. However, within the first ten minutes of the experiment, all peaks except one (shown in green in Figure 2) undergo an abrupt initial shift to higher ppm. The peak that does not show this initial shift to higher ppm is due to the residual ^{1}H nuclei in the D_2O solvent.

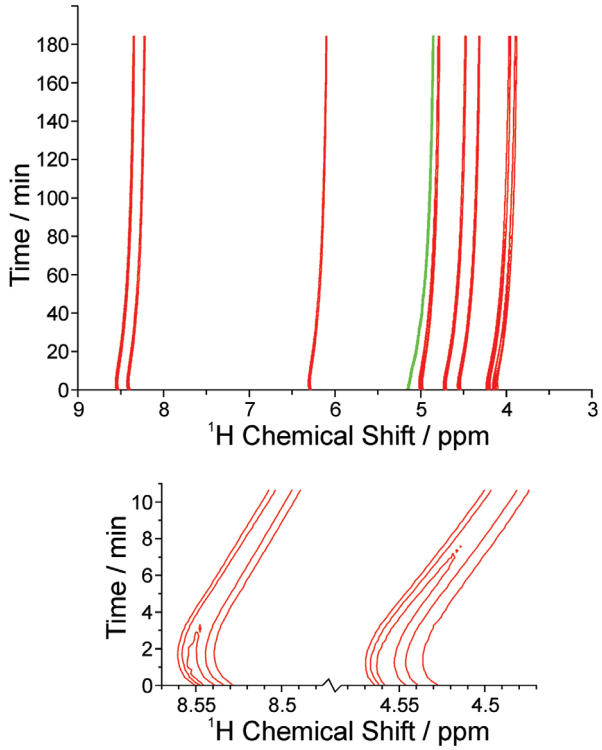

Figure 2. In-situ solution-state ^{1}H NMR spectra recorded as a function of time during crystallization of inosine from D_2O.

Furthermore, the peaks resulting from different regions of the inosine molecule exhibit small differences in behaviour with regard to these initial changes in chemical shifts, suggesting that the molecular association has a differing effect on different parts of the molecule. In particular, the three ^{1}H nuclei of the aromatic ring (with chemical shifts between 6 and 9 ppm) exhibit larger initial shifts to higher ppm than those in the ribose group (between 4 and 5 ppm). These observations are fully consistent with the association of inosine molecules in aqueous solution occurring by π–π stacking rather than hydrogen bonding, in agreement with the conclusion from the previous study.[5] Further analysis is revealing more detailed understanding of these small but significant changes in the solution-state ^{1}H NMR spectrum in the early stages of the crystallization process.

References

1. Hughes, C. E.; Harris, K. D. M. *J. Phys. Chem. A* **2008**, *112*, 6808.
2. Hughes, C. E.; Harris, K. D. M. *Chem. Comm.* **2010**, *46*, 4982.
3. Hughes, C. E.; Williams, P. A.; Peskett, T. R.; Harris, K. D. M. *J. Phys. Chem. Lett.* **2012**, *3*, 3176.
4. Burton, R. C.; Ferrari, E. S.; Davey, R. J.; Finney, J. L.; Bowron, D. T. *J. Phys. Chem. B* **2010**, *114*, 8807.
5. Chiarella, R. A.; Gillon, A. L.; Burton, R. C.; Davey, R. J.; Sadiq, G.; Auffret, A.; Cioffi, M.; Hunter, C. A. *Faraday Disc.* **2007**, *136*, 179.

Measurements of ^{15}N and ^{13}C Solid-State Relaxation as a Tool for Quantitative Description of Protein Dynamics

Jonathan M. Lamley,[1] Hans J. Sass,[2] Stephan Grzesiek[2] and Józef Lewandowski[1]

[1]*Department of Chemistry, University of Warwick*
[2]*Biozentrum, University of Basel, Switzerland*

Overview

Together with structure, protein dynamics are a crucial ingredient for understanding the molecular basis for protein function. Knowledge of molecular motions is pivotal for a number of important processes, including enzymatic catalysis, signaling, allosteric regulation, ligand binding and folding-unfolding. However, characterizing motions that span more than 12 orders of magnitude in terms of timescale is a challenging task that requires a diverse set of tools. For example, relaxation-based methods in solution are excellent for characterizing both amplitudes and timescales of the motions in the picosecond to nanosecond range. However, motions which occur on a timescale close to or longer than that of overall tumbling are then obscured. Since the overall tumbling is absent in solids, measurements of solid-state relaxation provide an attractive alternative for obtaining information on the timescales, amplitudes and possibly directions[1] of slower nanosecond-microsecond motions important for the understanding of protein functions. In spite of its tremendous potential, solid-state relaxation methodology is still plagued by a scarcity of observables that could be used for site-specific quantitative characterization of protein motions. In particular, measurement of motion-induced T_2 that is not obscured by (usually dominating) dipolar dephasing has been an elusive goal for a long time. Recently, we showed that such a goal can be achieved in the case of ^{15}N by combining fast magic angle spinning and $R_{1\rho}$ ($R_{1\rho} = 1/T_{1\rho}$) measurements.[2] As a continuation, one of the objectives for this project at the UK 850 MHz Solid-State NMR Facility was to introduce and validate ^{13}C $R_{1\rho}$ measurements for site-specific quantitative characterization of slow protein motions. The emerging picture of site-specific motions in the protein GB1 was contrasted with the picture emerging from other relaxation measurements, notably ^{15}N R_1 and $R_{1\rho}$ and ^{13}C R_1.[3]

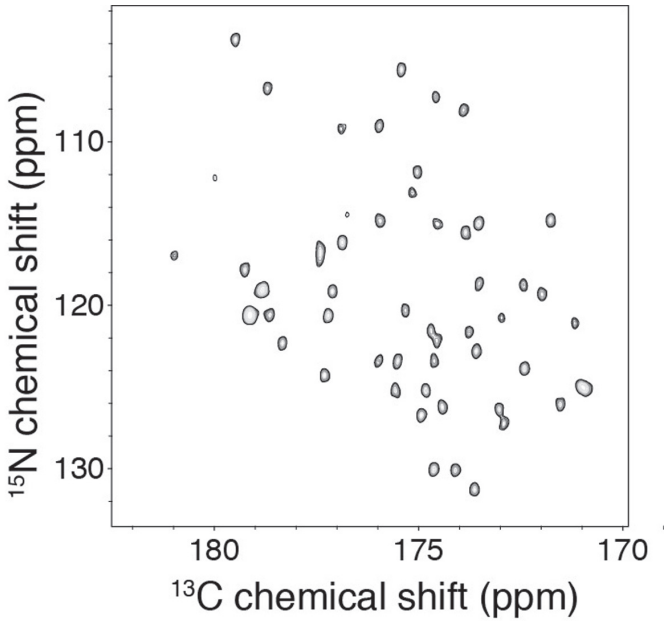

Figure 1. ^{15}N-^{13}C 2D NCO-S^{3}E correlation spectrum used as the basis for the site-specific measurement of ^{15}N and ^{13}C' R_1 and $R_{1\rho}$ rates in [U-^{13}C,^{15}N]GB1. The spectrum was obtained at $\omega_1/2\pi$ = 60 kHz and $\omega_{0H}/2\pi$ = 850 MHz, using the S^{3}E scheme to remove the effect of $^1J_{CC}$.

^{15}N and ^{13}C Relaxation Measurements on GB1 in the Solid State

We measured site-specific ^{15}N and ^{13}C' R_1 and $R_{1\rho}$ using ^{15}N-^{13}C 2D NCO-S^{3}E as the basis for obtaining site-specific dynamic information. Figure 1 shows an example ^{15}N-^{13}C 2D NCO-S^{3}E correlation spectrum of [U-^{13}C,^{15}N]GB1 with resolution improved by removing the effect of $^1J_{CC}$ by the S^{3}E "decoupling" scheme.[4] Figure 2 shows the measured R_1 and $R_{1\rho}$ rates projected onto the crystal structure of GB1. The substantial variation of the rates along the sequence highlights the fact that relaxation rates in the solid state are very sensitive probes of protein motions. Notably, a quantitative analysis of the relaxation data obtained at 850 MHz and 600 MHz (manuscript in preparation) reveals a detailed dynamical picture that is highly complementary and compatible with the picture emerging from extensive solution NMR studies.

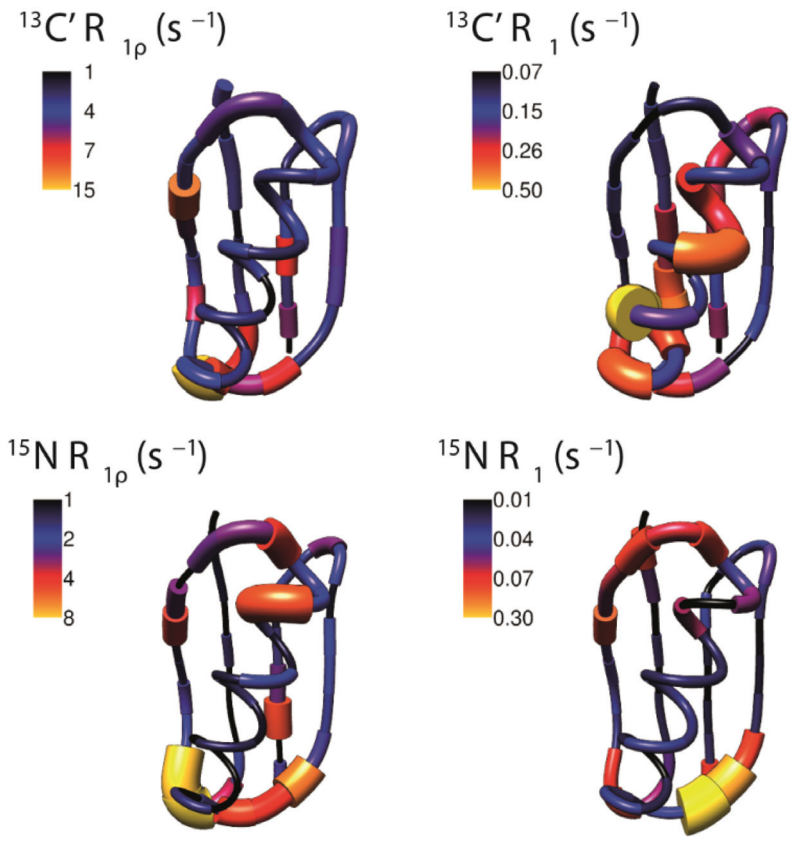

Figure 2. ^{15}N and $^{13}C'$ R_1 and $R_{1\rho}$ rates measured at $\omega_f/2\pi$ = 60 kHz and $\omega_{0H}/2\pi$ = 850 MHz projected onto the crystal structure of GB1. The magnitude of the measured rates is indicated both by color and the radius of the tube.

An interesting side note is that the measured ^{13}C $T_{1\rho}$ times provide a relaxation limit for the ^{13}C coherence lifetimes, i.e. ^{13}C coherence lifetimes that should be achievable under perfect heteronuclear decoupling. A classical benchmark for the efficiency of heteronuclear decoupling is measurement of T_2' for a CH_2 group in crystalline glycine. Currently the longest T_2' reported in the literature for this spin system under application of 400 kHz SPINAL-64 decoupling is ~250 ms.[5] The value we measured for the $T_{1\rho}$ of the glycine C_α exceeds 5 s, suggesting that there is still plenty of room for improvement of heteronuclear decoupling sequences before the relaxation limit is reached.

References

1. Lewandowski, J. R.; Sein, J.; Blackledge, M.; Emsley, L. *J. Am. Chem. Soc.* **2010**, *132*, 1246.
2. Lewandowski, J. R.; Sass, H. J.; Grzesiek, S.; Blackledge, M.; Emsley, L. *J. Am. Chem. Soc.* **2011**, *133*, 16762.
3. Lewandowski, J. R.; Sein, J.; Sass, H. J.; Grzesiek, S.; Blackledge, M.; Emsley, L. *J. Am. Chem. Soc.* **2010**, *132*, 8252.
4. Laage, S.; Lesage, A.; Emsley, L.; Bertini, I.; Felli, I. C.; Pierattelli, R.; Pintacuda, G. *J. Am. Chem. Soc.* **2009**, *131*, 10816.
5. Vasa, S. K.; Janssen, H.; Van Eck, E. R. H.; Kentgens, A. P. M. *Phys. Chem. Chem. Phys.* **2011**, *13*, 104–6.

An Investigation of $NaNbO_3$-Based Ferroelectric Perovskites

Martin D. Peel, Sharon E. Ashbrook and Philip Lightfoot

School of Chemistry, University of St Andrews

Overview

Perovskites have the general formula ABX_3 where A and B are cations of different size and X is typically oxygen. $NaNbO_3$ is one such perovskite, having enjoyed renewed interest recently as an alternative piezoelectric replacement for lead zirconium titanate.[1] Structurally, $NaNbO_3$ is composed of corner-sharing NbO_6 octahedra, and its high dielectric responses are derived from A- and B-site cation displacements within the structure. $NaNbO_3$ is a particularly complex perovskite as it can display a number of octahedral tilt modes, each resulting in its own space group and having different dielectric responses.

By doping Li and K onto the A-site, phase transformations are observed, and in many cases result in an increase in the dielectric responses. By combining solid-state NMR and X-ray diffraction, a more thorough understanding of both periodic and local structure can be gained, as well as information concerning disorder. Interestingly, the two techniques can yield very different results. For example, ^{23}Na MQMAS spectra of $K_xNa_{1-x}NbO_3$ (x = 0.03 – 0.08) suggest the presence of an additional phase, which is not observed in the diffraction data. High-field ^{39}K NMR is needed to significantly enhance the signal observed, while high-field ^{23}Na NMR provides improved resolution and sensitivity.

$K_xNa_{1-x}NbO_3$ (KNN)

The KNN series has enjoyed renewed interest[2] owing to its high piezoelectric responses. Small amounts of K-doping (x = 0.02 – 0.08) change the symmetry from centrosymmetric *Pbcm* to polar $P2_1ma$, giving rise to its electric properties. It does this by forcing the structure to undergo a change in the NbO_6 tilt mode to accommodate for the larger K^+ cations. Beyond this region, the structure resembles the $KNbO_3$ end member.

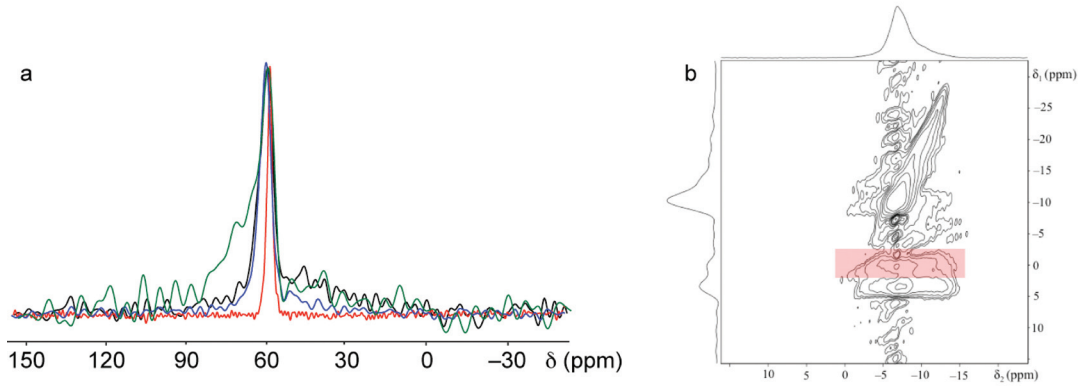

Figure 1: (a) ^{39}K (20.0 T) MAS NMR spectra of $K_{0.8}Na_{0.2}NbO_3$ (red), $K_{0.3}Na_{0.7}NbO_3$ (blue), $K_{0.2}Na_{0.8}NbO_3$ (black), and $K_{0.1}Na_{0.9}NbO_3$ (green). (b) ^{23}Na (14.1 T) sheared MQMAS z-filtered NMR spectrum of $K_{0.05}Na_{0.95}NbO_3$ showing the two distinct Na resonances and an additional low-intensity resonance (highlighted in pink).

^{23}Na (14.1 T) MQMAS spectra of $K_{0.05}Na_{0.95}NbO_3$ show two distinct Na resonances corresponding to the two sites in the $P2_1ma$ polymorph,[3] as well as an additional resonance corresponding to either an impurity or a second phase. The intensity of this additional resonance increases in the region x = 0.03 to 0.08, and it is present in multiple samples of each composition. Calcination temperature, time and cooling rate have all been varied, yet this resonance remains unaffected. ^{23}Na MQMAS NMR spectra,

in particular those acquired at 20.0 T, have allowed us to extract NMR parameters for the additional resonance, which may be a second Na-containing phase or impurity. Knowledge of any additional phase or impurity is important as it allows us to more accurately perform structure determinations for high temperature phases, which may be affected by the presence of such phases or impurities. Signs of a second phase or impurity are not observed in diffraction data, and so this additional information available from NMR spectra, in particular those acquired at 20.0 T, is extremely important.

Interestingly, ^{39}K (20.0 and 14.1 T) MAS NMR become substantially more broadened as the concentration of K is reduced. This is counter-intuitive – typically, increasing the concentration of a dopant introduces additional disorder and contributes to more broadening of resonances (x = 0.01 - 0.5). Preliminary analysis of ^{39}K MAS spectra where x = 0.05 and 0.08 continue to show broadening. There is no sign of two distinct resonances (thereby suggesting both Na sites are not substituted, or that the two are very similar) although this could be due to the poor sensitivity of ^{39}K.

$Li_xNa_{1-x}NbO_3$ (LNN)

The phase changes in this series, with increasing Li doping, are noticeably more complex than those of the KNN series. Similar to the KNN series, the $P2_1ma$ polymorph is stabilized when x = 0.02 to 0.08. At higher values of x, this phase can co-exist with a rhombohedral ($R3c$) phase depending on the synthetic and cooling conditions employed. These conditions can be manipulated to control the relative phase fractions of the two, and therefore alter the dielectric properties of the material. When $x < 0.2$, two rhombohedral phases co-exist through the series – one Na-rich and one Li-rich $LiNbO_3$-like phase. However, when x = 0.2 – 0.5, the Na content in one of these phases is too small to be detected using ^{23}Na NMR, and the presence of the phase is confirmed using XRD. ^{23}Na MAS spectra of several LNN compounds have allowed accurate Na ratios of the two rhombohedral phases to be calculated, and this is particularly true for spectra acquired at 20.0 T owing to the improved resolution. The occupancies of Na in each phase are difficult to accurately determine from diffraction methods, owing to the inherent insensitivity of fractional occupancy refinements using the Rietveld method. The values obtained allow us to understand in more detail the compositions of the phases, which in turn, allow us to more reliably interpret diffraction and electrical measurement data.

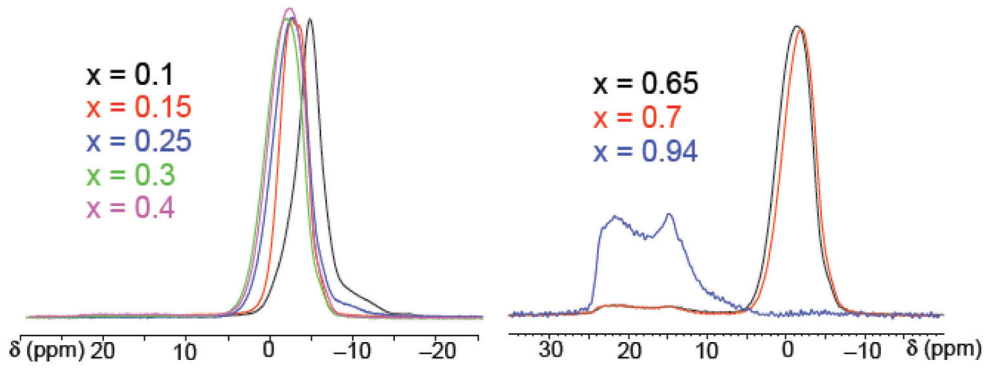

Figure 2: ^{23}Na (20.0 T) MAS NMR spectra of $Li_xNa_{1-x}NbO_3$ showing the subtle changes in chemical shift as x is varied, and the presence of two distinct phases at approximately –1 ppm and 19 ppm.

^{23}Na (20.0 T) MQMAS spectra confirm the presence of the $P2_1ma$ and $R3c$ phases (supported using CASTEP calculations), and also confirm that varying the synthetic conditions slightly can change the relative fractions of the two phases.

The KNN and LNN doped series show some interesting and complex phase behaviour. DFT calculations on the KNN series are underway to understand the ^{39}K MAS NMR spectra observed. XRD and neutron powder diffraction (NPD) data are currently being analysed for the LNN series, and temperature-dependent electrical profiles for every sample will also be obtained to investigate high temperature phase transitions. The experiments performed at the UK solid-state 850 MHz facility have allowed us to obtain the ^{39}K NMR spectra as the higher field is needed owing to poor sensitivity. The ^{23}Na spectra have improved resolution, allowing us to see more subtle changes in the MQMAS spectra, and provide additional information unavailable to us from diffraction data.

References

1. Saito, Y. *Nature,* **2004**, *432*, 84.
2. Baker, D. W.; Thomas, P. A; Zhang, N.; Glazer, A. M., *Appl. Phys. Lett.* **2009**, *95*, 91903.
3. Johnston, K. E.; Tang, C. C.; Parker J. E.; Knight, K. S.; Lightfoot, P.; Ashbrook S. E. *J. Am. Chem. Soc.,* **2010**, *132*, 8732.

New Paradigms for NMR of Organic Solids

Ilya Frantsuzov,[1] Steven P. Brown[2] and Paul Hodgkinson[1]

[1]*Department of Chemistry, Durham University*

[2]*Department of Physics, University of Warwick*

Overview

Resolution and sensitivity in solid-state NMR of organic compounds is limited by the relatively short decoherence times of ^{1}H and ^{13}C magnetisation. However, the relationship between radio-frequency (RF) decoupling sequences (for heteronuclear and homonuclear decoupling) and achievable decoherence times is still poorly understood. Building on early results reported last year, the goal of the project is to understand how to efficiently decouple the abundant protons over the steadily widening parameter space (increasing static magnetic fields, RF powers, and MAS rates).

Field-Dependence of Heteronuclear Decoupling

Figure 1a shows the decoherence time constant under a spin-echo, T_2', for several heteronuclear decoupling sequences with optimised parameters, at three different magnetic fields. The T_2' under TPPM, SPINAL64 and CW decoupling increases linearly with the inverse of the magnetic field, corroborating the theoretical analyses and simulations of such sequences as being limited by cross-terms between the ^{13}C,^{1}H dipolar coupling and ^{1}H chemical shift anisotropy.[1,2] Figure 1b shows that the reduced performance of TPPM at increased magnetic fields is independent of decoupling sequence parameters. In contrast, the decoupling performance using XiX shows a much weaker field dependence[3]. These and other results are helping to build up a comprehensive picture of heteronuclear decoupling performance, so that new strategies to optimise performance under different experimental conditions, e.g., high magnetic field, can be developed.

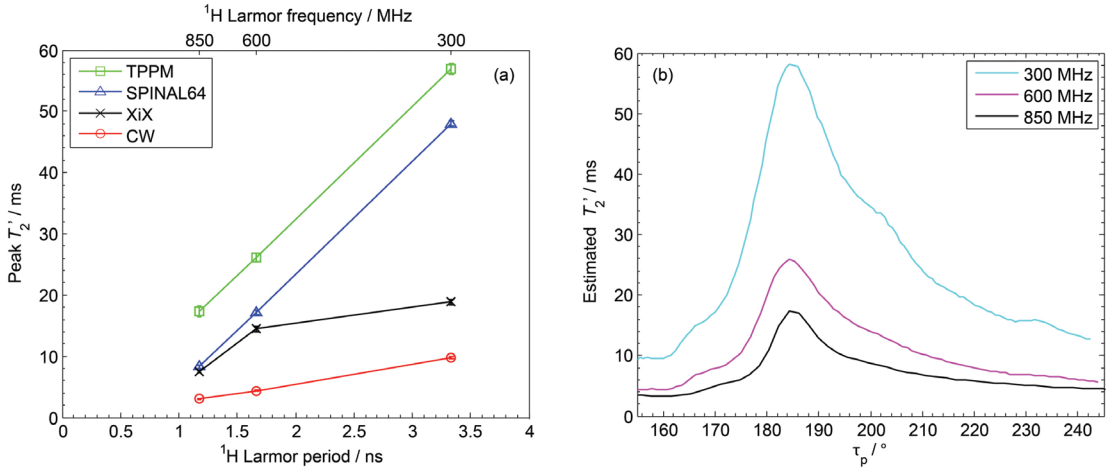

Figure 1. (a) Optimised T_2' of the ^{13}C signal of glycine-2-^{13}C,^{15}N as a function of magnetic field under different decoupling sequences. Consistent conditions of 12 kHz MAS and 105 kHz RF nutation rate were used. (b) TPPM T_2' as a function of pulse width and fixed phase of 6° shown for different magnetic fields.

References

1. Scholz, I.; Hodgkinson, P.; Meier, B.; Ernst, M. *J. Chem. Phys.* **2009**, *130*, 114510.
2. Ernst, M.; Samoson, A.; Meier, B. H. *J. Chem. Phys.* **2005**, *123*, 064102.
3. Ernst, M.; Geen, H.; Meier, B. H. *Solid State Nucl. Magn. Reson.* **2006**, *29*, 2.
4. Ernst, M.; Samoson, A.; Meier, B. H. *J. Magn. Reson.* **2003**, *163*, 332.

Investigating the Calcium Environment in Bioactive Glasses

Richard A. Martin,[1] Dinu Iuga,[2] Mark E. Smith[3] and John V. Hanna[2]

[1]*Aston Research Centre for Healthy Ageing & School of Engineering, Aston University*

[2]*Department of Physics, University of Warwick*

[3]*Vice-Chancellor's Office, University of Lancaster*

Overview

Melt-quenched silicate glasses containing sodium, calcium and phosphorus are of great importance due to their ability to bond chemically to bone and to stimulate new bone growth. Under physiological conditions these bioactive glasses slowly dissolve, releasing calcium and phosphorus into solution which can then redeposit as an amorphous calcium phosphate layer which then crystallises into hydroxyapatite forming new bone. The release of calcium ions from the glass is therefore the key step in the formation of new bone. In order to be able to model and predict the behaviour of these materials, and thereby optimise these glasses, it is necessary to understand the local structure of the glass, particularly the local calcium environment. Building on a diffraction and NMR study of the complex structure of archetypal 45S5 Bioglass®,[1,2] it has been suggested that incorporating yttrium into bioactive glasses could result in a new class of bioactive glasses with potential radiotherapy applications for bone tumours.[3,4,5] It is important to understand how the structure of these glasses will be modified with the addition of yttrium, with ^{43}Ca NMR being a potentially powerful probe of the structure of these new materials.

Results

Figure 1 presents ^{43}Ca NMR spectra of calcium and strontium containing glasses. ^{43}Ca NMR spectra of yttrium containing glasses recorded at 20 Tesla will be complemented by additional variable field measurements to determine the quadrupolar parameters.

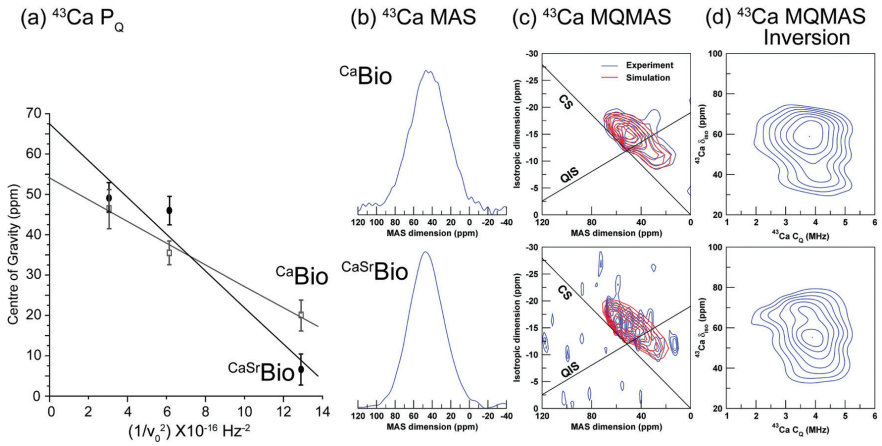

Figure 1. ^{43}Ca solid state MAS NMR data showing, (a) a plot of the resonance centre of gravity against the inverse square of the Larmor frequency υ_0, (b) 1D MAS spectra, (c) 3QMAS data and corresponding spectral simulation, and (d) the numerical inversion of the simulated 3QMAS data.[1]

References

1. Martin, R. A.; Twyman, H. L.; Rees, G. J.; Barney, E. R.; Moss, R. M.; Smith, J. M.; Hill, R. G.; Cibin, G.; Charpentier, T.; Smith, M. E.; Hanna, J. V.; Newport, R. J. *J. Mater. Chem.* **2012**, *22*, 22212.
2. Martin, R. A.; Twyman, H. L.; Rees, G. J.; Smith, J. M.; Barney, E. R.; Smith, M. E.; Hanna, J. V.; Newport, R. J. *Phys. Chem. Chem. Phys.* **2012**, *14*, 12105.
3. Christie, J. K.; Tilocca, A. *J. Mater. Chem.* **2012**, *22*, 12023.
4. Christie, J. K.; Malik, J.; Tilocca, A. *Phys. Chem. Chem. Phys.* **2011**, 13, 17749.
5. Cacaina, D.; Ylänen, H.; Simon, S.; Hupa, M. *J. Mater. Sci. Mater. Med.* **2008**, *19*, 1225.

Structural Analysis of Amyloid Fibrils Assembled from the Polypeptide Medin associated with Aortic Medial Amyloidosis

Hannah A. Davies, Jillian Madine and David A. Middleton

Institute of Integrative Biology, University of Liverpool

Overview

About 40 proteins and peptides are currently known to assemble into amyloid fibrils that are the pathological hallmark of human disease. The relationship between the structural and toxicological properties of amyloid fibrils, a question that is central to our understanding of these misfolding diseases, is poorly defined. Solid-state NMR has played a pivotal role in providing structural models for several amyloid protein assemblies, including the beta-amyloid polypeptide famously associated with Alzheimer's disease. Such information is useful for rationally designing therapeutic agents that block the assembly of these proteins into toxic species.

Aortic medial amyloid (AMA) is the most common form of localised amyloid and is found in 98% of the Caucasian population over the age of 50. The polypeptide medin, a 50-residue cleavage product of the protein lactadherin, is the principal protein component of amyloid fibrils found in the aorta and other large arteries, in close association with the internal elastic laminae. The fibrillar plaques are thought to contribute to age-related diminished elasticity of the blood vessels and experimental evidence suggests a role of AMA in sporadic thoracic aneurysm and dissection. In contrast to beta-amyloid, and despite the clinical relevance of AMA, virtually nothing is known about medin amyloid assemblies at the molecular level or about their structure-toxicity relationship. Here high-field solid-state NMR is used to investigate the structure of medin amyloid for the first time.

Results

Medin was prepared by recombinant expression in *E. coli* and purified by affinity chromatography. Medin assembly into amyloid fibrils was studied by monitoring the fluorescence enhancement of Thioflavin T, an amyloid-binding dye. A pronounced enhancement of Thioflavin T fluorescence, consistent with nucleation and rapid elongation of amyloid fibrils, occurs after incubation for 28 hours (Figure 1a). At the end-point of aggregation (50 hours), insoluble material is deposited with the characteristic amyloid-like fibril morphology when viewed by electron microscopy (Figure 1b).

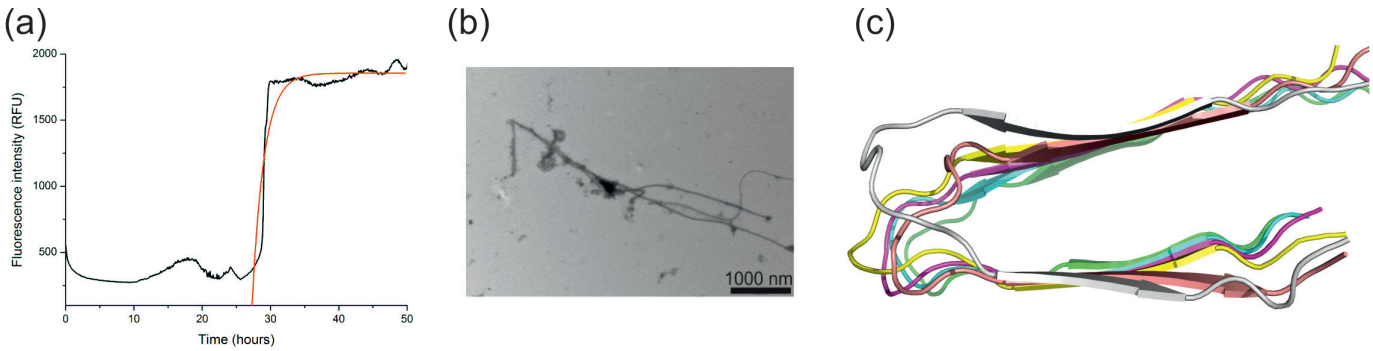

Figure 1. (a) Analysis of medin aggregation kinetics from the fluorescence intensity of thioflavin T. (b) A transmission electron micrograph of medin fibrils. (c) A model of the molecular organisation of medin fibres (viewed along the fibril long axis).

Medin shares a moderate sequence similarity with the amyloid beta peptide associated with Alzheimer's. Detailed structural models, based largely on solid-state NMR restraints, are available for the fibril organisation of the Aβ1-40 peptide.[1, 2] A homology model of the medin fibrils was constructed based upon the structure of Aβ1-40 (Figure 1c). Each medin molecule is modelled as two β-strands separated by a turn (this region has the highest similarity with the Aβ1-40 sequence) and the molecules are organised as parallel β-sheets along the intermolecular hydrogen-bonding axis (which runs approximately parallel with the fibril long axis). High-field solid-state NMR experiments were then conducted to test the validity of the model.

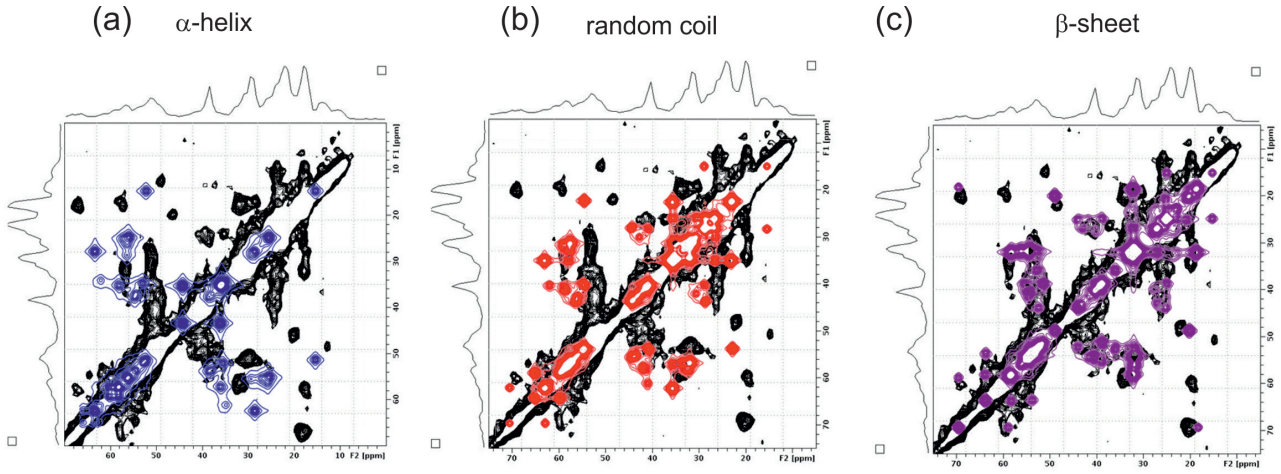

Figure 2. A high-field ^{13}C DARR spectrum (at 850 MHz) of medin fibrils (black) superimposed with three simulated spectra (blue, red or magenta) for different medin conformations.

A ^{13}C dipolar-assisted rotational resonance magic-angle spinning NMR spectrum was obtained for uniformly ^{13}C labelled medin fibrils (Figure 2). Measurement at 850 MHz provided excellent sensitivity but the line widths were somewhat broader than we had previously observed for Aβ1-40 fibrils. We were nevertheless able to extract valuable structural information from the spectrum. Comparison of the experimental spectrum with simulated spectra based on the mean chemical shift values for the 50 amino acid residues of medin in α-helical or random coil conformations revealed considerable differences across the entire spectrum (Figure 2, a and b). By contrast, a simulated spectrum for a β-sheet conformation (including documented chemical shifts for the residues of Aβ1-40 in the turn sequence homologous with medin) agrees well with the experimental spectrum (Figure 2c). The spectrum thus supports our homology model of medin, although clearly further restraints are required to confirm the model.

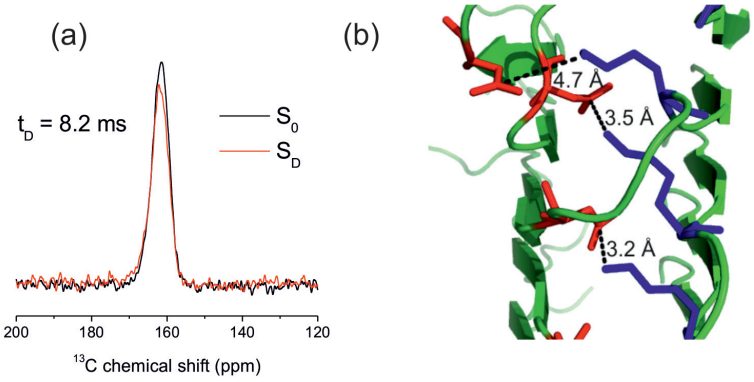

Figure 3. (a) Frequency selective REDOR spectrum of medin fibrils showing dephasing of the $^{13}C\gamma$ signal for D25 as a result of coupling to $^{15}N\zeta$ of K30. (b) A model of the medin fibril structure viewed from the side, showing distances across the proposed D25-K30 salt bridge in the turn region. The arrow denotes the fibril propagation axis.

There is growing evidence that salt-bridges between acidic and basic amino acid aide chains may play an important role in amyloidogenesis. It has been shown that Aβ1-40 fibrils are stabilised, in some morphologies, by an intermolecular salt bridge between residues D23 and K28.[1, 2] These residues occur in the region of high similarity with medin, where the corresponding residues are D25 and K30. To test the hypothesis that a similar salt bridge occurs in medin fibrils we used frequency selective REDOR to measure the distance between Cγ of D25 and Nζ of K30 in selectively labelled synthetic medin fibrils. The REDOR experiment detects a small dephasing of the ^{13}C signal detected for Cγ of D25, consistent with a Cγ-Nζ distance of <4.5 Å (Figure 3a), which is in the expected range for an Asp-Lys salt bridge (Figure 3b).

In summary, the first structural analysis of medin fibres, using solid-state NMR, support the hypothesis that some structural elements of medin fibrils are similar to those observed for the Alzheimer's Aβ1-40 polypeptide in amyloid fibrils. This work was supported by British Heart Foundation studentship grant FS/09/033/27742.

References

1. Petkova, A. T; Ishii, Y.; Balbach, J. J.; Antzutkin, O. N.; Leapman, R. D.; Delaglio, F.; Tycko, R. *Proc. Natl. Acad. Sci. USA* **2002**, *99*, 16742.
2. Paravastu, A. K.; Leapman, R. D.; Tau, W. M.; Tycko, R. *Proc. Natl. Acad. Sci. USA* **2008**, *105*, 18349.

Implications of 100 kHz Magic Angle Spinning for ^{1}H Detection and Protein Dynamics

Dinu Iuga,[1] Józef R. Lewandowski,[2] Andreas Oss,[3] Harri Parker[3] and Ago Samoson[1,3]

[1]*Department of Physics, University of Warwick*
[2]*Department of Chemistry, University of Warwick*
[3]*Tallinn University of Technology, Estonia*

Overview

Recent advances in fast magic angle spinning (MAS) technology has opened new exciting avenues for methodology development and applications in solid-state NMR. A new design based on 0.81 mm rotors developed in the Samoson laboratory allows spinning frequencies of 100 kHz to be achieved (reported at the 2012 EUROMAR conference). The narrowing of ^{1}H line widths afforded by 100 kHz MAS technology paves the way for routine application of ^{1}H spectroscopy of organic molecules without the need for homonuclear decoupling. In particular, thanks to excellent sensitivity per unit mass this methodology holds a great promise for structural and dynamics studies of sample size limited biological molecules.

Next Generation Magic Angle Spinning: Comparison of Experiments at 60 and 100 kHz Spinning Frequencies

We compared a series of experiments performed near 60 kHz spinning frequency (typical specification for a previous state-of-the-art generation of the instrumentation) and near 100 kHz spinning frequency (available through the latest design from the Samoson laboratory) using the same 0.81 mm MAS probe. We focused on quantifying improvements in ^{1}H resolution and ^{1}H,^{13}C and ^{15}N coherence lifetimes in a crystalline tripeptide N-Ac-[U-^{13}C,^{15}N]-*f*-MLF-OH.

Figure 1 shows 1D slices extracted at ^{13}C' frequencies from a ^{13}C-^{1}H 2D correlation spectra obtained at 61 and 96 kHz spinning frequencies. The benefit of the increased spinning frequencies for improving ^{1}H resolution is immediately apparent from this quick comparison. However, inhomogeneous broadening constitutes a significant fraction of the observed ^{1}H line width in the presented spectra. The full extent of the improved averaging of ^{1}H-^{1}H dipolar couplings is much better appreciated from the measurements of ^{1}H coherence lifetimes during a spin-echo experiment (T_2') where inhomogeneous broadening is removed. In the case of MLF-OH ^{1}H T_2' improve on average 2.3 times when going from 61 to 96 kHz spinning frequency (with the average T_2' ~ 3 ms and the longest T_2' > 7 ms at 96 kHz spinning frequency). This means that the homogenous ^{1}H line width achievable in a fully protonated peptide is now less than 50 Hz – a value that previously was reserved for perdeuterated samples with a highly diluted ^{1}H-^{1}H network.[1,2] In addition, we observed significant improvements in ^{13}C' and ^{15}N in coherence lifetimes under low power decoupling conditions, for example, when using slpTPPM[3] decoupling at 96 kHz spinning frequency, the MetC' T_2' reached ~260 ms (a ~1.7 times improvement compared to an analogous experiment at 61 kHz spinning frequency) and when using WALTZ decoupling at 96 kHz spinning, the MetN T_2' reached ~300 ms (~3.3 times improvement compared to an analogous experiment at 61 kHz spinning frequency). The improved averaging of the dipolar couplings at ~100 kHz spinning frequency leads to a situation where dynamics become the dominant factor affecting/influencing the length of ^{13}C' and ^{15}N coherence lifetimes, *e.g.* the MetC' T_2' is ~3 times longer than the T_2' of the other carbonyl carbons.

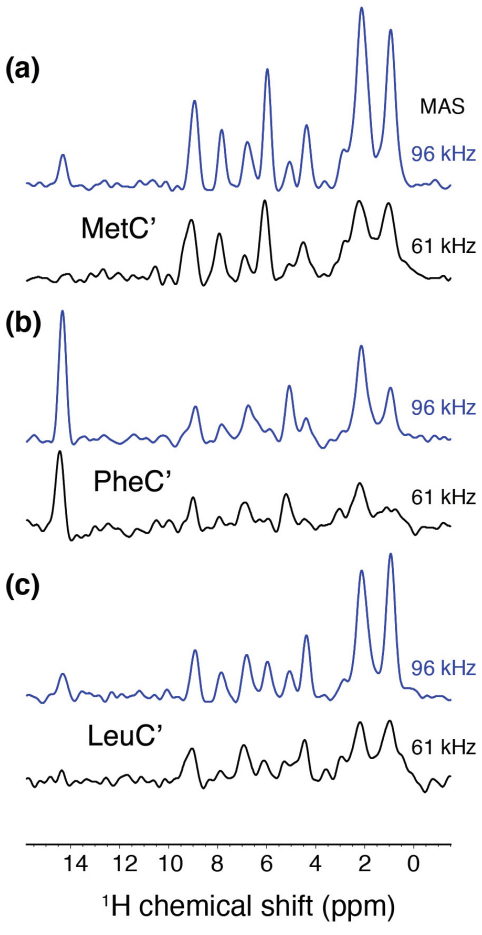

Figure 1. 1D slices from ^{13}C-^{1}H 2D correlation spectra measured on [U-^{13}C,^{15}N]-f-MLF-OH at 61 and 96 kHz spinning frequencies at $\omega_{0H}/2\pi$ = 850 MHz. The overall intensity was scaled in order to account for the differences in ^{1}H-^{13}C CP efficiency.

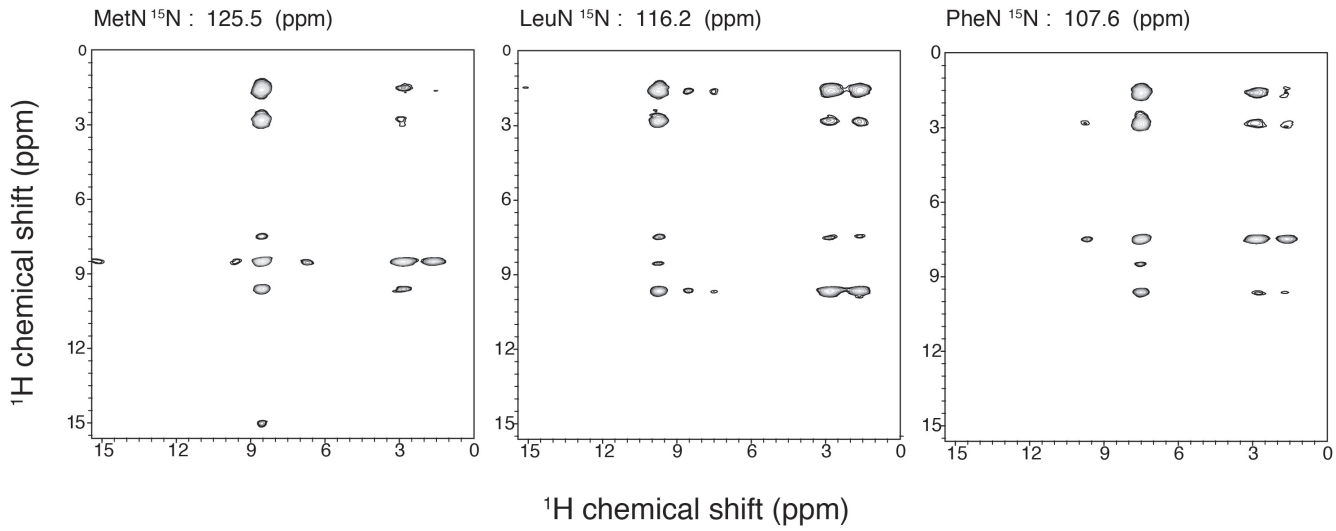

Figure 2. ^{1}H-^{1}H extracted at ^{15}N frequencies from ^{1}H-^{15}N-^{1}H 3D correlation spectrum measured on [U-^{13}C,^{15}N]-f-MLF-OH at 96 kHz spinning frequencies at $\omega_{0H}/2\pi$ = 850 MHz.

The combination of high field and improvements in resolution, coherence lifetimes and sensitivity in ^{1}H detected experiments performed at ~100 kHz spinning frequency allow rapid acquisition of high signal-to-noise well-resolved multidimensional spectra of organic and biological molecules in submilligram quantities. For example, Figure 2 shows 2D planes from a ^{1}H-^{15}N-^{1}H 3D spectrum obtained on [U-^{13}C,^{15}N]-*f*-MLF-OH in a few hours.

References

1. Chevelkov, V.; Rehbein, K.; Diehl, A.; Reif, B. *Angew. Chem. Int. Ed.* **2006**, *45*, 3878.
2. Lewandowski, J. R.; Dumez, J.-N.; Akbey, Ü.; Lange, S.; Emsley, L.; Oschkinat, H. *J. Phys. Chem. Lett.* **2011**, *2*, 2205.
3. Lewandowski, J. R.; Sein, J.; Sass, H. J.; Grzesiek, S.; Blackledge, M.; Emsley, L. *J. Am. Chem. Soc.* **2010**, *132*, 8252.

^{11}B MQMAS and DOR NMR of Boronic Acid-Saccharide Complexes

Emma-Rose Coad, Frédéric Blanc and Oren A. Scherman

Department of Chemistry, University of Cambridge

Overview

^{11}B solid-state NMR MQMAS[1-3] experiments offer an opportunity to probe boronic acid-saccharide interactions in the solid state rather than in solution where they are more routinely investigated.[4,5] This has allowed for an understanding of how these interactions differ with changes in boronic acid species, and opens up the possibility for designed interactions within boronic acid containing composite materials. ^{11}B MQMAS experiments performed by the authors at low field (400 MHz) showed the presence of multiple ^{11}B sites in the solid state, however resolution was poor. Employing the UK 850 MHz Solid-State NMR Facility instrument allowed for increased resolution of these signals. The results obtained during the MQMAS experiments were then confirmed through the use of the facility's DOR probe at varying spinning frequencies.

^{11}B Spectra

Figure 1 presents an example of the data gained from the MQMAS experiments, with a fairly well resolved spectrum being observed. This is a drastic improvement compared to the data obtained previously at lower field where the two sites that are distinguished in Figure 1 could not be fully resolved. Interestingly, the data presented here helps to confirm that although the intensity is low, a third minor site, around 12 ppm in the ^{11}B spectrum is present in the sample that could not be observed clearly at lower field. According to the standard coordination number – shift relationship in ^{11}B NMR,[6] both peaks at around 12 and 25 ppm are tri-coordinate boron species while the peak around 0 ppm is a tetra-coordinate boron species. We also note that there is clearly a distribution of chemical shifts as evidenced by the fact that most peaks are aligned with the +1 diagonal and indicate disorder in these polymers.

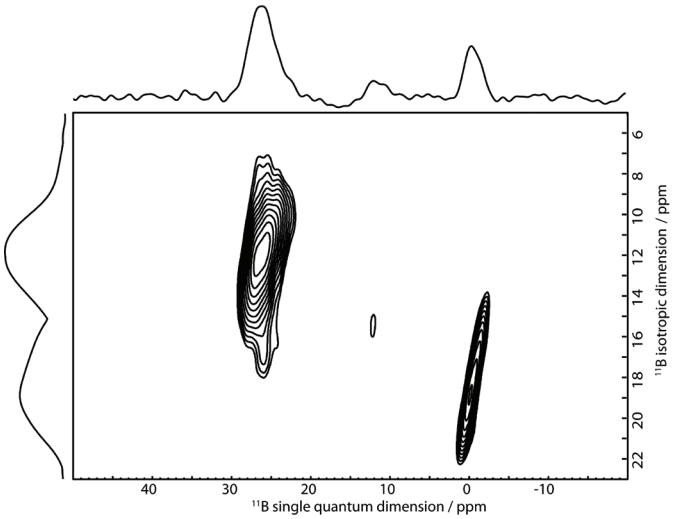

Figure 1. ^{11}B MQMAS (850 MHz, 12.5 kHz MAS) spectra with skyline projections of a boronic acid-saccharide complex.

In order to explore the possibility of acquiring high-resolution ^{11}B NMR spectra of the materials in a time efficient manner, ^{11}B double rotation (DOR)[7,8] spectra were also carried out at spinning speeds of 1400-1750 Hz and 7100-8000 Hz for the outer and inner rotors, respectively. The DOR experiments carried out were pulse-acquire experiments with simultaneous spinning of the two rotors[7,8] at two different angles (30.6° and 54.7°) with respect to the magnetic field B_0 in order to obtain high-resolution spectra of quadrupolar nuclei like ^{11}B by averaging out the second-order quadrupolar interaction and hence narrowing the line shape.

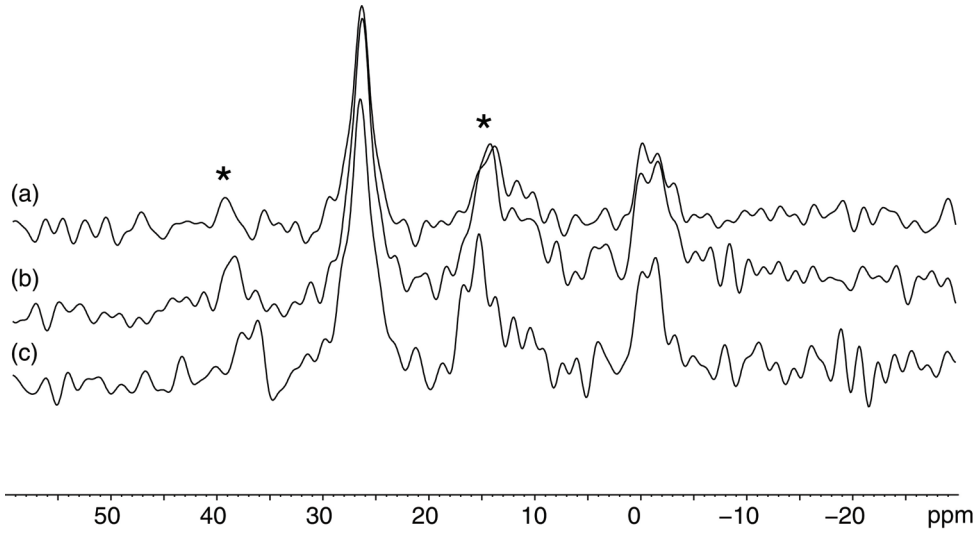

Figure 2. ^{11}B DOR spectra of boronic acid pendant polymer in the presence of polysaccharide. The spectra were obtained after background suppression of the spinner assembly. (a) inner rotor 8000 Hz, outer rotor 1750 Hz, (b) inner rotor 8000 Hz, outer rotor 1600 Hz (c) inner rotor 7100, outer rotor 1400 Hz. Asterisks (*) denote spinning side bands.

Figure 2 confirms the signals seen in Figure 1. However, the central peak (around 10 ppm) is in this case difficult to distinguish from the spinning side band. The MQMAS experiments together with the DOR experiments confirm the presence of multiple boronic acid sites within the solid material and the use of the higher field has allowed us to resolve these peaks with more confidence than was possible at lower field. This will in turn, together with knowledge of the coordination number of each species, aid assignment of the individual sites and hence allow for conclusions to be made as to the variable coordination potential of the different boronic acid species investigated.

References

1. Frydman, L.; Harwood, J. S. *J. Am. Chem. Soc.* **1995**, *117*, 5367.
2. Medek, A.; Hardwood, J. S.; Frydman, L. *J. Am. Chem. Soc.* **1995**, *117*, 12779.
3. Amoureux, J. P.; Fernandez, C.; Steuernagel, S. *J. Magn. Reson. A* **1996**, *123*, 116.
4. James, T. D.; Sandanayake, K. R. A. S.; Shinkai S. *Angew. Chem. Int. Ed.* **1996**, *35*, 1910.
5. Musto, C. J.; Suslick, K. S. *Curr. Opin. Cell Biol.* **2010,** *14*, 758.
6. MacKenzie, K. J. D.; Smith, M. E. *Multinuclear Solid-State NMR of Inorganic Materials*, in Pergamon Materials Series, Cahn, R. W., Ed.; University of Cambridge, Cambridge UK, **2002**.
7. Samoson, A.; Pines, A. *Rev. Sci. Instrum.* **1989**, *60*, 3239.
8. Wu, Y.; Sun, B. Q.; Pines, A.; Samoson, A.; Lippmaa, E. *J. Magn. Reson.* **1990**, *89*, 297.

Extension of WURST Excitation to ^{119}Sn and ^{87}Sr BRAIN-CP Experiments

Christian Bonhomme,[1] Danielle Laurencin,[2] John V. Hanna[3] and Mark E. Smith[3,4]

[1]*UPMC, Paris, France*
[2]*ICGM, Montpellier, France*
[3]*Department of Physics, University of Warwick*
[4]*Vice-Chancellor's Office, Lancaster University*

Overview

The combination of ultra-high magnetic field, broadband excitation schemes (WURST) and multiple echoes detection (CPMG) is extremely powerful for the measurement of very broad lineshapes such as those obtained for nuclei subjected to a strong quadrupolar interaction or CSA. Recently, we have shown that this approach was suitable for the detailed study of Sr-doped bioactive glasses by ^{87}Sr static NMR.[1] Schurko and co-workers have more recently extended the WURST concept to CP experiments enabling much wider excitation of the target nucleus (BRAIN-CP).[2] Here, we demonstrate the efficiency of ^{1}H-^{119}Sn BRAIN-CP experiments for the study tin oxoclusters, $\{(BuSn)_{12}O_{14}(OH)_6\}(OH)_2$, exhibiting both 5- and 6-fold coordinated Sn atoms.[3] The efficiency of BRAIN-CP over standard CP was clearly demonstrated and full spectra were recorded using a very limited number of offset frequencies. For the first time, we have applied the BRAIN-CP approach for the study of quadrupolar nuclei (^{1}H-^{87}Sr), using a ^{87}Sr-labelled strontium malonate sample. All experiments were performed using CPMG detection. The parameters related to (i) the WURST excitation scheme during very long contact times (up to 100 ms), and (ii) CPMG, were carefully optimised for each sample. Such experiments open new perspectives for the detailed characterisation of complex materials such as Sr-doped bioactive glasses after immersion in simulated body fluids, as they should allow discrimination of protonated from non-protonated Sr sites.

^{1}H-^{119}Sn spectra

Figure 1 presents ^{1}H-^{119}Sn CP spectra obtained with standard irradiation on both channels (Figure 1a) and with WURST excitation on the ^{119}Sn channel (Figure 1b). Each spectrum was obtained in ~ 10 min. A much wider excitation is obtained with WURST excitation. It allowed recording of a full spectrum in a short amount of experimental time (3 offsets, total experimental time ~ 30 min, (see the inset of Figure 1)). The resonances corresponding to the 5- and 6-fold coordinated Sn atoms are clearly distinguished.

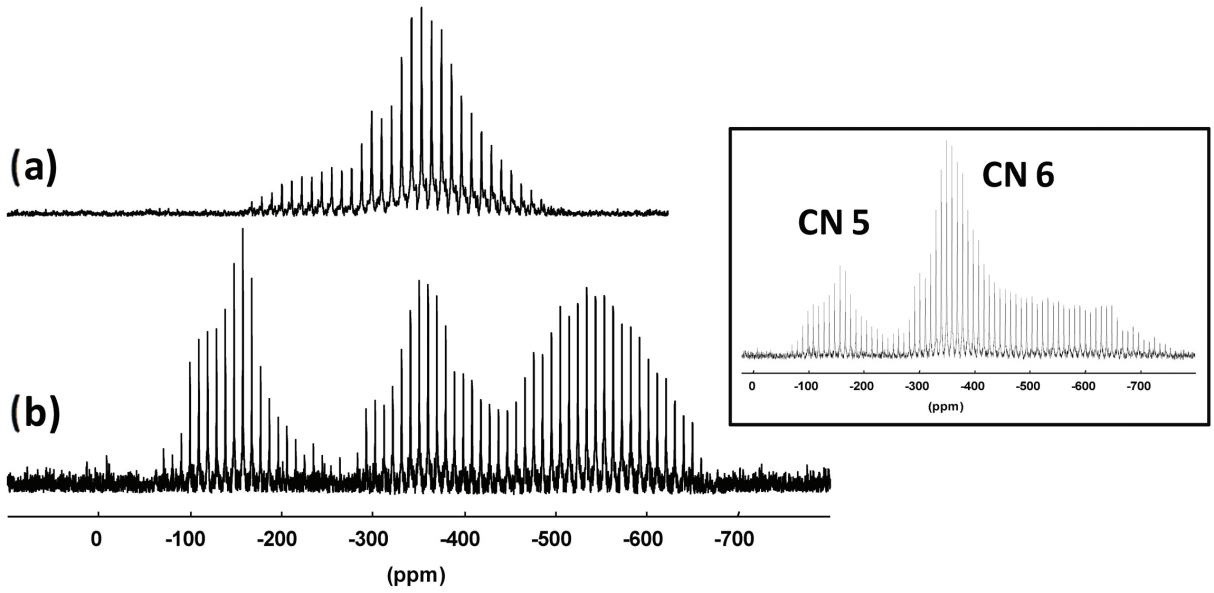

Figure 1. Static ^{1}H-^{119}Sn CP spectra for $\{(BuSn)_{12}O_{14}(OH)_6\}(OH)_2$ recorded with standard irradiation on both channels (a), and WURST irradiation on ^{119}Sn channel (b) (~ 10 min. for each spectrum). Inset: complete BRAIN-CP spectrum: 3 offsets, total experimental time ~ 30 min.

^{1}H-^{87}Sr spectra

For the first time we illustrate here the strength of the BRAIN-CP experiment for the case of large second-order quadrupolar broadening (^{87}Sr). The effect of BRAIN-CP is spectacular in comparison with normal CP, as one single offset is sufficient to extract the features of the quadrupolar lineshape for the unique ^{87}Sr site in the structure (Figure 2). In contrast, many offsets would be necessary in the case of standard CP experiments. Clearly, the impact of BRAIN-CP should be high in the materials science community. The introduction of the CP transfer in the detection of quadrupolar nuclei experiencing strong quadrupolar interactions (e.g. large second-order quadrupolar broadening) is a natural way to deeply investigate local dynamics through the modulation of the heteronuclear dipolar interaction.

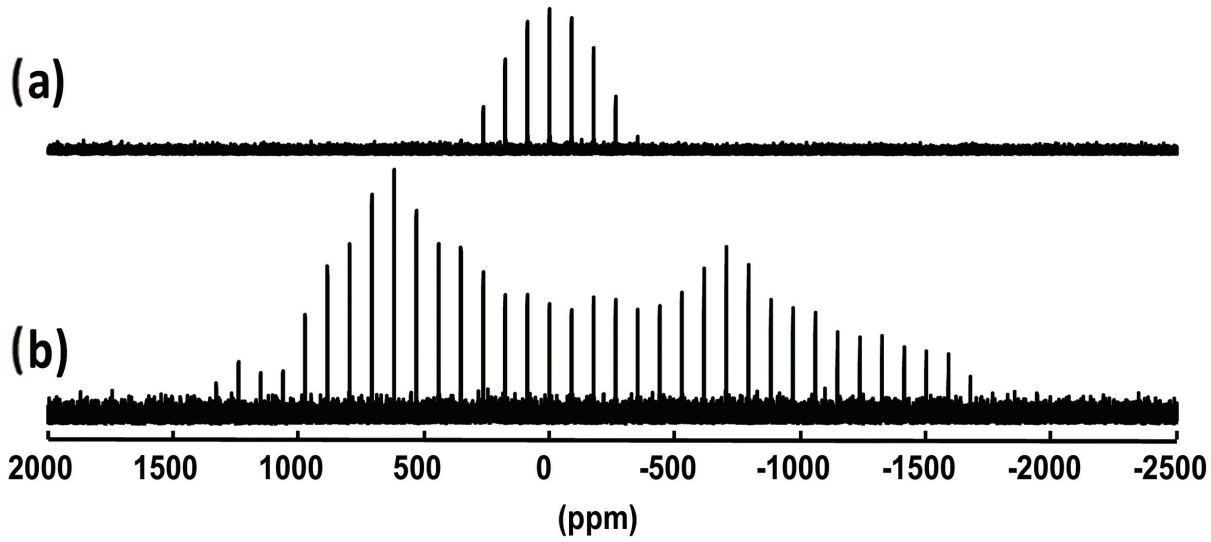

Figure 2. Static ^{1}H-^{87}Sr CP spectra for strontium malonate (labelled in ^{87}Sr) recorded with standard irradiation on both channels (a), and WURST irradiation on ^{87}Sr channel (b) (~ 3 h 30 min. for each spectrum).

Dr F. Ribot is warmly acknowledged for the preparation of $\{(BuSn)_{12}O_{14}(OH)_6\}(OH)_2$ and helpful discussions about the crystallographic structure of this compound.

References

1. Bonhomme, C.; Gervais, C.; Folliet, N.; Pourpoint, F.; Diogo, C. C.; Lao, J.; Jallot, E.; Lacroix, J.; Nedelec, J. M.; Iuga, D.; Hanna, J.V.; Smith, M. E.; Xiang, Y.; Du, J.; Laurencin, D. *J. Am. Chem. Soc.*. **2012**, *134*, 12611.
2. Harris, K. J.; Lupulescu, A.; Lucier, B. E. G.; Frydman, L.; Schurko, R. W. *J. Magn. Reson.* **2012**, *224*, 38.
3. Banse, F.; Ribot, F.; Tolénano, P.; Maquet, J.; Sanchez, C. *Inorg. Chem*. **1995**, *34*, 6371.

Measuring Proton Shift Anisotropies Using Ultrafast MAS

Habeeba Miah,[1] David Bennett,[1] Francesca Martini[2] and Jeremy J. Titman[1]

[1]*School of Chemistry, University of Nottingham*

[2]*Department of Chemistry and Industrial Chemistry, University of Pisa, Italy*

Overview

Hydrogen bonding plays a critical role in molecular self assembly, particularly in biological systems. Solid-state ^{1}H NMR spectroscopy provides a means to study hydrogen-bonded structures, since ^{1}H chemical shift parameters are known to depend on the hydrogen bond length.[1] For example, we have recently identified a correlation between calculated values of the ^{1}H chemical shift anisotropy (CSA) and the O–H –– O distance in galactose.[2] With increasing B_0 fields and faster MAS some progress has been made recently towards methodologies for measuring ^{1}H chemical shift parameters. Recently, Brouwer and Ripmeester proposed a novel two-dimensional ^{1}H anisotropic-isotropic correlation experiment[3] in which the ^{1}H CSA is measured in the indirect dimension using a symmetry-based recoupling sequence,[4] while different ^{1}H sites are resolved via their isotropic shifts in ν_2. Suitable pulse sequence symmetries recouple a single-quantum Hamiltonian which takes the form

$$\bar{H}^{(1)} = \sum_j \left(\omega_j T^j_{1-1} - \omega_j^* T^j_{1+1}\right)$$

to first order, where the index j runs over all the ^{1}H shift interactions and $T_{1\pm1}$ is an irreducible spherical tensor spin operator of rank 1. The coefficient ω_j depends on the CSA which in turn determines the width of the recoupled powder pattern observed in ν_1. In addition, suitable symmetries must suppress homonuclear dipolar interactions, isotropic chemical shifts and terms arising from RF inhomogeneity. Brouwer and Ripmeester chose the R18$_2^5$ recoupling sequence (specified here using the nomenclature in Ref.[4]) and demonstrated that ^{1}H CSAs could be measured in model systems. However, this choice restricts the maximum MAS rate to around 30 kHz, since otherwise the symmetry constraints require prohibitively high ^{1}H RF amplitudes. This means that homonuclear decoupling is required to resolve the ^{1}H isotropic shifts in ν_2.

Results

We have identified a number of new CSA recoupling sequences which produce the first-order Hamiltonian described above and result in acceptable scaling factors using RF amplitudes of less than 150 kHz at MAS rates around 60 kHz. The use of ultrafast MAS at high B_0 field optimizes the resolution of ^{1}H sites in ν_2 without the need for homonuclear decoupling. A number of these new CSA recoupling sequences were tested at 850 MHz. For example, Figure 1a shows an experimental (blue contours) ^{1}H anisotropic-isotropic correlation spectrum of ascorbic acid obtained using a R16$_3^2$ sequence with a MAS rate of 58.6 kHz and no homonuclear decoupling in t_2.

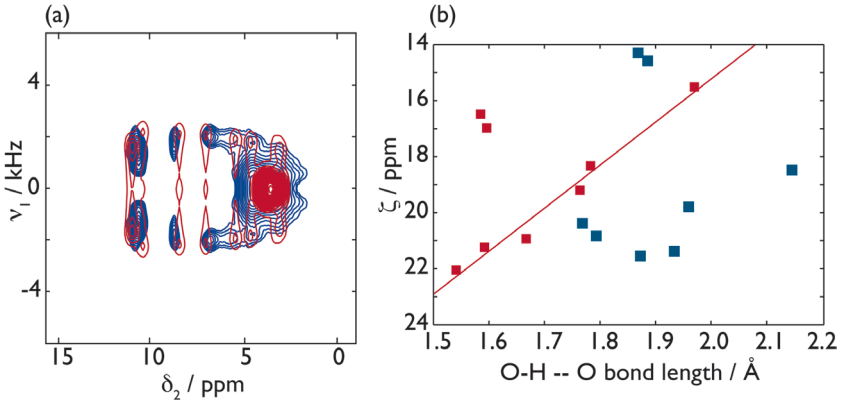

Figure 1(a). (blue contours) Experimental ^{1}H anisotropic-isotropic correlation spectrum of ascorbic acid recorded with a R16$_3^2$ sequence to recouple the ^{1}H CSA during the indirect dimension. The Larmor frequency was 850 MHz and the MAS rate was 58.6 kHz. (red contours) Simulated ^{1}H anisotropic-isotropic correlation spectrum of ascorbic acid spectrum based on calculated shift parameters obtained using DFT after an initial geometry optimization step. (b). DFT calculated values of ^{1}H CSA (blue points) based on the X-ray structure and (red points) after geometry optimization. Note the good correlation (red line) between the CSA and the bond length for the six hydrogen bonds with a hydroxyl acceptor group.

The results were compared with CASTEP DFT[5] calculations of the ^{1}H CSAs based on the ascorbic acid X-ray structure. Initially, the chemical shift parameters were extracted directly from the X-ray structure[6] using a gauge-including projector-augmented wave (GIPAW) approach. The calculated value of the ^{1}H CSA (blue points) is plotted as a function of the X-ray-derived hydrogen bond length in Figure 1b. The calculated shift parameters were used to simulate the ^{1}H anisotropic-isotropic correlation spectrum (not shown), but the match with the experimental data was very poor. As expected, much better agreement was obtained when an initial geometry optimization step was carried out, in which all the atom positions were allowed to vary. The chemical shift parameters extracted using a GIPAW approach from the optimized structure are also shown in Figure 1b (red points). It is clear that significant changes in the hydrogen positions occur during geometry optimization and these are reflected in substantial changes to the ^{1}H CSA. These optimized shift parameters were used to simulate the ^{1}H anisotropic-isotropic correlation spectrum shown in Figure 1a (red contours). The agreement between the simulated and experimental spectra is good. In addition, after geometry optimization, there is a clear correlation between the ^{1}H CSA and the hydrogen bond length as shown in Figure 1b (red line). Note that the six hydrogen bonds which show the correlation involve hydroxyl acceptor oxygen atoms, while the two outliers involve carbonyl acceptor oxygen atoms.

In addition, we have identified a number of new sequences which still operate with acceptable RF amplitudes at even higher MAS rates up to 80 kHz. Some of these were tested at 850 MHz using the Facility's new Jeol 1 mm MAS probe which spins at rates up to 80 kHz. For example, Figure 2 shows an experimental ^{1}H anisotropic-isotropic correlation spectrum of ascorbic acid obtained using a $R10_3^1$ sequence with a MAS rate of 78.1 kHz and an RF amplitude of 130 kHz.

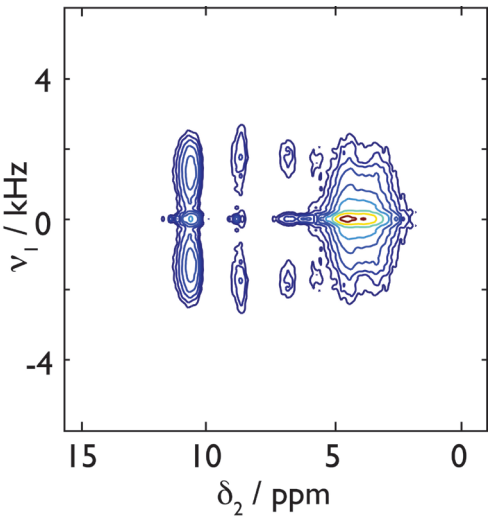

Figure 2. (blue contours) Experimental ^{1}H anisotropic-isotropic correlation spectrum of ascorbic acid recorded with a $R10_3^1$ sequence to recouple the ^{1}H CSA in the indirect dimension. The Larmor frequency was 850 MHz and the MAS rate was 78.1 kHz.

References

1. Jeffrey, G. A.; Yeon, Y. *Acta Crystallogr. B*, **1986**, *42*, 410.
2. Kibalchenko, M.; Lee, D.; Shao, L.; Payne, M. C.; Titman J. J.; Yates J. R. *Chem. Phys. Lett.*, **2010**, *498*, 270.
3. Brouwer, D. H.; Ripmeester, J. A. *J. Magn. Reson.*, **2007**, *185*, 173.
4. Carravetta, M.; Edén, M.; Zhao, X.; Brinkmann A.; Levitt, M. H. *Chem. Phys. Lett.*, **2000**, *321*, 205.
5. Clark, S. J.; Segall, M. D.; Pickard, C. J.; Hasnip, P. J.; Probert, M. J.; Refson, K. Payne, *Z. Kristallogr.*, **2005**, *220*, 567.
6. Milanesio, M.; Bianchi, R.; Ugliengo, P.; Roetti, C.; Viterbo, D.; *J. Mol. Struct.*, **1997**, *419*, 139.

A Solid-State NMR Study of an Immobilised Enzyme

Nicole Fauré,[1] Peter J. Halling[2] and Stephen Wimperis[1]

[1]*School of Chemistry and WestCHEM, University of Glasgow*

[2]*Department of Pure and Applied Chemistry and WestCHEM, University of Strathclyde*

Overview

Enzymes, as catalysts, possess the astonishing virtue of leading to product formation at mild and environmentally friendly conditions with a high specificity. A core technology is the immobilisation of enzymes – the conversion of the soluble protein molecules into a solid particle form that can be easily separated from the reaction mixture. This allows the expensive enzyme catalyst to be recovered and re-used and avoids protein contamination of the product streams. Since the advent of immobilisation of single enzymes in the 1940s, innumerable methods have been developed. Despite extensive study on different systems, there is no clear approach for a given process and enzyme. One reason for this is that little is known about the state of the protein molecules in the preparation except what is deduced from the catalytic activity.

Enzymes, being proteins, possess an inherent flexibility to different environmental conditions that affect their functionality. This issue is related to the fact that proteins do not occupy one structure but rather they are more accurately described by an equilibrating set of time-dependent structures.[1] With the aim of evaluating these conformational aspects, solid-state NMR has become a powerful tool to visualise biological processes in space and time at atomic resolution, specifically for insoluble biological systems that are not accessible by X-ray crystallography or solution-state NMR.[2] As mentioned previously, little is known about the protein state in the preparation, therefore it is not possible to guide in a more rational way the immobilisation of enzymes owing to this lack of knowledge. Consequently the study of heterogeneous enzyme systems via solid-state MAS NMR becomes an appropriate approach and an entirely novel one.

Results

α-Chymotrypsin covalently immobilised on epoxide silica has been our first system of study by solid-state MAS NMR. With this heterogeneous enzymatic and inorganic support system, we have used the 850 MHz NMR Facility to characterise our support system (glycidoxypropyltrimethoxysilane, GOX, grafted onto surface of silica gel – see Figure 1b) using cross-polarisation (CP) experiments and have obtained ^{13}C CPMAS spectra where our immobilised enzyme is visible and been able to correlate different species present in our sample (see Figures 1 and 2a).

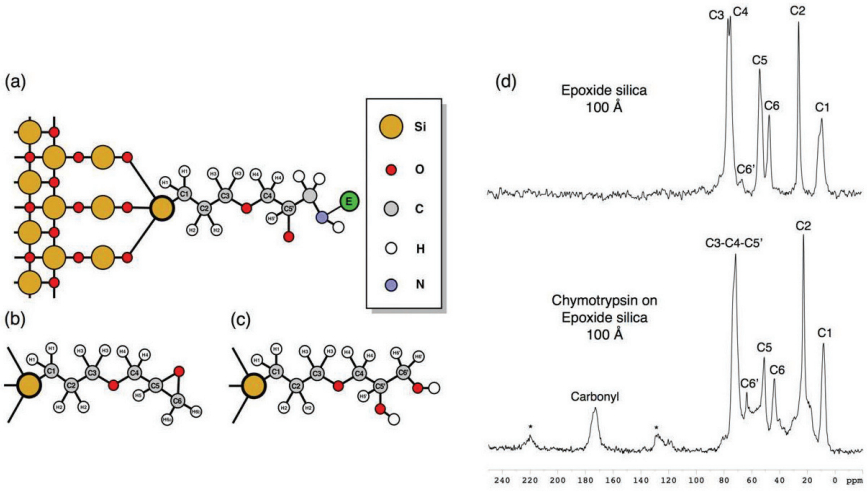

Figure 1. (a) Scheme of α-chymotrypsin (E) covalently immobilised in epoxide silica. (b) Scheme of GOX grafted on to silica surface. (c) Scheme of opened epoxide ring. (d) ^{13}C CPMAS NMR spectra with ^{1}H decoupling (ν_R = 10 kHz) of epoxide silica and immobilised enzyme at 20 T.

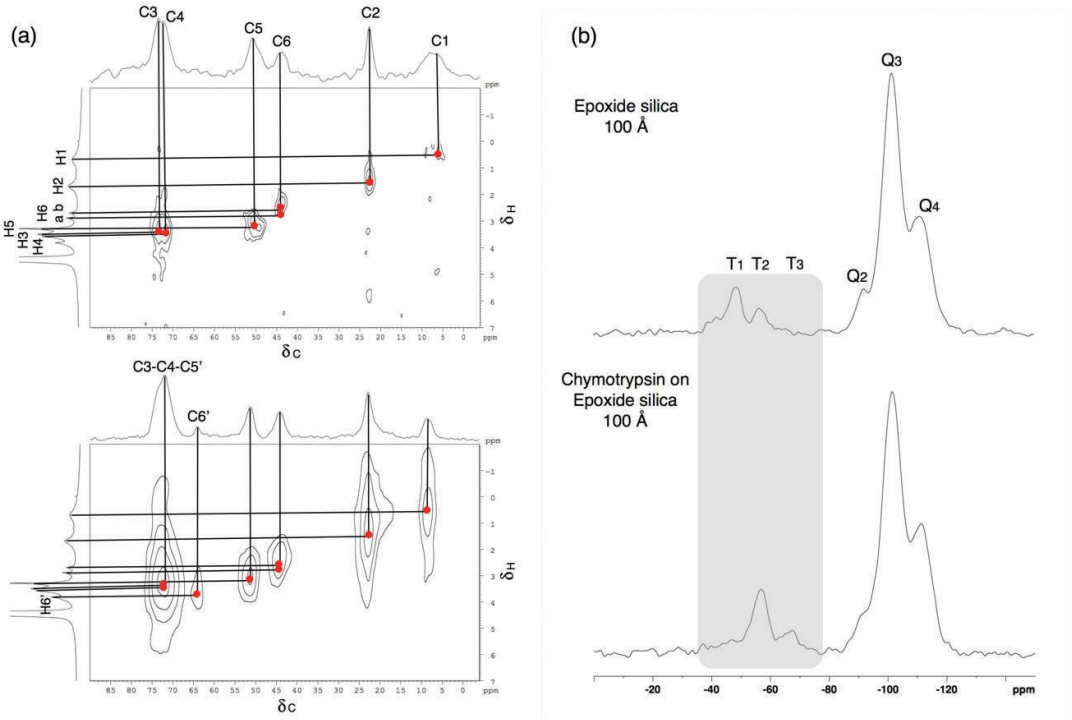

Figure 2. (a) Two-dimensional ^{1}H-^{13}C HETCOR spectra with ^{1}H decoupling (ν_R = 10 kHz) of epoxide silica and immobilised enzyme recorded at 20 T. (b) ^{29}Si CPMAS NMR spectra with ^{1}H decoupling (ν_R = 10 kHz) of epoxide silica and immobilised enzyme at 20 T.

It was observed during the process of immobilisation (epoxide silica and enzyme in contact for 20 hours in aqueous system) that the oxirane functional groups are opened by nucleophilic attack by water molecules,[3] thereby yielding a diol (see Figure 1c); this can be noted from the relative increase in intensity of C6' and the decrease for oxirane carbons (the C5 and C6 decrease is also due to the immobilisation of the enzyme) (Figure 1d).

Two-dimensional ^{1}H-^{13}C HETCOR spectra of the epoxide silica and immobilised enzyme materials were recorded (Figure 2a). The epoxide silica sample has been treated with D_2O so that only non-exchangeable ^{1}H nuclei related with the grafted linker remained. Analysing the results for the support and immobilized enzyme jointly, it was possible to assign the various species labelled in Figures 1 and 2a.

Unexpectedly, the ^{29}Si CPMAS NMR spectra shown in Figure 2b reveal changes in the surface species of epoxide silica after the enzyme immobilisation, a process that is distant from any silicon atoms. The covalent bonds between the grafted molecule (GOX) and the surface of silica gel may be characterised as mono-, bi- or tri-dentate (T_1, T_2 or T_3). After the immobilisation procedure, it can be observed that the ^{29}Si T_1 signal is negligible, T_2 is significantly increased and T_3 has appeared for the first time; small changes can also be observed in the Si-coordinated Q_2, Q_3 and Q_4 species. These changes are because residual Si-OH groups become cross-linked to give Si-O-Si, with T_1, T_2 and Q_2 species becoming T_2 or T_3, T_3 and Q_3, respectively, after the immobilisation. Further experiments have ruled out that the enzyme is involved in this process. The hydrolysis and condensation (cross-linking process) of organofunctional alkoxysilanes is a well known process used in industry to increase adhesive strength.[4] However, it has not been extensively studied on surfaces, and not at all in the type of system studied here.

References

1. Boehr, D. D.; Dyson, H. J.; Wright, P. E. *Chem. Rev.* **2006**, *106*, 3055.
2. McDermott, A. E. *Curr. Opin. Struc. Biol.* **2004**, *14*, 554.
3. Templin, M.; Wiesner, U.; Spiess, H. W. *Adv. Mater.* **1997**, *9*, 814.
4. Osterholtz, F. D.; Pohl, E. R. *J. Adh. Sci.* **1992**, *6*, 127.

Global Supplier of stable isotope enriched products & NMR consumables

Contact & Address:
Philippe Corcos, CEO
15/17, rue des Tilleuls
78960 Voisins-Le-Bretonneux, France
Tel: +33 (0)1 30 12 11 31
pcorcos@cortecnet.com

cortecnet
INNOVATION ACCELERATOR IN LIFE SCIENCE

Company

Since more than 15 years, CortecNet is known as one of the most reliable supplier of NMR consumables and stable isotope enriched products. CortecNet is composed of a team of analytical engineers capable to understand and fulfill all your needs. Over the years, CortecNet has developed a strong professional network including thousands of academic labs and industrial companies all around the world.

Products

CortecNet has developed strong partnerships with key analytical suppliers like Bruker, New Era, Wilmad, SGE.... CortecNet is specialized in NMR & EPR consumables (rotors, inserts, NMR tubes) as well as fully and selectively ^{13}C, ^{15}N, ^{2}H stable isotope enriched compounds, deuterated solvents, metals (^{29}Si, ^{43}Ca, ^{87}Sr), ^{17}O-labeled water and gases.

^{29}Si-Teos and ^{17}O-labeled compounds

Cortecnet is now moving one step forward by providing specialty labeled compounds in order to meet the growing scientist needs in selectively labeled intermediates and compounds. We are now able to provide ^{29}Si enriched Teos, a precursor widely use in sol-gel methods, that is going to be essential for the characterization of zeolite structures, microelectronic and fuel cell components. We will also soon be able to provide others ^{17}O-labeled compounds.

We recently expanded our line of services by providing high quality labeled protein standards for liquid and solid state NMR spectroscopy (Giotto Biotech).
We kindly invite you to visit our website (www.cortecnet.com) to discover all our products, download our catalogs and take advantage of our incredible weekly discounts on selected products.

www.cortecnet.com

JEOL-NMR Probes

advanced technology and performance

Royal Probe:

High 1H sensitivity
Improved inverse detection
Broad (LF) tuning range
Auto-tuning
Wide VT capability

1mm CPMAS Probe:

MAS Speeds 1KHz to 80KHz
Spinning stability <10Hz
Sample Volume 0.8µL
Excellent 1H sensitivity and resolution
Strong RF field

+44 (0)1707 377117

JEOL
www.jeol.com

euro.sales@jeol.com

BRUKER

Analyse Everything

Cutting Edge Instrumentation

For Results You Can Rely On

One of the world's largest ranges of analytical instrumentation available under one brand, including flexible research systems and push-button routine solutions based on Magnetic Resonance, Mass Spectrometry, Vibrational Spectroscopy, X-Ray and Surface Analysis.

Find the solution to your analytical question:
www.bruker.com **info@bruker.co.uk** **024 7685 5200**

Innovation with Integrity

Design by Mustard: www.mustardhot.com

Advantage West Midlands
www.advantagewm.co.uk

BBSRC
bioscience for the future

EPSRC
Engineering and Physical Sciences Research Council

investing in your future
European Regional Development Fund
European Union

Dr Dinu Iuga (Facility Manager)
Department of Physics
University of Warwick
Coventry CV4 7AL
T +44 (0) 24 761 50814
F +44 (0) 24 761 50897
E D.Iuga@warwick.ac.uk
W http://go.warwick.ac.uk/850mhz/

UNIVERSITY OF CAMBRIDGE
Durham University
University of Glasgow
The University of Nottingham
UNITED KINGDOM · CHINA · MALAYSIA
University of St Andrews
THE UNIVERSITY OF WARWICK